# DEVELOPMENT OF A REGENERATIVE MEDICINE STRATEGY FOR THE TREATMENT OF DUCHENNE MUSCULAR DYSTROPHY

by
Kenneth Michael Estrellas

A dissertation submitted to Johns Hopkins University in conformity with the requirements for the degree of Doctor of Philosophy

Baltimore, Maryland
March 2017

## Abstract

Despite decades of work, Duchenne Muscular Dystrophy (DMD) remains a deadly disease with no cure. Recent advances in stem cell biology, immunology, and bioengineering suggest an interdisciplinary approach to the treatment of DMD. Towards this end, we created a multifunctional hydrogel composed of hyaluronic acid and skeletal muscle extracellular matrix that is cytocompatible, injectable, and biodegradable. The hydrogel facilitates the controlled release of myostatin inhibitors *in vitro* and increases their bioactivity *in vivo*. The hydrogel also promotes macrophage polarization towards CD206 expression, elevates anti-inflammatory cytokine levels, and co-injection of hydrogel with myostatin inhibitor yields a significant increase in $Foxp3^{+}$ regulatory T cells. Finally, human embryonic stem cell derived myoblasts transplanted with the hydrogel demonstrated greater survival at 7-10 days post-injection, and increased engraftment after 4 months in immunodeficient dystrophic mice. Overall, this study represents a promising advance in regenerative medicine therapies for DMD.

## Advisors / Thesis Readers

Jennifer Elisseeff, Ph.D.

Department of Biomedical Engineering, Johns Hopkins University

Kathryn Wagner, M.D. Ph.D.

Departments of Neurology and Neuroscience, Johns Hopkins University School of Medicine

## Acknowledgements

To Kathryn and Jennifer, for your guidance, mentorship, insight, and patience.

To Kaitlyn for introducing me to the world of immunology, Matt and Liam for helping me analyze endless FACS samples, Shoumyo for helping with rheology, and everyone else in the Elisseeff lab for being awesome.

To Lindsay, for being the best undergraduate mentee a grad student could ever ask for. To Tracy and Naili for teaching me how to cryosection and harvest muscle, to Jyothi for correcting me, and everyone else in the Wagner lab for being awesome.

To Colleen, Leslie, Rajini, Bob, and everyone else in the CMM program for giving me the opportunity to train at such an amazing place.

To my CMM Class of 2011, and everyone I've met at Hopkins, it's been a wonderful journey. To all those still in the process – you'll get there soon!

To Edith, Dan, and Sorin for introducing me to the world of biomedical research. Thank you for taking your chances on an inexperienced undergraduate!

To BDCP, Project D, imPulse, and the greater urban dance community for giving me a second life outside of science, and friends no matter where I go.

To all my friends from Kindergarten to College, for always being there for me.

To Mom, Dad, Tita, Jeff, and Sheryll, thank you for instilling and supporting my love for science since childhood. I literally wouldn't be here without you.

To Jean, for everything. I love you with all of my heart, and look forward to us forever.

# Table of Contents

# List of Abbreviations

| | |
|---|---|
| AAV | Adeno-Associated Viral Vector |
| CD | Cluster of Differentiation |
| CTX | Cardiotoxin |
| DMD | Duchenne Muscular Dystrophy |
| dSKM | Decellularized Skeletal Muscle |
| DYS | Dystrophin |
| ECM | Extracellular Matrix |
| FACS | Fluorescence Activated Cell Sorting |
| H&E | Hematoxylin and Eosin |
| hESC | Human Embryonic Stem Cell |
| hESMyo | hESC-derived myoblast |
| hiPSC | Human Induced Pluripotent Stem Cell |
| hLAC | Human Lamin A+C |
| hLAM | Human Laminin |
| HA | Hyaluronic Acid |
| HA-NHS | Hyaluronic Acid Succinimidyl Succinate |
| IF | Immunofluorescence |
| IFN | Interferon |
| IL | Interleukin |
| MFI | Mean Fluorescence Intensity |
| NHS | *N*-hydroxysuccinimide |
| NRG | NOD-Rag1$^{null}$-IL2rg$^{null}$ |
| NSG | NOD-SCID-IL2rg$^{null}$ |
| Pax7 | Paired Box 7 |
| PBS | Phosphate-Buffered Saline |
| SC | Satellite Cell |
| SKM | Skeletal Muscle |

# List of Tables

## Chapter 3

# List of Figures

## Chapter 2



## Chapter 3



## Chapter 4

# Chapter 1: Introduction

## Overview

In **Chapter 1**, I will introduce Duchenne Muscular Dystrophy (DMD), current and future treatment options for DMD including cell therapy and myostatin inhibition, the role of the immune system in skeletal muscle repair and regeneration, and the application of biomaterials and regenerative medicine principles to skeletal muscle. **Chapter 2** describes the synthesis of the materials utilized in this study, the fabrication of an injectable biomaterial-based hydrogel, and its initial characterization *in vitro* and *in vivo*. Cytocompatibility, biocompatibility, and growth factor delivery are assessed. **Chapter 3** characterizes the effects of the hydrogel and myostatin inhibitor on the local immune microenvironment in dystrophic mice, in terms of immunofluorescence visualization, cytometric characterization of local cell populations, and cytokine expression. **Chapter 4** describes work characterizing human pluripotent stem cell derived skeletal muscle myoblasts and the application of the hydrogel to skeletal muscle cell therapy. Finally, **Chapter 5** presents the conclusion of this work and describes potential future experimental directions for this project.

## Duchenne Muscular Dystrophy (DMD)

Skeletal muscle disorders pose a significant public health burden, decreasing the quality of life of hundreds of thousands of patients worldwide [1]. The most common of these disorders is Duchenne Muscular Dystrophy (DMD), an X-linked recessive disease which affects approximately 1:5000 boys annually [2]. Due to mutations in the dystrophin gene, DMD patients have a complete absence of the dystrophin protein, which has key structural and signaling roles [3]. Without dystrophin, skeletal muscle undergoes a constant cycle of degeneration and regeneration, ultimately leading to replacement with fat and fibrotic tissue [4]. Depending upon genetic and environmental factors and standard of care, DMD patients generally lose the ability to ambulate as children, progressing to loss of upper limb function, and death by early adulthood due to cardiomyopathy and/or respiratory failure [4].

Dystrophin is one of the largest genes in the human body, consisting of 79 exons and 8 promoters [5] encoding a 427 kDa protein [6] that links the skeletal muscle sarcolemma to the underlying extracellular matrix through an N-terminal actin-binding domain, a cysteine-rich sarcoglycan-binding domain, and a C-terminal dystroglycan binding domain, all linked with a rod domain [7]. A variety of mutations can occur within the dystrophin gene, including missense [8] and nonsense [9] mutations; roughly 60% of mutations in DMD occur between exons 45-55 [10] and all have the potential to severely compromise the concentration and overall function of dystrophin. The dystrophin linkage is key to maintaining the complex architecture of skeletal muscle and

its ability to transduce force; absence or malfunction of dystrophin leads to a loss of stability between skeletal muscle and basal lamina, resulting in breakdown of components of the dystrophin glycoprotein complex, mis-localization of key proteins such as neuronal nitric oxide synthase, and compromise of the integrity of the sarcolemmal membrane [7], ultimately leading to ineffective skeletal muscle repair [4].

## Treatments and Therapies for DMD

Duchenne patients are typically maintained on corticosteroids such as prednisone [11] and the recently-approved deflazacort [12] whose mechanism of action in this disease is not entirely understood but likely results in modulation of local inflammation. However, as of 2017 two therapies to promote restoration of Dystrophin have received regulatory approval. Restoring even low levels of Dystrophin has the potential to confer clinical benefit, recapitulating the symptomatic profile of Becker Muscular Dystrophy, a less severe disease characterized by reduction of functional dystrophin but maintenance of some dystrophin function [13]. Ataluren, a compound designed to promote read-through of premature stop codons [14] caused by nonsense mutations in the dystrophin gene, was approved by the EMA [15] despite a lack of consensus over the efficacy of the drug as determined by uncertainty over the use of luminescence-based assays to measure its effectiveness [16]. Eteplirsen, an agent designed to promote exon 51 skipping and restore the reading frame of dystrophin [17], was also approved by the FDA [18] for use in DMD patients [19]. Despite the approval of these therapies, they appear to provide only a small benefit and are far from a cure [20].

Several other therapies for DMD are currently in various stages of development [20]. Dissociative immunomodulators such as VPB15 stabilize the sarcolemmal membrane and mediate inhibition of NF-κB without nonspecific immunosuppression, ameliorating DMD symptoms [21]. Several evaluated compounds upregulate the expression of compensatory proteins such as utrophin and biglycan that confer membrane-stabilizing functions. One modulator of utrophin, an autosomal analog of Dystrophin which maintains similar functions and can mediate disease severity in animal models of DMD [22], has recently completed phase I clinical trials [23]. Recombinant human biglycan, an ECM protein which has been shown to recruit the dystrophin glycoprotein complex proteins dystrobrevin, syntrophin, and neuronal nitric oxide synthase [24] as well as utrophin [25] to the sarcolemmal membrane, is also approaching clinical evaluation.

Gene therapy approaches to replacing or editing non-functional Dystrophin have benefited from recent significant advances in molecular biology, particularly with the use of adeno-associated viral vectors (AAVs) [26]. Despite the 4.7 kb packaging limit of AAVs, micro- and mini- Dystrophin constructs [27] with truncated rod domains but functional N- and C- termini can be delivered via AAVs to treat dystrophic mice [28]. Micro-dystrophin therapies are currently undergoing industrial development for eventual clinical application [29]. Alternative strategies utilize AAV-mediated delivery of the CRISPR-Cas9 genome editing system, a highly specific prokaryote-derived mechanism that can readily edit genomic DNA [30, 31]. Several groups have utilized this system to treat dystrophic mouse muscle [32, 33] and local muscle progenitor cells [34],

and utilized targeting vectors for muscle-specific delivery [35]. In addition to virally mediated gene editing and replacement, one additional strategy to replace Dystrophin has undergone significant development– cellular therapies.

## Cellular Therapies in DMD

Young, healthy skeletal muscle has an enormous capacity for regeneration from resident and circulating myogenic precursor cells [36]. The primary progenitor population consists of Pax7+/MyoD- satellite cells (SCs), which are located between the basal lamina and the sarcolemma of individual muscle fibers. These cells remain quiescent until stimulated to divide by cytokines or growth factors released during muscle injury [37]. Satellite cells divide asymmetrically, with one daughter cell repopulating the SC niche and the other undergoing either myogenic differentiation (expressing MyoD, Myf5, myogenin, and MRF4), or transdifferentiating into adipocyte or fibroblast lineages in ineffective regeneration [38, 39].

Cell based therapies, which involve transplanting healthy skeletal muscle progenitor cells into diseased muscle, are widely considered as a potential treatment for DMD. Preclinical trials have demonstrated that transplanted muscle progenitor cells integrate with existing muscle, restoring the dystrophin protein in dystrophic mice [40] and dogs [41]. Notably, an alternative strategy involving the transplantation of bone marrow derived stem cells has also been used to restore dystrophin in dystrophic mice [42]. Dystrophin-deficient muscle progenitor cells derived from induced pluripotent stem

cells corrected *ex vivo* via micro-utrophin delivery [43] or CRISPR-Cas9 editing [44] have also been used to restore Dystrophin *in vivo*. Consequently, several cell types have been tested in various clinical trials, ranging from donor myoblasts from a father into affected progeny [45] to vessel-associated mesoangioblasts [46]. However, these trials have all failed to produce clinically significant outcomes [47]. The majority of transplanted muscle progenitor cells do not survive transplantation, and those that do are introduced into a fibrotic environment that inhibits their proper differentiation, integration, and maturation into myofibers [47].

## Role of Myostatin Inhibition in DMD

One class of compounds that has undergone significant development includes inhibitors of myostatin, an endogenous TGF-β family member that negatively regulates muscle regeneration [48, 49]**.** Genetic depletion or postnatal pharmacological inhibition of myostatin can lead to increased muscle growth [50, 51]**.** This phenomenon, which was first observed in mice, was confirmed in multiple species including humans, specifically in a hypermuscular child with a homozygous myostatin mutation whose Olympic sprinter mother also presented with a heterozygous myostatin mutation. Muscle growth has been observed with various pharmacological inhibitors of myostatin in healthy human subjects [51]. Blockade of myostatin results in faster regeneration of skeletal muscle and reduced fibrosis in mouse models of acute and chronic muscle injury [52]. Additionally, the Wagner lab has worked extensively with ActRIIB-Fc, a soluble form of activin receptor IIB conjugated to an Fc immunoglobulin domain, which binds free

myostatin and other activin proteins. ActRIIB-Fc not only enhances myoblast proliferation and differentiation, but also inhibits fibroblast proliferation and collagen production [53]. Fibrosis of muscle is counterproductive to muscle regeneration and can be partially reversed by treatment with ActRIIB-Fc [54].

Despite these promising pre-clinical results with ActRIIB-Fc, clinical trials evaluating the systemic delivery of similar soluble activin receptors were terminated due to unacceptable side effects which were determined to be off-target effects of the drug [55]. However, several other myostatin inhibitors have reached clinical stages and two are currently undergoing Phase 2 clinical evaluation for the treatment of DMD [20]. One of these compounds is a humanized [56] version of RK35, a highly potent and specific monoclonal neutralizing antibody against myostatin [57]. Although the effects of myostatin and its inhibition on skeletal muscle hypertrophy and fibrosis have been extensively characterized, relatively little is known about how these factors affect the immune microenvironment in skeletal muscle.

## Skeletal Muscle and the Immune System

The complex cellular and signaling machinery of the immune system has, in addition to maintaining host defense against pathogens, been shown to play a significant role in the repair and regeneration of skeletal muscle [58]. Macrophages, which can adopt a variety of phenotypes, can exert numerous effects on skeletal muscle [59]. M1 macrophages, which infiltrate immediately following neutrophils in the earliest stages of muscle repair,

secrete IGF-1 which promotes the proliferation of local muscle progenitor cells [60]. Pro-inflammatory cytokines upregulated during this phase not only perpetuate local inflammation, but also directly influence myogenesis. IFN-Y signaling upregulates the class II transactivator CIITA, which directly binds and inhibits myogenin [61] and other myogenic factors [62]. TNF signaling upregulates the histone methyltransferase EZH2, leading to epigenetic silencing of Pax7 [63] and Notch1 [64].

Switching from the generally proinflammatory M1 phenotype to the generally proregenerative M2 phenotype is closely associated with downregulation of the cell surface marker CD86. This phenomenon is notably mediated by IL-10 released from $Foxp3^{+}$ regulatory T cells [65]. The transition to the M2 phenotype eventually leads to the induction of IL-4 signaling and expression of the cell surface markers Fizz1 CD206 [59]. M2 macrophages also facilitate phagocytosis and clearance of dead muscle fibers and other apoptotic cells such as neutrophils, Inhibiting the pro-inflammatory TNF and promoting TGF-B, which is key to secretion of ECM required for long-term repair [66, 67]. Additionally at this stage, one group demonstrated that local eosinophils secrete IL-33, potentially signaling local fibro-adipo progenitor cells (FAPs) to adopt a phenotype that promotes debris clearance and repair in cardiotoxin-injured mice, while also inhibiting their fatty, degenerative phenotype [68]. In conditions of chronic injury or disease these mechanisms can go awry, leading to pathological inflammation and fibrosis that can impede normal myogenesis [58]. This lends credence to the concept of targeting the immune system to resolve pathogenic inflammation in DMD [69].

## Biomaterials and Regenerative Medicine in Skeletal Muscle

To promote skeletal muscle regeneration, recent advances in the fields of tissue engineering and regenerative medicine have greatly expanded the use of biomaterial scaffolds in a number of applications ranging from volumetric repair and delivery of cells and growth factors to skeletal muscle [70, 71] to 3D-printed artificial muscle constructs [72]. Encouraging results have been reported using small intestinal submucosal scaffolds with endothelial cells, murine myoblasts and foreskin fibroblasts [73], and an injectable polyethylene glycol-fibrinogen hydrogel with human mesoangioblasts [74, 75]. One group has utilized hydrogels to deliver VEGF and IGF-1 in a model of ischemia [6].

Several studies have been reported using decellularized skeletal muscle extracellular matrix, created by removing cellular and nuclear material while retaining pro-regenerative growth factors. This material has been utilized in numerous applications including skeletal [76] and cardiac muscle [77], and has been used to treat volumetric muscle loss [78]. Notably, the field of biomaterials-mediated regenerative immunology has characterized the role of these materials in modulating the immune system to induce pro-regenerative outcomes [79], including the use of extracellular matrix scaffolds to promote CD206 macrophage polarization [80] and type 2 immune signaling [81], facilitating myogenesis. These biomaterials could potentially be utilized towards the development of injectable hydrogels [82] that have the capability to deliver growth factors [70] and create a pro-regenerative immune microenvironment that can be characterized to determine the effects of the material on surrounding tissue [83].

## Overall Summary

Here we utilize an injectable biomaterial composed of hyaluronic acid (HA), a glycosaminoglycan upregulated during muscle hypertrophy [84], and decellularized porcine skeletal muscle extracellular matrix, which has demonstrated considerable utility in previous regenerative medicine applications [78]. HA is conjugated to *N*-hydroxysuccinimide [85], allowing it to readily form a cytocompatible hydrogel at physiological temperatures *in vitro*. The hydrogel is injectable and biodegradable, and promotes the delivery of myostatin inhibitors [57] *in vivo*.

Additionally, injection of hydrogel is associated with a shift in macrophage polarization away from CD86 and towards CD206 expression in both wild type and dystrophic mice, as well as the elevated expression of anti-inflammatory cytokines. When combined with a neutralizing antibody against myostatin, the hydrogel synergistically promotes the induction of regulatory T cells in the local immune microenvironment, revealing potentially novel insights into the interplay between the immune system, myostatin inhibition, and the host response to biomaterials. Finally, the hydrogel also promotes the viability and myogenic capacity of transplanted hESC derived skeletal muscle myoblasts [86], leading to some observed restoration of the dystrophin protein in dystrophic mice. By utilizing biomaterials to create a pro-regenerative environment, this study represents a novel approach to the treatment of Duchenne Muscular Dystrophy.

# Chapter 2: Fabrication and Characterization of Skeletal Muscle Hydrogel

## Abstract

A number of biomaterials have been developed for tissue engineering and regenerative medicine in various applications, ranging from bone and cartilage to skeletal muscle. Here we describe the preparation of an injectable biomaterial, known as a hydrogel, utilized throughout this study. The hydrogel consists of hyaluronic acid (HA) conjugated to *N*-hydroxysuccinimide (NHS), and decellularized skeletal muscle extracellular matrix (dSKM-ECM). These materials were combined to form a cytocompatible hydrogel *in vitro*, and determined to be injectable and biodegradable *in vivo*. Additionally, the hydrogel promoted the controlled release of myostatin inhibitors *in vitro,* and increased their bioactivity *in vivo*. **Chapter 2** outlines the fabrication and characterization of an injectable, multifunctional biomaterial with potential regenerative applications in skeletal muscle.

## Introduction

Hydrogels, defined as networks of "water-insoluble crosslinked hydrophilic polymers" [82], have been adopted by the field of tissue engineering for several applications in skeletal muscle, ranging from culturing muscle progenitor cells [87] to growth factor delivery [88] and cell delivery [74, 89, 90]. A number of materials can be used to create hydrogels, including hyaluronic acid, a glycosaminoglycan upregulated during skeletal muscle hypertrophy [84] that has been used as a hydrogel in cardiac tissue applications to deliver cardiomyocytes [85], as well as decellularized extracellular matrix, which has been used alone to form hydrogels that repair cardiac [91] and skeletal [92] muscle.

Although myostatin inhibitors have demonstrated efficacy in ameliorating symptoms in an animal model of DMD [48], systemic administration of one soluble activin receptor during clinical trials led to telangiectasia and epistaxis, leading to termination of the trial [55]. In order to promote site-specific myostatin inhibition in conjunction with the longer-term goal of creating a microenvironment to promote muscle regeneration, we developed a hyaluronic acid / extracellular matrix hydrogel designed to be injectable, cytocompatible *in vitro*, and biocompatible *in vivo*. Functionality of the hydrogel as a drug delivery vehicle was tested utilizing RK35, a potent anti-myostatin antibody [57], as a candidate compound.

## Materials and Methods

*HA-NHS Synthesis*

Hyaluronic acid functionalization with NHS (HA-NHS) was performed as described previously [85]. Briefly, 10% (w/v) sodium hyaluronate (MW 13-16 kDa, LifeCore Biomedical) was reacted with 67% N-(3-Dimethylaminopropyl)-N'-ethylcarbodiimide (EDC, Sigma) and N-hydroxysuccinimide (NHS, Sigma) in phosphate buffered saline (Gibco) at 37°C for 10 minutes. The resulting mixture was then frozen at -80°C for 1 hour, then precipitated using 100% ethanol pre-cooled to -20°C. Precipitate was centrifuged, washed with -20°C 100% ethanol 9 times, then dried under high vacuum overnight. Functionalization was confirmed by hydroxamate assay [93].

*Skeletal Muscle ECM Processing*

Skeletal muscle extracellular matrix (M-ECM) was prepared in the same manner as previously described [81]. Yorkshire porcine hindlimb skeletal muscle (Wagner Meats) was trimmed of fat and connective tissue, minced using a knife mill (Retsch) into pieces no larger than 5 mm, then rinsed with distilled water to remove blood and loose particulates. The tissue was then incubated with 3% peracetic acid (Sigma) for 1 hour under constant agitation, followed by replacement with fresh acid solution and an additional 3 hours of agitation at 37°C. Sample was re-equilibrated to neutral pH with several rinses of distilled water and verified with pH indicator strips (Macherey-Nagel), then transferred to 1% Triton X-100 (Sigma) + 2 mM sodium EDTA (Sigma) solution on a room temperature stir plate at 400 rpm for 3 days, changing the solution daily. The

sample was rinsed with distilled water until no bubbles formed from agitation, indicating complete removal of the Triton/EDTA solution, then transferred to 600 units/mL DNAse I (Roche) + 10 mM magnesium chloride (J.T. Baker) + 10% Antifungal-Antimycotic (Gibco) for 1 day. Tissues were rinsed with distilled water, frozen at -80°C overnight, then lyophilized for three days. A sample of the resulting dried particulate was fixed in formalin, embedded with paraffin, and sections were taken and stained with Hematoxylin and Eosin (Sigma) to verify proper decellularization. The remaining particulate was pulverized into a powder with a SPEX SamplePrep Freezer/Mill (SPEX CertiPrep) and stored at -20°C prior to use. Phenol chloroform extraction was used to isolate DNA and confirm endogenous DNA degradation using gel electrophoresis.

*Rheological Testing*

An ARES G2 Rheometer (TA Instruments) with a solvent trap plate, Peltier solvent trap, and evaporation blocker were used in the mechanical characterization of the material. All tests were performed at 37°C. Gelation testing was performed on 1 mL samples of freshly prepared HA-NHS (15 mg/mL), M-ECM (45 mg/mL), or 6% HA-NHS:M-ECM 1:3 hydrogel. Gelation test parameters were determined as described previously [94] with frequency at 2.0 Hz and oscillation strain at 5.0%; storage and loss moduli were observed over the course of 250 minutes. Data were analyzed via ordinary one-way ANOVA using Tukey's multiple comparisons test in Prism (Graphpad).

*In vitro Cytocompatibility Assay*

In order to evaluate the cytocompatibility of the hydrogel, $0.5x10^6$ LHCN-LUC7 immortalized human myoblasts [95] were combined with 45 mg/mL M-ECM in sterile phosphate-buffered saline (PBS), then combined with 15 mg/mL HA-NHS in sterile PBS, yielding a final concentration of $0.5x10^6$ cells / 1 mL 6% w/v HA-NHS:M-ECM 1:3 hydrogel. Cell-laden hydrogels were added to the wells of a 24-well plate, incubated at 37°C for 50 minutes, then covered with 1 mL human myoblast medium (Medium 199:DMEM 4:1 + S0% fetal bovine serum + 2% penicillin / streptomycin + 0.02 M HEPES + 0.03 µg/mL $ZnSO_4$ + 1.4 µg/mL Vitamin B12 + 0.055 µg/mL Dexamethasone + 2.5 ng/mL HGF + 10 ng/mL bFGF). Cells were allowed to grow for four days, and then viability was determined using a Live/DEAD Assay Kit (Thermo Fisher). 2 sets of live and dead 10x channel images from n=4 100 µL gels were taken with an EVOS FL microscope (Thermo Fisher), live and dead cells present in each field were counted. Counts were used to calculate the percentage of live and dead cells, which were compared with a two-way ANOVA using Sidak's multiple comparisons test in Prism (Graphpad).

*In vivo Degradation Assay*

6-week old female wild-type C57BL/6 mice (Jackson Laboratories) were anesthetized under constant isoflurane and their hind limbs were shaved. Each limb was restrained and a 1 cm incision was made above the tibialis anterior muscle to expose the fascia. 50 µL 6% HA-NHS:M-ECM 1:3 hydrogel was injected into the subfascial space of the tibialis anterior with a 1 mL tuberculin syringe (BD) fitted with a 22G needle (Exel). Both legs

were injected for each mouse, and wounds were closed with surgical staples (Roboz). n=2 mice were harvested at 7, 14, and 21 days post-injection, flash frozen with chilled isopentane, serially cryosectioned, stained with Hematoxylin and Eosin, and visualized with an Axio Imager.M2 microscope (Zeiss). 10x H&E images with 10% overlap were taken across the entire section and stitched with Image Composite Editor (Microsoft).

*Myostatin Inhibitor In Vitro Release Kinetics*

6% w/v HA-NHA:M-ECM 1:3 hydrogels loaded with 66.67 ng RK35 [56, 57] (Pfizer) were added to a 48-well plate (Corning), allowed to gellate at 37°C for 30 minutes, then 500 µL collection medium (McCoy's 5A + 0.1% bovine serum albumin) was added to each well. Collection medium was harvested at 1, 3, and 5 days post-encapsulation, combined with recombinant myostatin (R&D Systems) at 10 ng/mL, then incubated at 37°C for 30 minutes. Each sample was analyzed via luminescence-based assay to measure myostatin bioactivity [96] on a Luminoskan Ascent luminometer (Fisher Scientific) and compared to a standard dilution curve of RK35 + myostatin to calculate the amount of RK35 present, which was then used to calculate % RK35 released. N=3 gels were harvested per timepoint, and n=3 technical replicates were analyzed per sample.

*Myostatin Inhibitor In Vivo Bioactivity*

In order to verify the validity of saline vs. hydrogel controls, 4 month old dystrophic male *mdx*-5$^{Cv}$ mice (Jackson Laboratories) were injected with 50 µL PBS or 50 µL 6% w/v HA-NHS:M-ECM 1:3 hydrogel into the subfascial space of the left TA. Each contralateral

limb was used as an internal negative control. 5 days after injection all TAs were weighed and compared via student's T test in Prism (Graphpad). In order to assess myostatin inhibitor activity, 2 month old dystrophic male *mdx*-$5^{Cv}$ mice (Jackson Laboratories) were injected with 50 µL PBS, 50 µL PBS + 10.75 µg RK35, or 50 µL 6% w/v HA-NHS:M-ECM 1:3 hydrogel + 10.75 µg RK35 (n=5 per group) into the subfascial space of the left TA muscle. Each contralateral limb was used as an internal negative control.

5 days after injection all TAs were weighed and compared via one-way ANOVA with Tukey's multiple comparisons test in Prism (Graphpad). RK35-injected TA muscles were flash frozen in chilled isopentane and cryosectioned. Two 7 µm sections from regions at least 300 µm apart were analyzed from each muscle. Slides were fixed in cold methanol, blocked with 20% normal goat serum in 2% bovine serum albumin (BSA), then incubated overnight with primary antibody against embryonic myosin (DSHB F1.652-s, mouse IgG1 anti-MYH3). Primary antibody was removed, then slides were incubated with Goat Anti-Mouse Alexa Fluor 647 (Thermo Fisher) secondary antibody at 1:500 in 20% NGS + 2% BSA for 1 hour at room temperature. Slides were rinsed in PBS, mounted in Vectashield + DAPI (Vector), and 20x immunofluorescence mosaics were taken with an Axio Imager.M2 microscope (Zeiss). Images were analyzed in ImageJ to determine overall cross-sectional area and embryonic myosin heavy chain signal in terms of integrated density. Slides stained without primary antibodies were used as a negative control, and the strongest eMHC signal field from one hydrogel+RK35 injected muscle was used as a positive control to set exposure constant at 13 ms.

## Results

*Hydrogel synthesis and characterization.*

Hyaluronic acid was combined with *N*-hydroxysuccinimide (NHS) and reacted with carbodiimide, creating HA-NHS via formation of sulfo-NHS-esters from locally available carboxylic acid groups **(Figure 2.1A)**. A hydroxamate assay was performed to verify conjugation, revealing that 22.41% of the carboxylic acid groups present on HA formed sulfo-NHS-esters (data not shown). Porcine skeletal muscle tissue was separated from fatty and connective tissue, rinsed, minced, and subjected to a standard processing protocol [81] to yield decellularized skeletal muscle extracellular matrix (M-ECM) **(Figure 2.1B)**. Decellularization was verified by extracting DNA from the processed ECM sample and comparing it to a standard DNA ladder, revealing that only small fragments of nuclear material remained (**Figure 2.1C).** Further characterization was performed by histological assessment of the processed ECM material, which revealed a lack of visibly apparent cellular and nuclear material after staining for hematoxylin and eosin **(Figure 2.1C).** 30 mg/mL HA-NHS and 90 mg/mL M-ECM were combined to yield a final 6% w/v HA-NHS:M-ECM 1:3 (HA-ECM) composite which formed a hydrogel at physiological temperatures *in vitro.* Time sweep rheology [94] revealed a steady increase and eventual plateau of the hydrogel storage modulus not observed with either component alone **(Figure 2.2).**

*Hydrogel cytocompatibility and biocompatibility.*

In order to assess cytocompatibility, immortalized human myoblasts [95] were combined with the hydrogel and seeded *in vitro*. Cell viability was assessed at 4 days post-encapsulation via Live/DEAD visualization of two fields in four gels **(Figure 2.3A, Supplementary Figure 2.1)**, and almost no dead cells were observed **(Figure 2.3B).** The hydrogel was injected into the subfascial space above the tibialis anterior (TA) muscles of wild-type C57BL/6 mice in order to assess its biocompatibility *in vivo*. Labeling the hydrogel with blue dye allowed for visualization of the hydrogel spreading across the entire intertendinous space of the TA when injected subfascially **(Figure 2.4A).** Harvest and histological evaluation of hydrogel-injected muscles revealed that the hydrogel degrades over the course of 21 days *in vivo* with no long-standing myotoxic effects (**Figure 2.4B).**

*Hydrogel-mediated delivery of cells and myostatin inhibitors in vivo.*

Since biomaterials have demonstrated several applications in skeletal muscle, we assessed the multifunctionality of the hydrogel by determining its ability to deliver growth factors *in vivo*. Growth factor delivery was assessed with hydrogels containing the anti-myostatin antibody RK35 [57] both *in vitro* and *in* vivo **(Figure 2.5).** A luminescence-based assay [96] was used to generate a standard curve of myostatin inhibition **(Supplementary Figure 2.2)**, which was then used to quantify the amount of RK35 present in supernatant samples taken from RK35-laden hydrogels *in vitro*, allowing for determination of the percentage of RK35 release over time. Controlled release of

RK35 from the hydrogel was observed over the course of five days, peaking at 20% release of the encapsulated compound **(Figure 2.5A).** *Mdx*-$5^{Cv}$ mice, which serve as a model of Duchenne Muscular Dystrophy [97], were used to evaluate RK35 bioactivity when delivered to uninjured TA muscles via saline or hydrogel *in vivo* **(Figure 2.5B-D, Supplementary Figures 2.3-2.4).** Saline-injected muscles were demonstrated to have similar weights to hydrogel-injected muscles, and thus were deemed appropriate as a treatment-free control **(Supplementary Figure 2.3).** RK35-hydrogel injected muscles showed greater weight and overall cross-sectional area compared to muscles injected with RK35 in saline **(Figure 2.5 B-C).** Immunofluorescence labeling of embryonic myosin heavy chain (eMHC), a marker of regeneration, revealed greater eMHC signal density in muscles injected with RK35 and hydrogel compared to saline **(Figure 2.5D, Supplementary Figure 2.4).**

## Discussion

Given the previously demonstrated utility of biomaterial hydrogels in regenerative medicine applications [82] and drug delivery [98], we sought to apply these principles to the treatment of DMD. Here, we have utilized the techniques of carbodiimide chemistry and tissue decellularization to create a hyaluronic acid / ECM composite hydrogel. The gel was demonstrated to be cytocompatible with immortalized human skeletal muscle myoblasts **(Figure 2.3)**, injectable **(Figure 2.4A)**, and biocompatible **(Figure 2.4B).** Additionally, the hydrogel facilitated the controlled release of the myostatin inhibitor RK35 *in vitro* **(Figure 2.5A)** and promoted its bioactivity *in vivo* **(Figure 2.5B)**.

Some limitations do arise in the preparation of each of the hydrogel component materials. Even though only 22.41% of the available carboxyl groups present on the hyaluronic acid backbone were reacted, this is in line with previous results describing this chemical conjugation to chondroitin sulfate [93] and actually exceeds the 16.67% conjugation previously observed with hyaluronic acid [85]. Despite extensive processing of porcine-derived skeletal muscle, some nuclear material remained **(Figure 2.1C).** Although it may not be possible to remove all exogenous nuclear material, the standard DNAse I treatment is sufficient to remove large fragments, leaving only small traces of nuclear material that are relatively non-immunogenic.

Rheology **(Figure 2.2)** revealed that gelation of the material composite takes a relatively long time *in vitro*, and the low terminal storage modulus indicates that this is a relatively weak gel. Skeletal muscle itself adopts an elastic modulus of 13-18 kPa [70], roughly two orders of magnitude stronger than this material, which exhibited a peak storage modulus of approximately 30 Pa. However, the primary design factor of the hydrogel was not necessarily structural repair but implantation, creating a material that modulates the local environment to support the effective regeneration *in vivo*, complemented by localized delivery of the myostatin inhibitor. The fact that HA-NHS and decellularized skeletal muscle ECM were unable to individually exhibit gelation properties similar to that of the composite material demonstrates that some crosslinking does occur between conjugated *N*-hydroxysuccinimide groups on the HA backbone and locally available primary amines in the ECM.

The increased viscosity of this material, as well as the opportunity for NHS groups to react with primary amines in local tissue, facilitates the retention of the hydrogel *in situ*, potentially contributing to the increased bioactivity of the myostatin inhibitor RK35 *in vivo* **(Figure 2.5 B-D).** Because the hydrogel itself does not swell appreciably **(Figure 2.2)**, nor does it significantly contribute to the weight of injected muscles *in vivo* **(Supplementary Figure 2.3)**, the observed increase in muscle weights and overall cross-sectional areas was most likely due to the hypertrophic effects of myostatin inhibition associated with RK35 **(Figure 2.5B-C).** This was confirmed upon observation of the increased staining density of embryonic myosin heavy chain **(Figure 2.5D).**

RK35 is a highly specific, direct inhibitor of myostatin [56, 57], contrasted with ActRIIB-Fc, a soluble activin receptor decoy which despite positive results *in vitro* has been previously tested and retracted from clinical trials due to side effects [55], presumably from off target effects on other activin signaling pathways. Although RK35 already has higher potency, specificity, and half-life compared to soluble activin receptors [56], targeted specific delivery to muscles most severely affected by DMD could still confer a number of benefits: further reduction of off-target effects, decreased overall concentrations of drug used to treat patients, and, in concert with the presence of pro-myogenic growth factors in the locally crosslinked decellularized skeletal muscle extracellular matrix, the creation of a pro-myogenic microenvironment that could have direct effects on any muscle progenitor cells transplanted with this hydrogel.

## Figures

**A.**

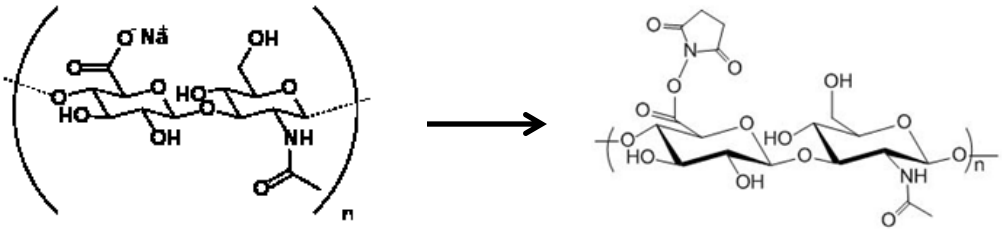

**B.**

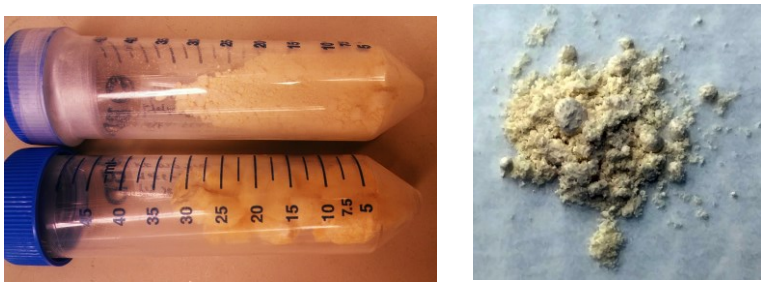

**C.**

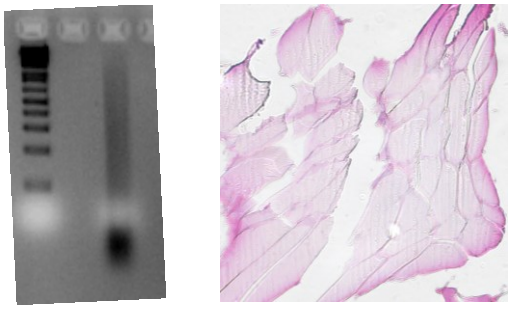

**Figure 2.1. Hydrogel components.** (A) Sodium hyaluronate (left) was reacted with *N*-hydroxysuccinimide to form hyaluronic acid succinimidyl succinate (HA-NHS) (right). Chemical structures taken from Wikipedia.com and www.creativepegworks.com. (B) Yorkshire porcine skeletal muscle was processed to yield decellularized skeletal muscle extracellular matrix (dSKM-ECM). (C) dSKM-ECM characterization. (Left) DNA electrophoresis gel confirms removal of major nuclear material. (Right) H&E image of processed skeletal muscle confirms removal of nuclear and cellular material.

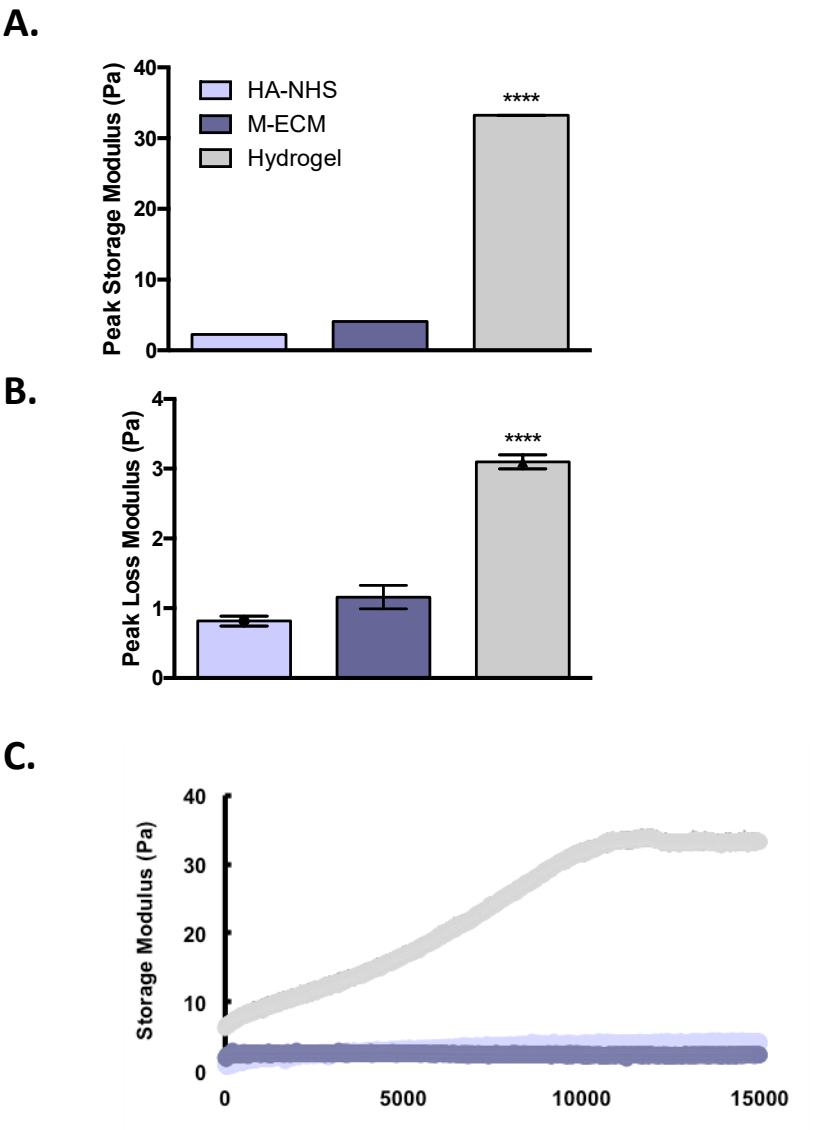


**Figure 2.2. Mechanical characterization of HA-ECM hydrogel.** Time sweep rheology of HA-NHS, M-ECM, and hydrogel over 250 minutes. Frequency = 2.0 Hz, oscillation strain = 5.0%. Peak storage (A) and loss moduli (B) shown in bar graphs, storage moduli shown in curve (C). Legend applies to all figures. N=3 samples per condition. Data represent means +/- SEM. Legend applies to all figures. **** $p < 0.0001$.

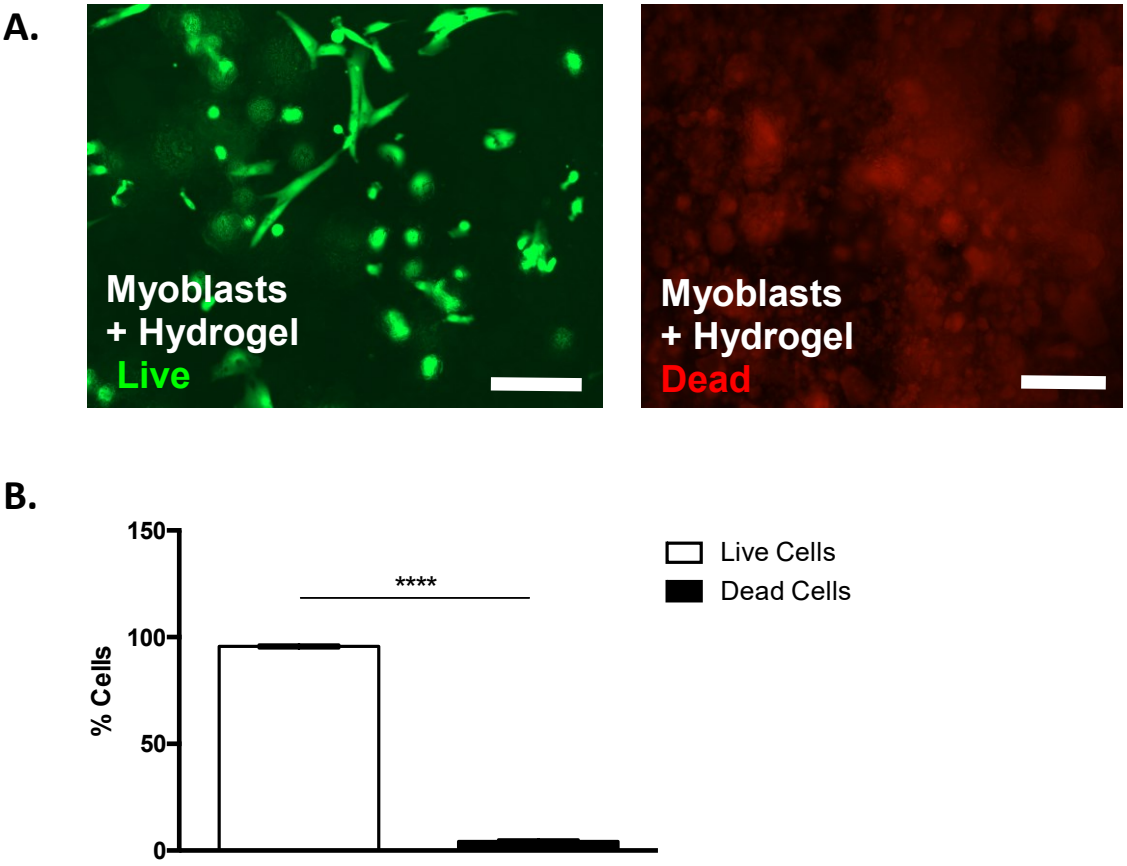


**Figure 2.3. Cytocompatibility of HA-ECM hydrogel.** 0.5x$10^6$ LHCN-LUC7 immortalized human myoblasts were seeded into hydrogels in vitro and assessed for cytocompatibility after 4 days. (A) Fluorescence images of live (green) and dead (red) immortalized human myoblasts at 4 days post-hydrogel encapsulation *in vitro*. Scale bars = 200 microns. (B) Quantification of observed live and dead cells from 2x sets of live/dead images from N=4 gels. All error bars represent means +/- SEM, **** = $p < 0.0001$.

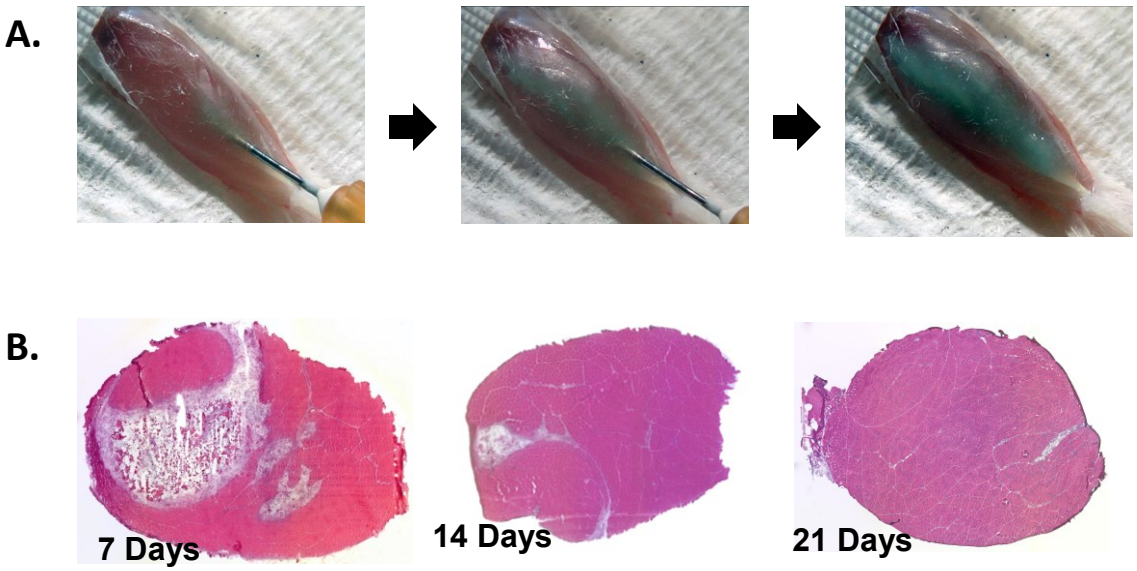


**Figure 2.4. Injectability and biocompatibility assessment of HA-ECM hydrogel.** (A) Subfascial injection of dye-labeled hydrogel (blue) into murine TA muscle spreads from tendon to tendon. (B) H&E mosaics of whole C57BL/6 WT TA muscles injected with hydrogel at 7, 14, 21 days post-injection.

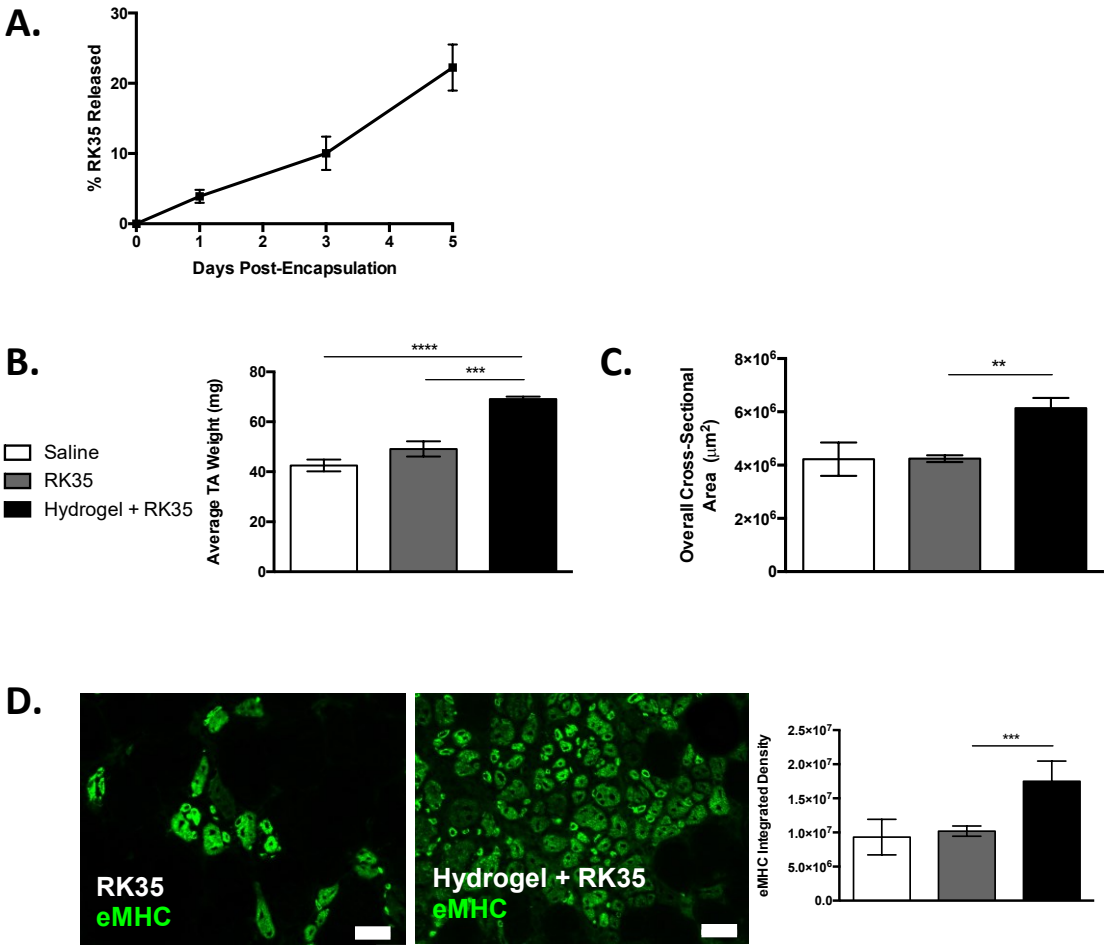


**Figure 2.5. HA-ECM hydrogel delivery of myostatin inhibitors in vitro and in vivo.** (A) Release kinetics of myostatin inhibitor (RK35) from hydrogels *in vitro*, quantified with a luminescence-based assay up to 5 days post-encapsulation. N=3 gels per timepoint. (B-D) Increased bioactivity of hydrogel-encapsulated RK35 at 5 days post-injection *in vivo*. (B) Average injected TA weights. (C) Average injected TA cross-sectional areas. (D) Immunofluorescence images and integrated density quantification of embryonic myosin heavy chain (green) in injected TAs. Scale bars = 50 microns. Saline n=2, RK35 and hydrogel+RK35 n=5. Legend applies to all figures. All error bars represent means +/- SEM. ** $p < 0.01$, *** $p < 0.001$, **** $p < 0.0001$.

## Supplementary Data

**Gel 1:**

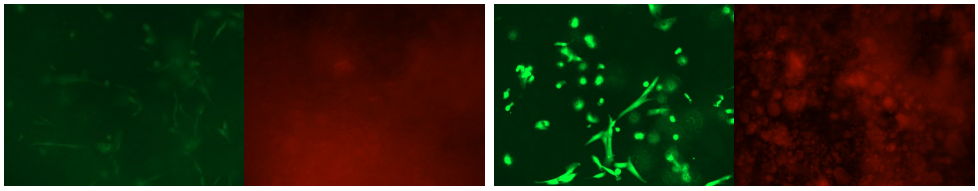

**Gel 2:**

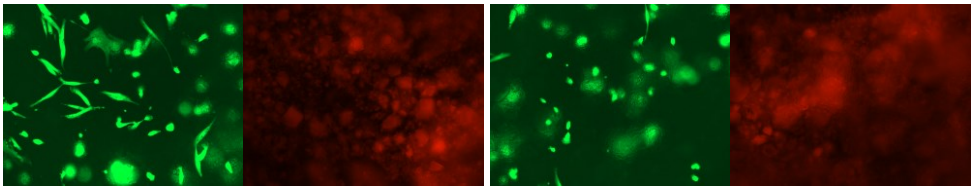

**Gel 3:**

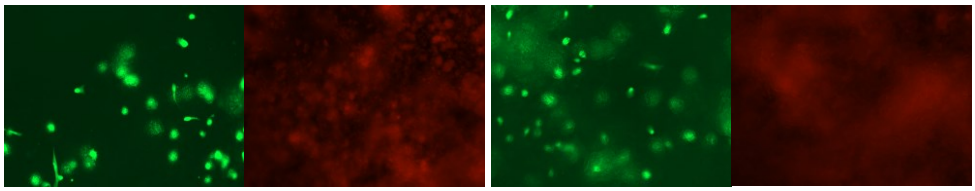

**Gel 4:**

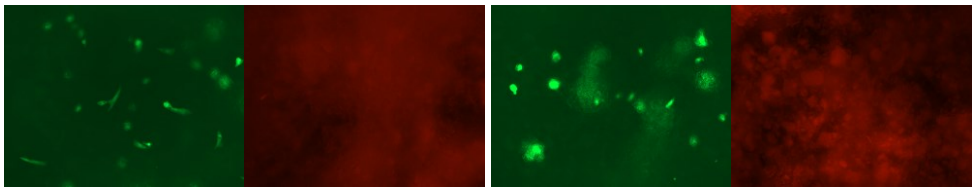

**Supplementary Figure 2.1. Representative images used to determine cell viability in hydrogel.** $0.5x10^6$ LHCN-LUC7 immortalized human myoblasts were seeded into hydrogels in vitro and assessed for cytocompatibility after 4 days. Fluorescence images of live (green) and dead (red) immortalized human myoblasts at 4 days post-hydrogel encapsulation *in vitro*. 2 live and dead fields were imaged from N=4 gels. All images taken at 10x.

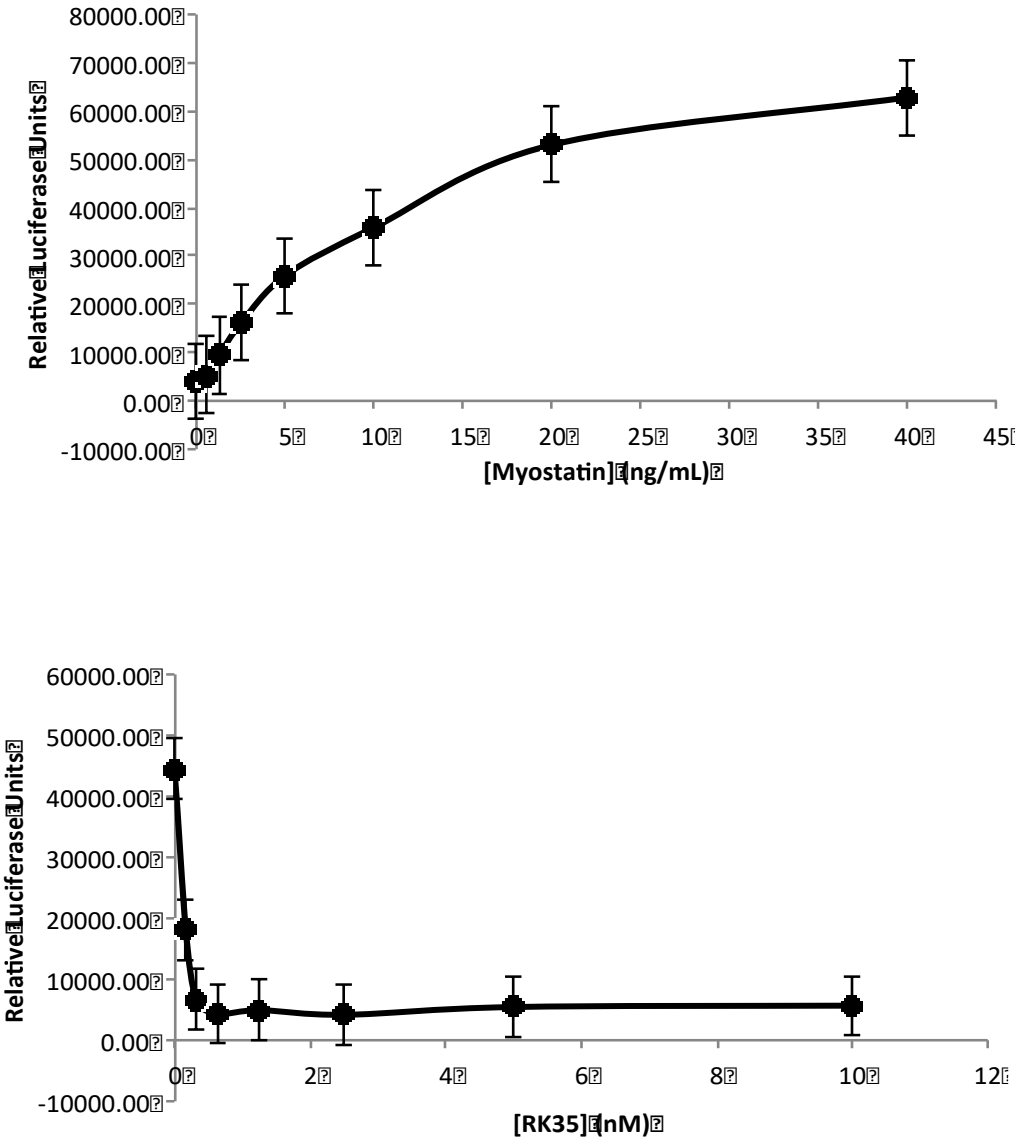


**Supplementary Figure 2.2. TA204 + myostatin response curve.** Serum-starved TA204 cells were treated with several concentrations of myostatin (160-0 ng/mL, top panel) or with 10 ng/mL myostatin and various concentrations of RK35 (0-10 nM, bottom panel). Response levels were determined by differential emission of luciferase. N=3 technical replicates per data point.

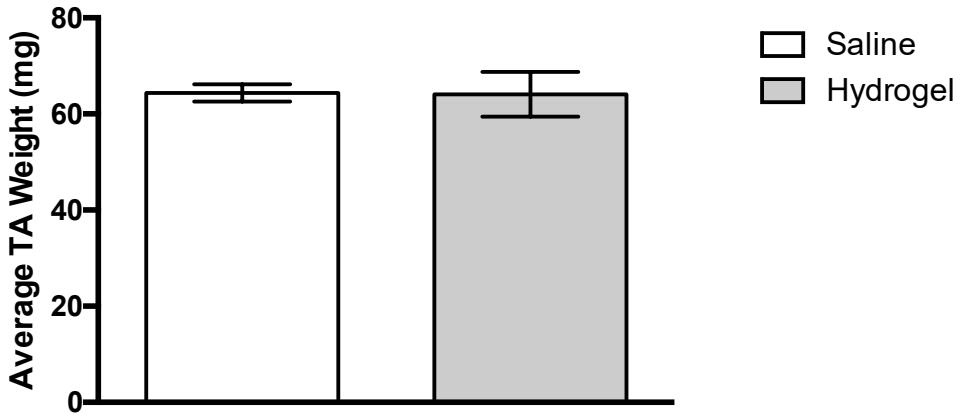


**Supplementary Figure 2.3. Saline and hydrogel-injected TAs used to verify controls.** N=5 TAs were injected with 50 µL PBS or hydrogel, harvested at 5 days post-injection, and weighed. TA weights were compared via student's T test in Prism (Graphpad).

# Chapter 3: Hydrogel-Mediated Effects on the Immune Microenvironment

## Abstract

Several studies have implicated the immune system as a significant mediator of skeletal muscle repair and regeneration, and extracellular matrix-based biomaterials have been shown to play a role in polarizing the immune microenvironment towards pro-myogenic outcomes. However, the study of the immune response to biomaterials has not been evaluated within the context of DMD. Towards this end, we have utilized a previously established method to characterize the overall immunological response to the HA-ECM hydrogel described in **Chapter 2.** The hydrogel promotes the infiltration of scaffold-associated macrophages and expression of anti-inflammatory cytokines in both wild type and dystrophic mice. Notably, combining the hydrogel and myostatin inhibitor Rk35 affects T cell polarization, and yields a substantial increase in $Foxp3^{+}$ regulatory T cells - an effect not observed with any individual component of the hydrogel or RK35 alone **Chapter 3** outlines the analysis of immune cell populations present around (and possibly influenced by the presence of) the hydrogel scaffold, known as the scaffold immune microenvironment, as well as the effects of the hydrogel on proximal systemic cytokine expression *in vivo*.

## Introduction

A number of recent studies [58] have explored the complex interplay between the processes of skeletal muscle repair and activation of the immune system, particularly within the context of DMD [69]. The population of immune cells and soluble factors such as cytokines form a distinct immune microenvironment that has direct effects on the process of myogenesis, ranging from effects on satellite cell proliferation and differentiation to normal versus pathological induction of fibrosis. This has been further studied within the context of the response to biomaterials in skeletal muscle. Previous work has demonstrated the presence of M2-like $CD206^+$ scaffold-associated macrophages [83] modulated by biomaterials in skeletal muscle that work with type 2 signaling through IL-4 and $CD4^+$ T-cells to promote regeneration [81].

Despite these advances, the immunological response to biomaterials has not been evaluated within the context of DMD, and the effects of myostatin inhibition on the dystrophic immune microenvironment are still unknown. Here, we evaluated the effects of the hydrogel described in **Chapter 2**, its individual components, and myostatin inhibitors on the immune microenvironment in wild type and dystrophic *mdx* mice. We used immunofluorescence and flow cytometry to characterize modulated cell populations, and qPCR to evaluate cytokine expression in local draining lymph nodes proximal to the injected biomaterial. Overall, we observed polarization towards a pro-regenerative immune microenvironment in the presence of the hydrogel and myostatin inhibitor in *mdx* mice.

## Materials and Methods

*Materials Implantation*

1 month old female WT C57BL/6 and dystrophic mdx-5$^{Cv}$ mice (Jackson Laboratories) were bilaterally injected with 50 µL PBS or 6% w/v HA-NHS:M-ECM 1:3 hydrogel. 2-5 month old male dystrophic mdx-5$^{Cv}$ mice (Jackson Laboratories) were bilaterally injected with 50 µL PBS, 30 mg/mL HA-NHS, 90 mg/mL M-ECM, 6% w/v HA-NHS:M-ECM 1:3 hydrogel, PBS + 10.75 µg RK35, or 6% w/v HA-NHS:M-ECM 1:3 hydrogel + 10.75 µg RK35. In all cases, mice were anesthetized with isoflurane and shaved prior to injection. Each limb was restrained and a 1 cm cutaneous incision was made above the tibialis anterior muscle to expose the fascia. All materials were injected into the subfascial space of the tibialis anterior (TA) muscle with a 1 mL tuberculin syringe (BD) fitted with a 22G needle (Exel). Both legs were injected for each mouse, and wounds were closed with surgical staples (Roboz). All animals were sacrificed at 1 week post-injection.

*Proximal Lymph Node Cytokine Analysis*

Upon harvest, inguinal lymph node pairs (n=4) were visually identified, isolated from each animal, and frozen. Lymph node pairs were then minced and homogenized in Trizol (Invitrogen). RNA was extracted from each sample with chloroform, and then isolated using an RNEasy Extraction Kit (Qiagen). RNA concentration for each sample was determined with a Nanodrop 2000 spectrophotometer (Thermo Scientific), and 1 µg RNA was used to produce cDNA using an iScript cDNA Synthesis Kit (Bio-Rad). qPCR was performed with PowerUP SYBR (Thermo Fisher) on a CFX Connect (Bio-Rad) with

primers diluted to 20 µm **(Table 3.1).** Data were analyzed as calibrated normalized relative quantities (CNRQ) over saline group for each genotype, and statistically compared via one-way ANOVA with Tukey's multiple comparisons test in qBase+ (Biogazelle). Graphs were rendered in Prism (Graphpad).

*Immune Characterization*

Upon harvest, both tibialis anterior (TA) muscles were harvested from each animal. N=4 animals from each group were used for FACS analysis, and n=1 spleen was processed and split for use in unstained, viability, single-color, and full-panel control samples. Samples were minced, then digested with Liberase TL (Roche) for 45 minutes or Liberase TM (Roche) with DNAse I (Roche) in RPMI-1640 medium (Gibco) for 30 minutes under constant agitation at 37°C. The resulting single-cell suspensions were filtered through a 100 micron filter (Fisher Scientific) and counted with a Countess II FL (Thermo Fisher) **(Supplementary Table 3.1).** All samples were treated with ACK lysing buffer (Quality Biological), subjected to cytokine stimulation, stained with FACS antibodies (BioLegend, Thermo Fisher, or BD) and viability dye (eBiosciences) **(Table 3.2-3.3),** fixed in Cytofix (BD), and analyzed with an LSR II or Fortessa (BD). Data were analyzed and gated **(Supplementary Figures 3.1, 3.4)** in FloJo (Treestar) or Diva (BD), population percentages were calculated in terms of %$CD45^+$ cells, then normalized to cell counts to yield absolute cell numbers. Overall mean fluorescence intensity (MFI) was also calculated for the fluorescent channels corresponding to CD86 and CD206 in each experiment as another overall determinant of macrophage polarization.

*Immunohistochemistry*

Upon harvest, both tibialis anterior (TA) muscles were harvested from n=1 animal from each group. Each TA was flash frozen in chilled isopentane and cryosectioned. Six 7 µm sections were stained per muscle from regions spread at least 150 µm apart. Immunofluorescence slides were fixed in cold methanol for 10 minutes, rinsed with PBS for 5 minutes, blocked with 20% normal goat serum (NGS) in 2% bovine serum albumin (BSA), then incubated with primary antibodies against F4/80 (BioLegend BM8, Rat IgG2a anti-mouse F4/80) and Fizz1 (Peprotech 500-P215, Rabbit Polyclonal anti-Mouse RELMβ) at 1:500 20% NGS + 2% BSA at 4°C overnight. Primary antibody was removed from sections, then incubated with Goat Anti-Rat Alexa Fluor 488 and Goat Anti-Mouse Alexa Fluor 647 secondary antibodies (Thermo Fisher) at 1:500 in 20% NGS + 2% BSA for 1 hour at room temperature. Slides were rinsed in PBS and mounted in Vectashield + DAPI (Vector). 20x immunofluorescence mosaics and 40x oil objective single extended focus images were taken with an Axio Imager.M2 microscope and rendered in Axiovision (Zeiss).

## Results

*Immunomodulatory effects of hydrogel in wild type and dystrophic mice.*

Potential immunomodulatory effects of the hydrogel were tested in comparison to saline in both wild-type C57BL/6 and dystrophic *mdx*-5$^{Cv}$ mice. Cryosections of injected TA muscles revealed the presence of F4/80$^{+}$Fizz1$^{+}$ macrophages in hydrogel-injected muscles, but not saline **(Figure 3.1).** Single-cell suspensions were obtained from each muscle and analyzed by FACS **(Supplementary Figure 3.1).** Macrophages (CD45$^{+}$CD11b$^{+}$F4/80$^{+}$MHCII$^{+}$) were prominent in all hydrogel-injected conditions **(Figure 3.2)** with significantly more CD206$^{+}$ macrophages found in hydrogel-injected wild type and dystrophic mice **(Figure 3.2C).** CD86$^{+}$CD206$^{+}$ macrophages were most prominent in saline-injected dystrophic mice. Analysis of mean fluorescence intensity (MFI) **(Supplementary Figure 3.3)** indicated reductions in CD86-associated fluorophore signal in hydrogel-injected mice compared to saline, which was significant in dystrophic mice. No significant differences were observed in CD206-associated fluorophore MFI between groups, but corresponding decreases in CD86-fluorophore signal indicate an overall polarization away from CD86 and towards CD206 in hydrogel-injected mice.

Inguinal lymph nodes, which are most proximal to injected muscles, showed significantly elevated expression of IL-4 in hydrogel-injected mice of both genotypes, but differences in IL-10 expression were only observed in wild-type mice **(Figure 3.3).**

*Effects of hydrogel and myostatin inhibitor on macrophage populations.*

In addition to the HA-ECM hydrogel, each of its individual components (HA-NHS, M-

ECM) was injected into aged *mdx*-5$^{Cv}$ mice to evaluate their immunomodulatory properties. Since the hydrogel demonstrated the ability to deliver RK35 *in vivo* **(Figure 2.5),** additional mice were injected with RK35 in saline and hydrogel. Immunofluorescence revealed F4/80$^{+}$Fizz1$^{+}$ macrophages in ECM, hydrogel, and hydrogel + RK35 mice **(Figure 3.4).** Cytometric analysis **(Figure 3.5)** revealed significantly reduced numbers of CD11b$^{+}$ cells in M-ECM and RK35 injected mice. **(Supplementary Figure 3.5), and** significantly greater percentages of CD86$^{+}$ (M1) and CD86$^{+}$CD206$^{+}$ macrophages in mice injected with HA-NHS. Hydrogel injected mice exhibited significantly more CD206$^{+}$ macrophages; co-delivery of RK35 with the hydrogel also induced the CD86$^{+}$CD206$^{+}$ population. MFI analysis revealed a shift in macrophage polarization towards CD86 in HA-NHS treated mice **(Supplementary Figure 3.3)**.

*Effects of hydrogel and myostatin inhibitor on T cell populations and cytokine signaling.* Mice injected with hydrogel + RK35 exhibited elevated levels of CD3$^{+}$ T cells compared to all other groups **(Supplementary Figure 3.5).** FACS revealed significantly greater numbers of CD4$^{+}$ cells **(Figure 3.6A)** and Foxp3$^{+}$ regulatory T cells **(Figure 3.6B)** in mice injected with both RK35 and hydrogel, more than any other group. Mice injected with hydrogel + RK35 also exhibited elevated levels of IL-17$^{+}$ T cells **(Supplementary Figure 3.5).** Inguinal lymph nodes showed elevated expression of IL-4 in ECM, hydrogel, and hydrogel+RK35 injected mice. No substantial differences were detected in IL-10, and a slight TNF-α increase was detected in hydrogel+RK35-injected mice **(Figure 3.7)**. No other significant differences were observed in IL-17, IL-6, IL-1β, IFN-ϒ, Arg1, or Retn1α.

## Discussion

This set of experiments represents the first evaluation of the effects of implanted biomaterials and myostatin inhibition on the skeletal muscle immune microenvironment in DMD. Immunofluorescence images of hydrogel-injected muscles revealed the presence of $CD206^+$ macrophages **(Figure 3.1, Figure 3.4)**, which was further confirmed with flow cytometry **(Figure 3.2, 3.5)**. Additionally, mice injected with the hydrogel demonstrated significantly elevated interleukin-4 expression in local draining lymph nodes **(Figure 3.3, 3.6)**. Finally, analysis of $CD3^+$ T cell populations via flow cytometry revealed significantly elevated numbers of $CD3^+$ T cells, $CD3^+CD4^+$ T helper cells, $CD3^+CD4^+Foxp3^+$ regulatory T cells, and IL-$17^+$ secreting T cells in mice injected with the myostatin inhibitor RK35 delivered via hydrogel **(Figure 3.5, Supplementary Figure 3.5)**.

The modulation of M2-like $CD11b^+F4/80^+CD11c^{+/-}CD206^{hi}CD86^+MHCII^+$ scaffold-associated macrophages by implanted biomaterials has been established previously [83], and their role alongside $CD4^+$ T cells in promoting regenerative outcomes in biomaterials-implanted mice is also well known [81]. Although there is significant potential for mechanisms of the immune system to go awry within the context of chronic injury or diseases such as DMD [58], macrophage polarization remained intact in dystrophic mice at one week post-injection **(Figure 3.1).** $Foxp3^+$ regulatory T cells, an immune cell population responsible for mediating overall immune responses and facilitating the transition of macrophages from the M1 to the M2 phenotype in skeletal muscle [58], have been previously targeted for upregulation in dystrophic *mdx* mice via

treatment with IL-2/anti-IL-2 complexes that specifically act on these cells, leading to consequent increases in IL-10, reduced expression of cyclooxygenase-2, and reduction of pathologic muscle inflammation and injury [99]. Here, we observed a substantial upregulation of $Foxp3^+$ regulatory T cells in mice injected with both hydrogel and the myostatin inhibitor RK35, a phenomenon not observed with RK35, the hydrogel, or any of the individual hydrogel components **(Figure 3.5).** This elevation of the regulatory T cell population was, however, insufficient to significantly increase expression of interleukin 10 in inguinal lymph nodes of dystrophic *mdx* mice **(Figure 3.6)**, as observed in comparable wild-type animals **(Figure 3.3).** Nonetheless, this synergistic upregulation observed with both hydrogel and myostatin inhibitor delivered together suggests the existence of a novel immunomodulatory function for this combination. Future studies with co-delivery of hydrogel and RK35 separately administered systemically, intramuscularly, or in other controlled release vehicles such as polymeric fibers or spheres could be used to determine whether this effect is simply due to the presence of RK35 in conjunction with hydrogel, or its localization and/or sustained release.

A great deal of work remains in determining the underlying mechanisms driving the pro-regenerative effect of the hydrogel and myostatin inhibitor. Given the complex temporal kinetics of immune-mediated regulation of muscle [58], characterization of the scaffold immune environment at shorter or longer timepoints may add an additional layer of understanding to the host response to this material. In addition to the extracellular matrix present in the hydrogel, hyaluronic acid also has complex, variable effects on the

immune system through direct interaction with RHAMM and CD44 [100] that may affect local immune responses to the material. Myostatin inhibition has previously been shown to ameliorate TNF-α-mediated rheumatoid arthritis in mice [101], but its effects on muscle immunology are still relatively unknown. Specific isolation and transcriptome characterization of isolated specific immune cell populations present could clarify the signaling mechanisms modulated in response to the hydrogel or RK35.

Additionally, some limitations are also present with the mouse model. Even though *mdx*-5$^{Cv}$ mice demonstrates profound defects compared to wild-type mice [97], hindlimb skeletal muscles are not as symptomatically severe as those of DMD patients, or even other muscles within the same animal, such as the diaphragm. Evaluation of these materials in dystrophic mice with or without myostatin inhibitor in more profoundly affected muscles such as the diaphragm, or in conjunction with injuries such as myotoxin, cryogenic, burn, or volumetric injury [102] may further elucidate the underlying mechanisms that shape the immune microenvironment in Duchenne Muscular Dystrophy. Comparative assessment of the hydrogel and myostatin inhibitor under healthy and injured conditions in both wild type and dystrophic mice could also potentially determine the effects of the immune environment and biomaterial on functional regeneration and repair, either through *ex vivo* physiologic assessment of individual muscles or whole-animal studies such as grip strength tests, hanging tests, rota-rod balance assessment, or endurance-based treadmill testing [103].

## Figures

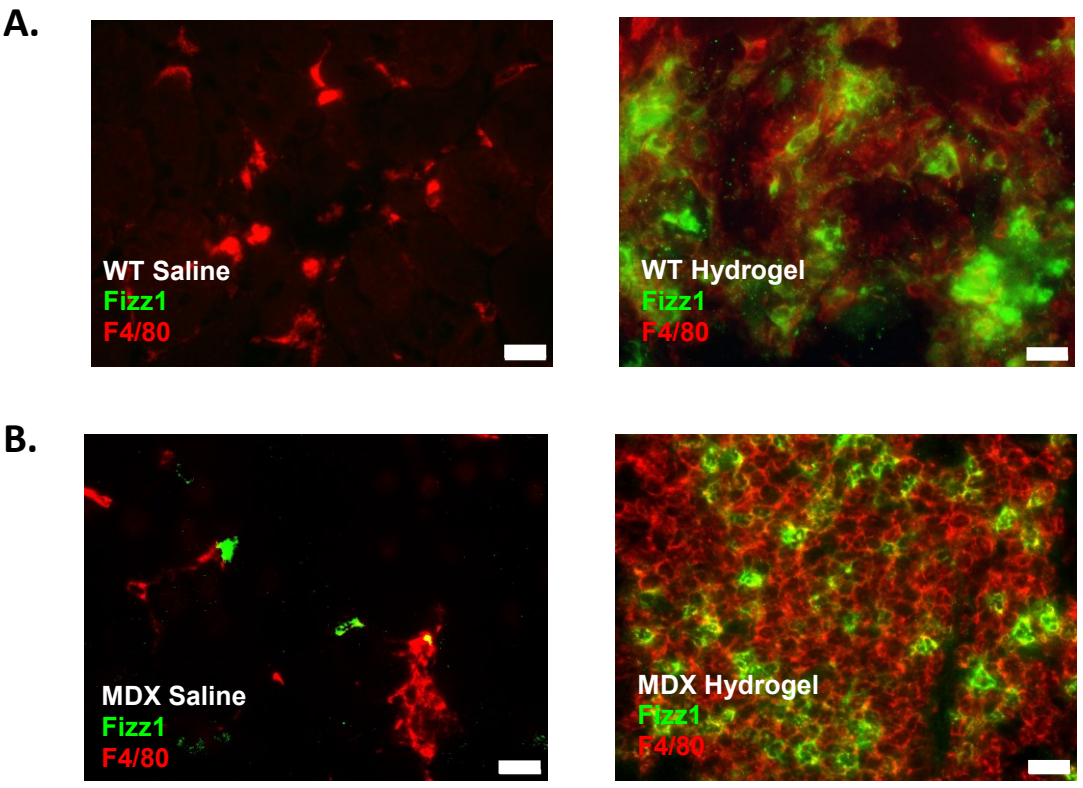


**Figure 3.1. Macrophage immunofluorescence in wild type and dystrophic mice.** WT C57BL/6 (A) and *mdx*-5$^{Cv}$ (B) mice injected with saline (left images) or hydrogel (right images) were harvested at 7 days post-injection. Immunofluorescence images of cryosectioned TAs depict the presence of M2 macrophages (Fizz1, green) and general macrophage populations (F4/80, red). Scale bars = 50 microns.

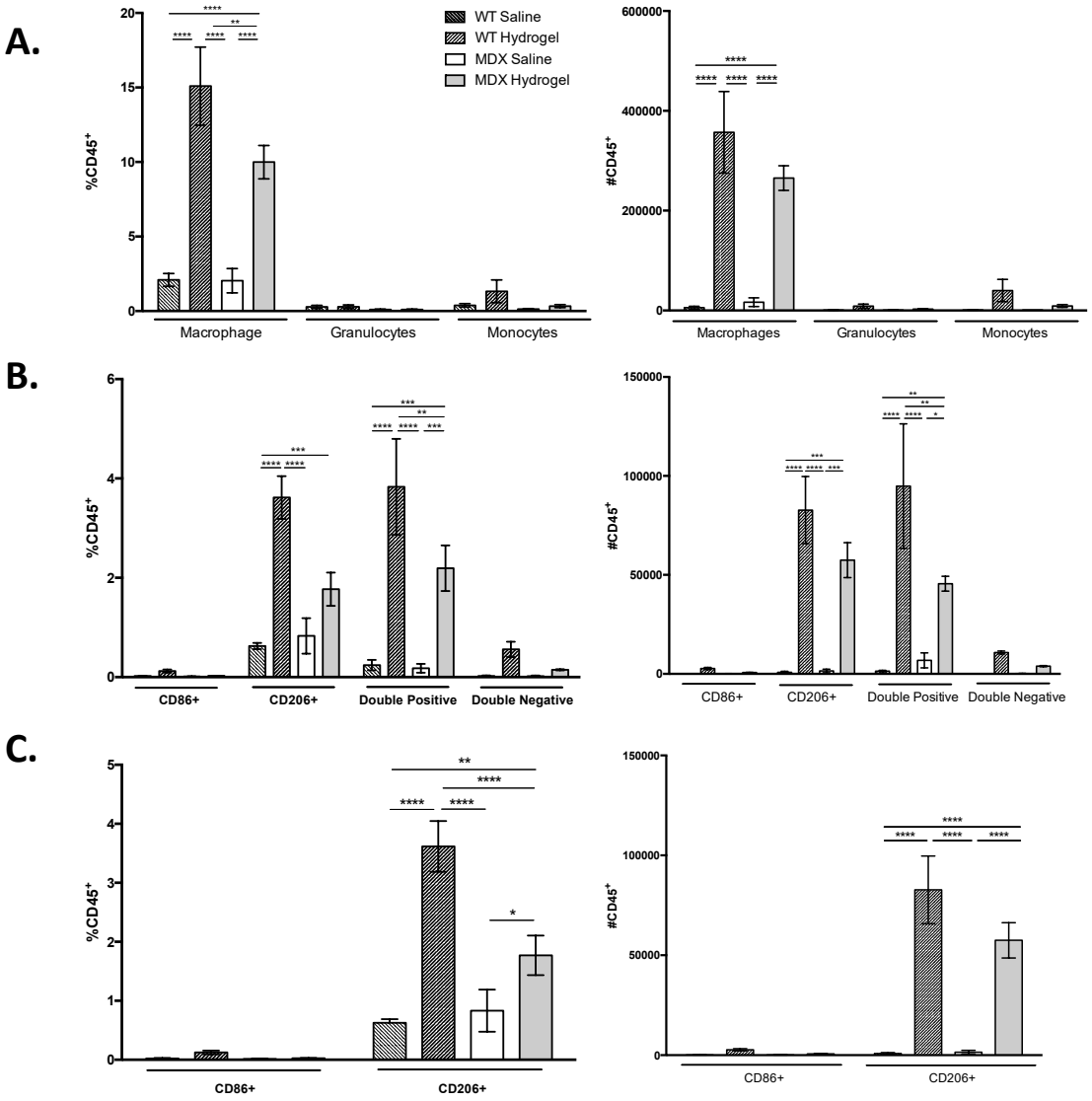


**Figure 3.2. Macrophage polarization affected by hydrogel.** Wild type C57BL/6 and *mdx*-5$^{Cv}$ TAs injected with saline or hydrogel harvested at 7 days post-injection were analyzed via FACS. (A) General myeloid populations. (B) CD86$^{+}$CD206$^{-}$, CD86$^{-}$CD206$^{+}$, CD86$^{+}$CD206$^{+}$, and CD86$^{-}$CD206$^{-}$ macrophages. (C) CD86$^{+}$CD206$^{-}$ and CD86$^{-}$CD206$^{+}$ macrophages. Legend applies to all figures. Populations shown as % CD45$^{+}$ cells (left) and absolute number of CD45$^{+}$ cells (right). Error bars are means +/- SEM, N=4 TA pairs per group. * p<0.05, ** p<0.01, *** p<0.001, **** p<0.0001.

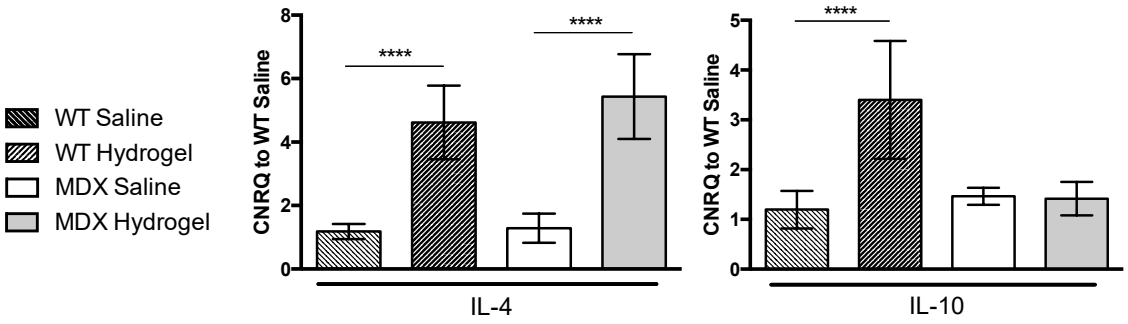


**Figure 3.3. Cytokine expression in wild type and dystrophic mice.** WT C57BL/6 and *mdx*-5$^{Cv}$ mice injected with saline or hydrogel were harvested at 7 days post-injection. RNA was isolated from inguinal lymph nodes and used to determine local gene expression. IL-4 and IL-10 expression are presented as calibrated normalized relative quantities (CNRQ) over WT saline, normalized to B2M and TBP. Legend applies to all figures. All error bars are means +/- SEM, N=4 inguinal lymph node pairs per group. **** $p<0.0001$.

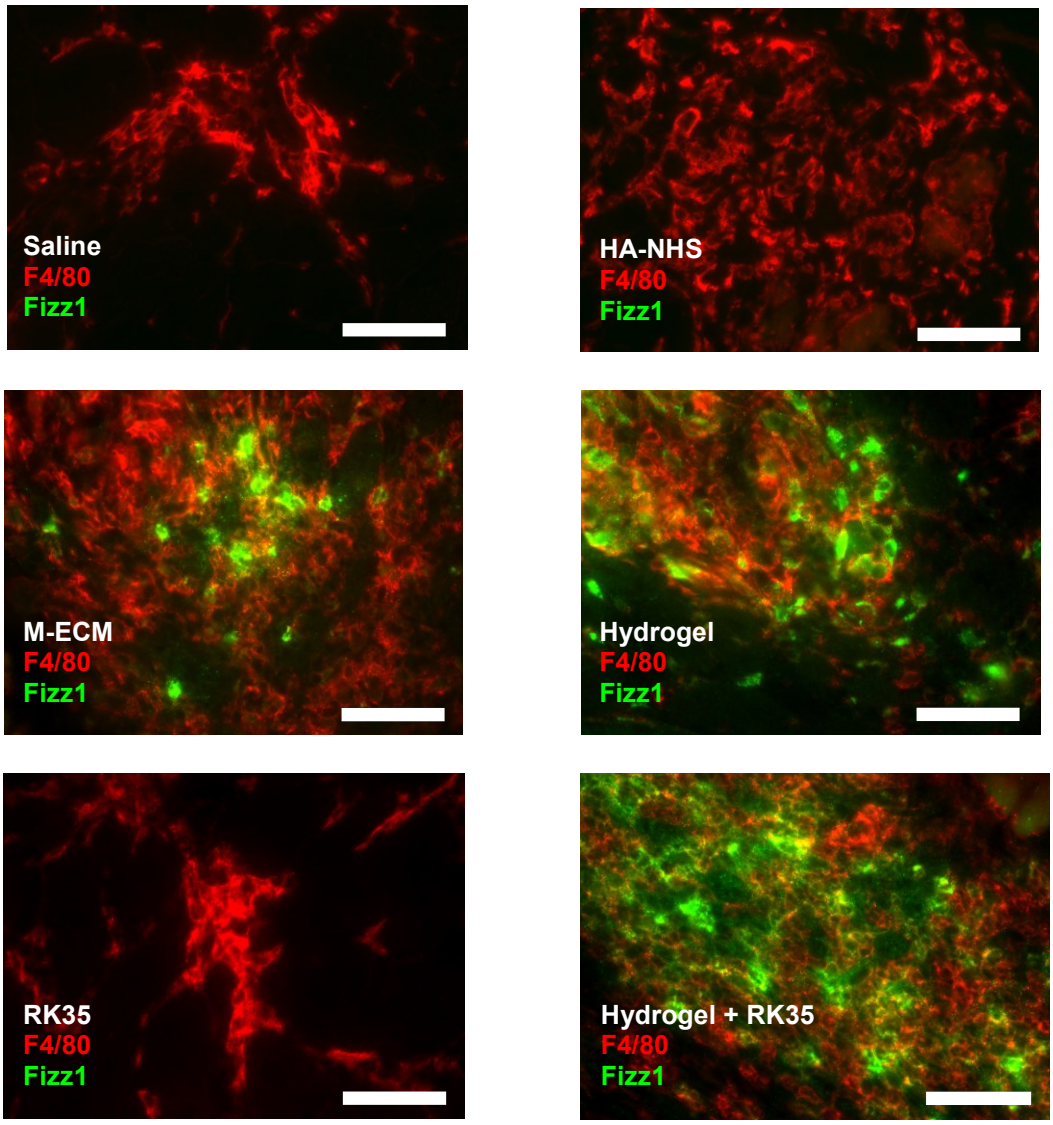


**Figure 3.4. Fizz1+ macrophages in hydrogel component- injected dystrophic mice.** *mdx-5*$^{Cv}$ mice injected with hydrogel components and/or RK35 were harvested at 7 days post-injection. Immunofluorescence images of cryosectioned TAs depict the presence of M2 macrophages (Fizz1, green) and general macrophage populations (F4/80, red). Scale bars = 50 microns.

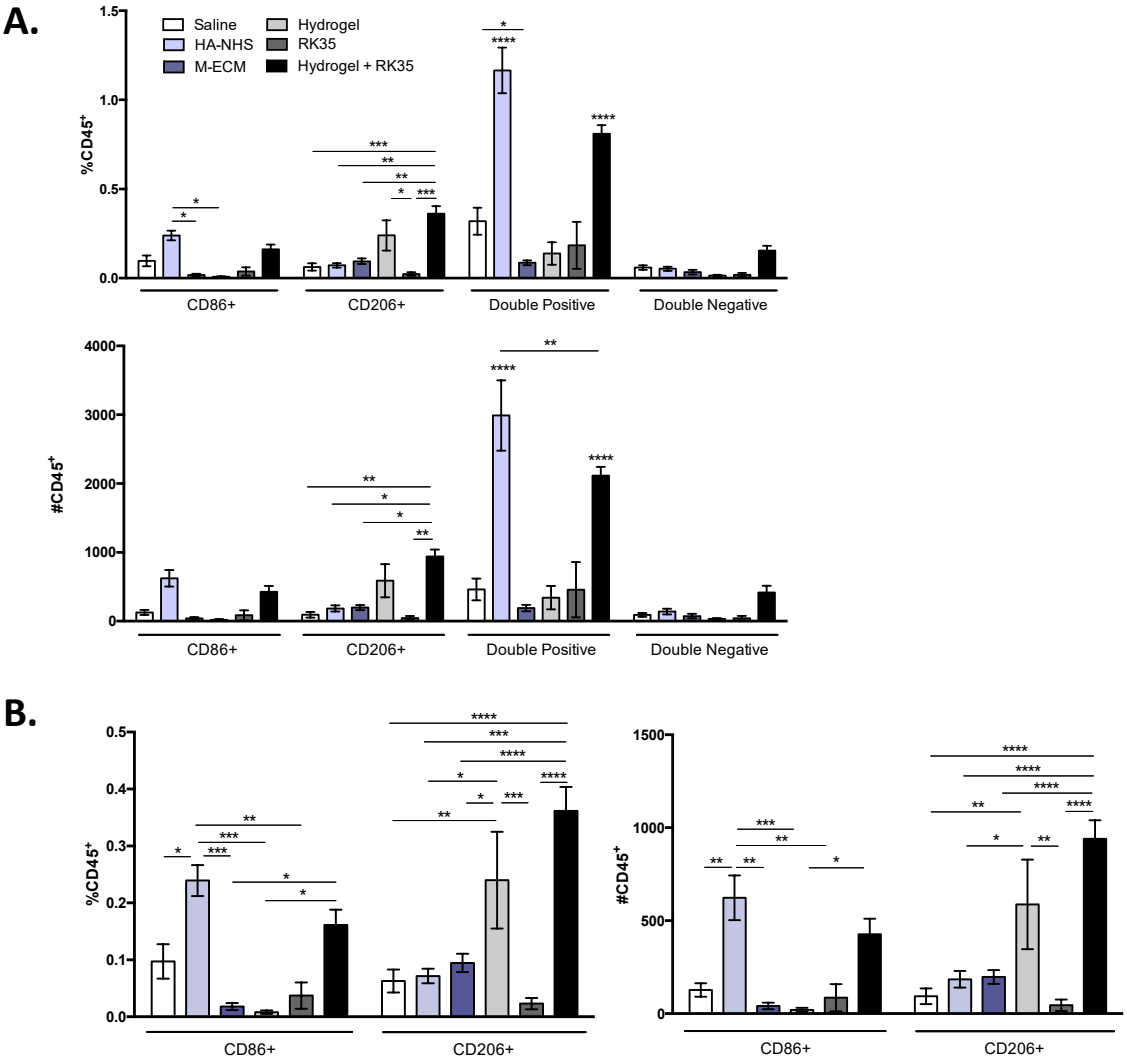


**Figure 3.5. HA-ECM hydrogel and RK35 affect M2 macrophage polarization.** *Mdx*-5$^{Cv}$ TAs injected with hydrogel components and/or RK35 harvested at 7 days post-injection were analyzed via FACS. (A) CD86$^{+}$CD206$^{-}$, CD86$^{-}$CD206$^{+}$, CD86$^{+}$CD206$^{+}$, and CD86$^{-}$CD206$^{-}$ macrophages. (B) CD86$^{+}$CD206$^{-}$ and CD86$^{-}$CD206$^{+}$ macrophages. Legend applies to all figures. Populations shown as % CD45$^{+}$ cells (top/left) and absolute number of CD45$^{+}$ cells (bottom/right). Legend applies to all figures. Error bars are means +/- SEM, N=4 TA pairs per group. * p<0.05, ** p<0.01, *** p<0.001, **** p<0.0001.

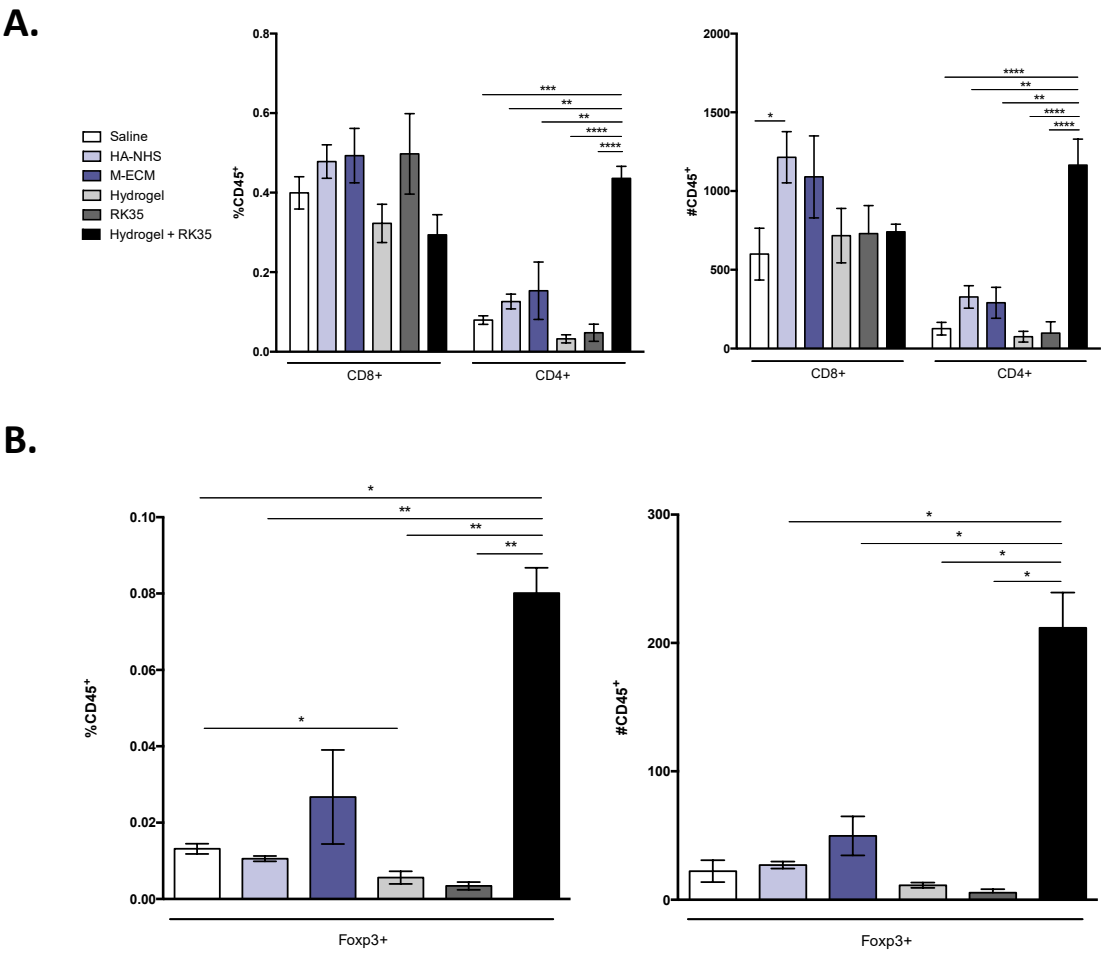


**Figure 3.6. HA-ECM hydrogel and RK35 affect T cell polarization.** *Mdx*-5$^{Cv}$ TAs injected with hydrogel components and/or RK35 harvested at 7 days post-injection were analyzed via FACS. (A) CD8$^+$ and CD4$^+$ T cells. (B) Foxp3$^+$ regulatory T cells. Populations shown as % CD45$^+$ cells (left) and absolute number of CD45$^+$ cells (right). Legend applies to all figures. Error bars are means +/- SEM, N=4 TA pairs per group. * p<0.05, ** p<0.01, *** p<0.001, **** p<0.0001.

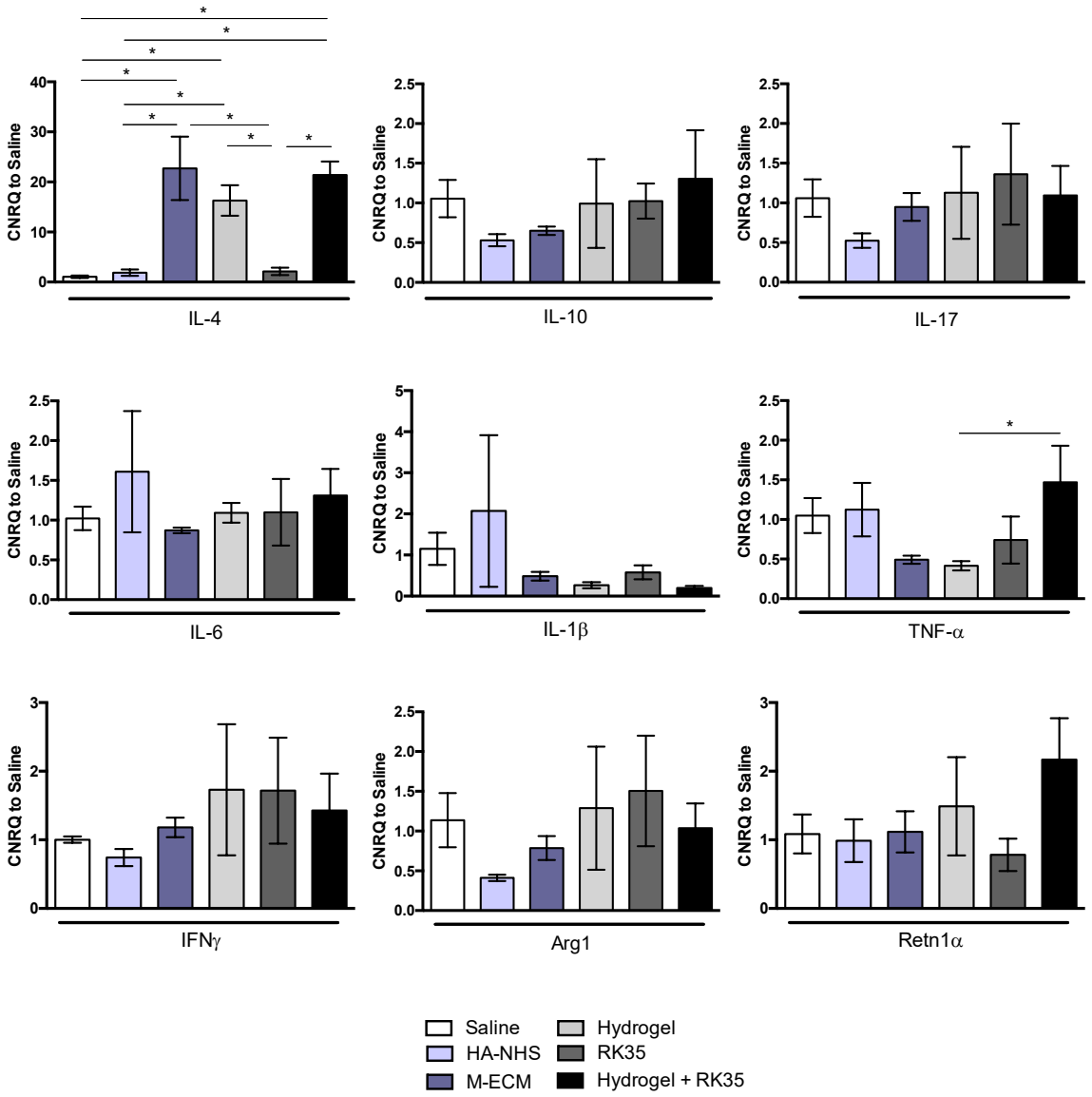


**Figure 3.7. Cytokine expression in hydrogel component-injected mice.** *Mdx*-5$^{Cv}$ mice injected with hydrogel components and/or RK35 were harvested at 7 days post-injection. RNA was isolated from inguinal lymph nodes and used to determine local gene expression. Expression levels are presented as calibrated normalized relative quantities (CNRQ) over saline, normalized to B2M and TBP. Legend applies to all figures. Legend applies to all figures. Error bars are means +/- SEM, N=4 inguinal lymph node pairs per group. * p<0.05, ** p<0.01, *** p<0.001, **** p<0.0001.

| Gene | Forward Primer (5’ → 3’) | Reverse Primer (5’ → 3’) |
|---|---|---|
| B2M | CACTGAATTCACCCCCACTGA | TCTCGATCCCAGTAGACGGT |
| TBP | AGTGCCCAGCATCACTATTT | GGTCCATGATTCTCCCTTTCTT |
| IL-4rα | GGTCACAGGAGAAGGGACGC | AGCACCTTGGAAGCCCTACA |
| IL-10 | CAGGACTTTAAGGGTTACTTGGGT | GCCTGGGGCATCACTTCTAC |
| IL-17α | TCAGCGTGTCCAAACACTGAG | CGCCAAGGGAGTTAAAGACTT |
| IL-6 | CCAGGTAGCTATGGTACTCCAGAA | GCTACCAAACTGGATATAATCAGGA |
| IL-1β | TGCCACCTTTTGACAGTGATG | AAGCTGGATGCTCTCATCAGG |
| TNFα | ATGGCCTCCCTCTCATCAGT | TGGTTTGCTACGACGTGGG |
| IFNϒ | TCAAGTGGCATAGATGTGGAA | TGAGGTAGAAAGAGATAATCTGG |
| Arg1 | ACAAGACAGGGCTCCTTTCAG | TAAAGCCACTGCCGTGTTCA |
| Retn1α | CAGCTGATGGTCCCAGTGAAT | AGTGGAGGGATAGTTAGCTGG |

**Table 3.1. qPCR primer sequences used for proximal lymph node cytokine analysis.**

| Antigen | Clone | Fluorophore | Dilution |
|---|---|---|---|
| CD45 | 30-F11 | Brilliant Violet 605 | 1:100 |
| CD11b | M1/70 | Alexa Fluor 700 | 1:400 |
| CD11c | N418 | Allophycocyanin | 1:250 |
| F4/80 | BM8 | Phycoerythrin - Cy7 | 1:250 |
| CD86 | GL-1 | Brilliant Violet 510 | 1:200 |
| CD206 | C068C2 | Phycoerythrin | 1:250 |
| MHCII (I-A/I-E) | M5/114.15.2 | Alexa Fluor 488 | 1:200 |
| Ly6c | HK1.4 | Peridinin Chlorophyll / Cy5.5 | 1:400 |
| Ly6g | 1A8 | Pacific Blue | 1:400 |
| Viability | -- | eFluor780 | 1:2000 |

**Table 3.2. FACS antibodies used for wild type vs. *mdx* immune study.**

| Antigen | Clone | Fluorophore | Dilution |
|---|---|---|---|
| CD3 | 145-2C11 | Brilliant Violet 786 | 1:200 |
| CD4 | RM4-5 | Phycoerythrin – Texas Red | 1:200 |
| CD8 | SK1 | Peridinin Chlorophyll / Cy5.5 | 1:200 |
| Foxp3 | FJK-16s | Fluorescein Isothiocyanate | 1:100 |
| IL-17 | TC11-18H10.1 | Alexa Fluor 700 | 1:300 |
| CD45 | 30-F11 | Horizon V500 | 1:300 |
| MHCII (I-A/I-E) | M5/114.15.2 | Brilliant Violet 711 | 1:2000 |
| F4/80 | BM8 | Phycoerythrin – Cy7 | 1:500 |
| CD86 | GL-1 | Allophycocyanin | 1:400 |
| CD206 | C068C2 | Phycoerythrin | 1:300 |
| CD11b | M1/70 | Pacific Blue | 1:400 |
| Viability | | Viability Aqua | 1:2000 |

**Table 3.3. FACS antibodies used for *mdx* hydrogel immune study.**

## Supplementary Data

| | | | |
|---|---|---|---|
| **WT Saline 1** | 152500 | **MDX Saline 1** | 556000 |
| **WT Saline 2** | 264000 | **MDX Saline 2** | 821000 |
| **WT Saline 3** | 88000 | **MDX Saline 3** | 375000 |
| **WT Saline 4** | 146600 | **MDX Saline 4** | 352000 |
| | | | |
| **WT Hydrogel 1** | 868000 | **MDX Hydrogel 1** | 251900 |
| **WT Hydrogel 2** | 223200 | **MDX Hydrogel 2** | 645000 |
| **WT Hydrogel 3** | 709000 | **MDX Hydrogel 3** | 446000 |
| **WT Hydrogel 4** | 387000 | **MDX Hydrogel 4** | 826000 |

**Supplementary Table 3.1. Cell counts for samples in wild type vs. mdx study.** Cell counts from each sample determined by "live" gating with Countess II-FL cell counter (Thermo Fisher), counted twice and averaged.

| | | | |
|---|---|---|---|
| **MDX Saline 1** | 199400 | **MDX Hydrogel 1** | 157200 |
| **MDX Saline 2** | 264000 | **MDX Hydrogel 2** | 146600 |
| **MDX Saline 3** | 58600 | **MDX Hydrogel 3** | 256000 |
| **MDX Saline 4** | 105600 | **MDX Hydrogel 4** | 334000 |
| | | | |
| **MDX HA-NHS 1** | 292000 | **MDX RK35 1** | 98600 |
| **MDX HA-NHS 2** | 274000 | **MDX RK35 2** | 210000 |
| **MDX HA-NHS 3** | 167800 | **MDX RK35 3** | 69200 |
| **MDX HA-NHS 4** | 290000 | **MDX RK35 4** | 288000 |
| | | | |
| **MDX M-ECM 1** | 137200 | **MDX Hydrogel + RK35 1** | 268000 |
| **MDX M-ECM 2** | 199400 | **MDX Hydrogel + RK35 2** | 194800 |
| **MDX M-ECM 3** | 260000 | **MDX Hydrogel + RK35 3** | 306000 |
| **MDX M-ECM 4** | 268000 | **MDX Hydrogel + RK35 4** | 290000 |

**Supplementary Table 3.2. Cell counts for samples in mdx hydrogel study.** Cell counts from each sample determined by “live” gating with Countess II-FL cell counter (Thermo Fisher), counted twice and averaged.

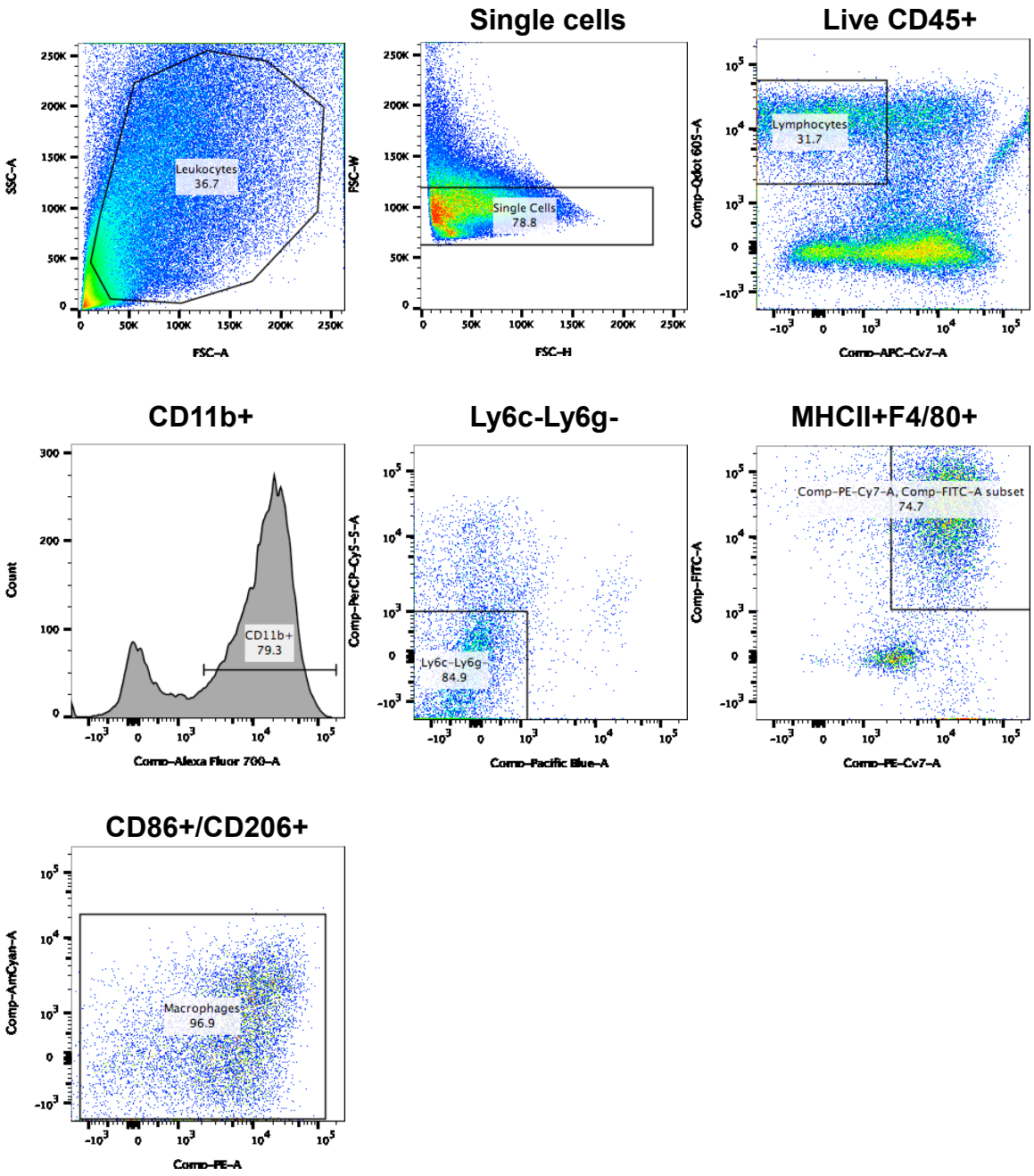


**Supplementary Figure 3.1. FACS gating schematic for macrophage populations.** Note: Ly6c / Ly6g not used for *mdx* hydrogel component study.

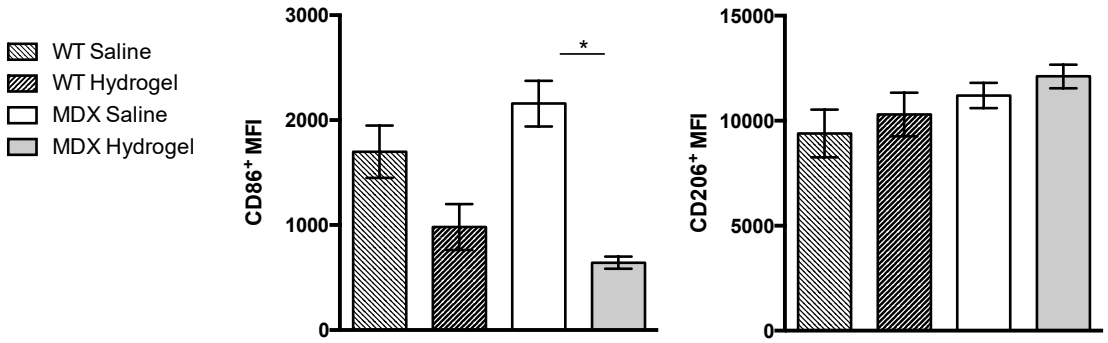


**Supplementary Figure 3.2. Macrophage MFI in wild type vs. mdx hydrogel experiment.**

Left: CD86 (BV 510 signal). Right: CD206 (PE signal). Legend applies to all figures. Error bars are means +/- SEM, N=4 TA pairs per group. * $p<0.05$.

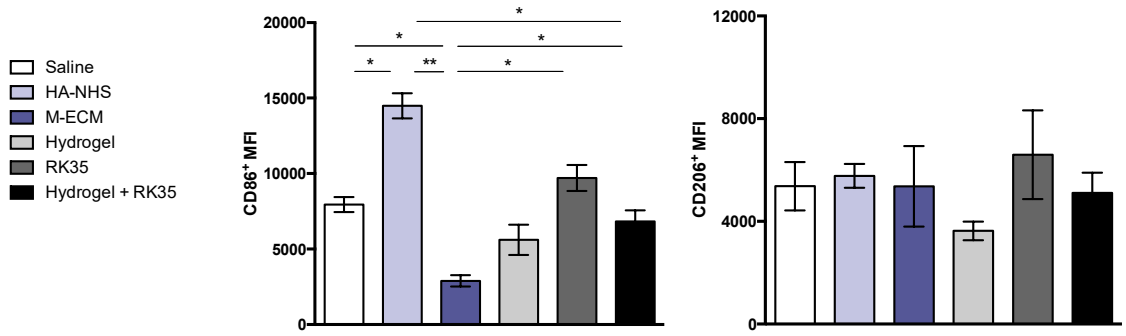


**Supplementary Figure 3.3. Macrophage MFI in mdx hydrogel component experiment.** Left: CD86 (APC signal). Right: CD206 (PE signal). Legend applies to all figures. Error bars are means +/- SEM, N=4 TA pairs per group. * $p<0.05$, ** $p<0.01$.

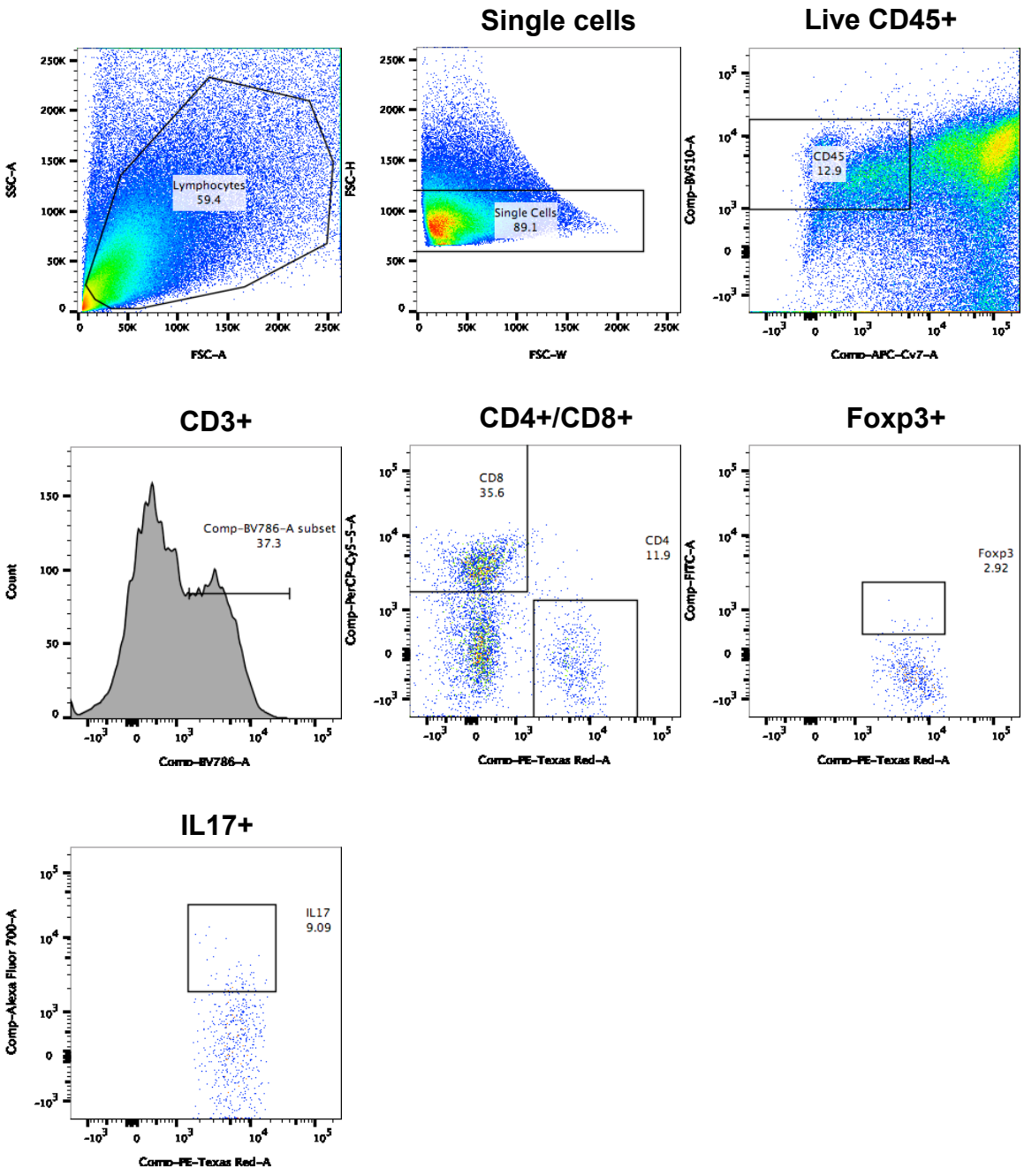


**Supplementary Figure 3.4. FACS gating schematic for T cell populations.**

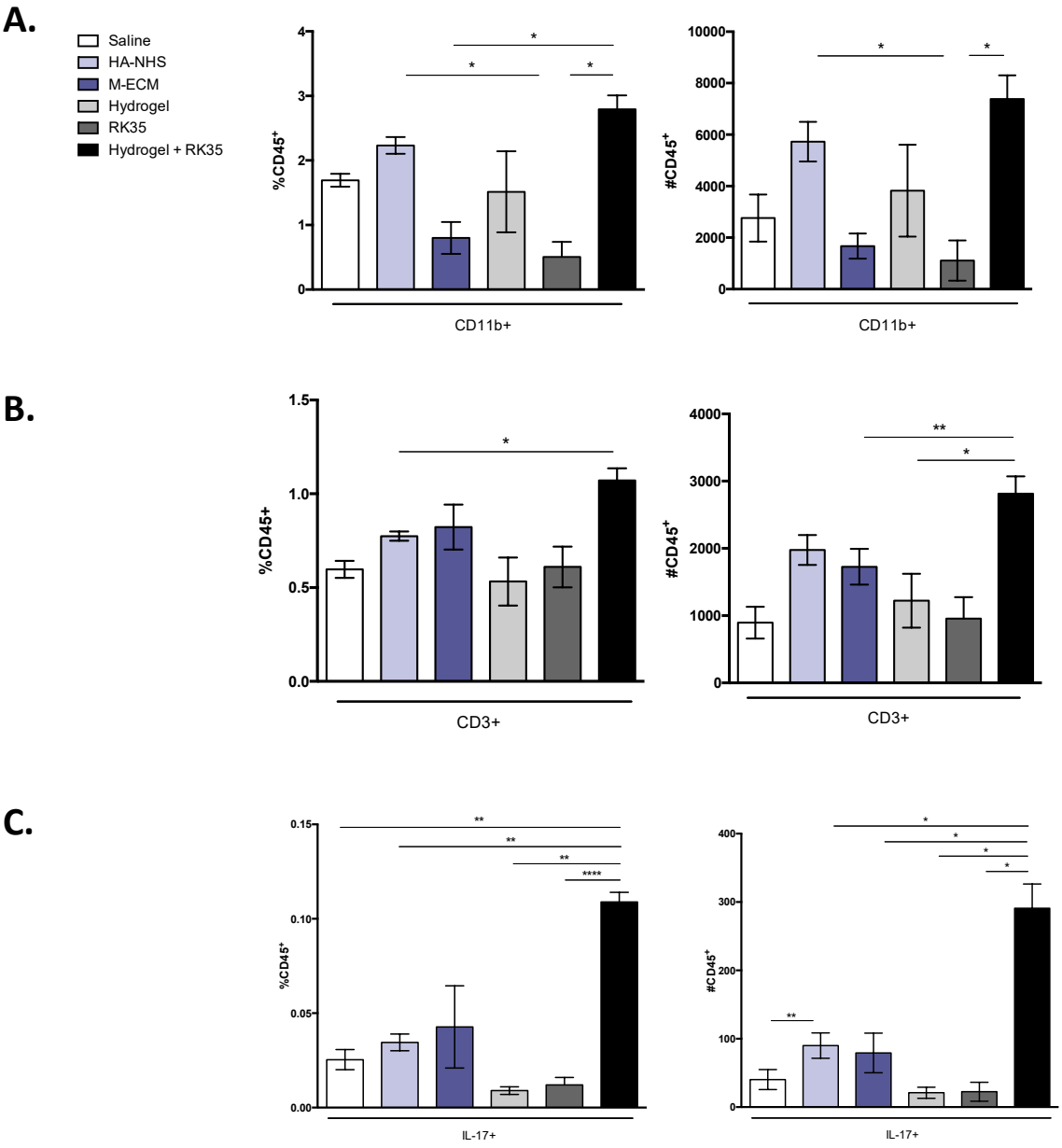


**Supplementary Figure 3.5. Hydrogel and RK35 affect CD11b+, CD3+, and IL-17+ populations.** *Mdx*-5$^{Cv}$ TAs injected with hydrogel components and/or RK35 harvested at 7 days post-injection were analyzed via FACS. (A) CD11b$^{+}$ cells. (B) CD3$^{+}$ T cells. (B) IL-17$^{+}$ T cells. Populations shown as % CD45+ cells (left) and absolute number of CD45+ cells (right). Legend applies to all figures. Error bars are means +/- SEM, N=4 TA pairs per group. * p<0.05, ** p<0.01, **** p<0.0001.

# Chapter 4: Hydrogel-Mediated Transplantation of Skeletal Muscle Cells

## Abstract

Despite decades of development, cellular therapies for the treatment of DMD have remained largely ineffective. Here we describe the *in vivo* characterization of a novel population of human embryonic stem cell derived muscle progenitor cells for use in cell therapy, as well as the application of the injectable biomaterial hydrogel described in **Chapter 2** to increase the effectiveness of their transplantation. Human stem-cell derived myoblasts injected into immunodeficient mice formed human muscle fibers *in vivo* and occupied the local progenitor cell niche, driving long term repair after injury. Transplantation of cells with the hydrogel promoted their viability at short-term timepoints, and a long-term pilot study revealed their capability to restore Dystrophin in immunodeficient dystrophic mice. **Chapter 4** describes the first application of an injectable biomaterial to increase the effectiveness of stem cell transplantation in DMD.

## Introduction

The transplantation of healthy skeletal muscle progenitor cells into dystrophic recipients in order to partially or completely restore Dystrophin expression has been explored and evaluated by numerous groups since the late 1980s [40]. However, even after numerous preclinical and clinical trials, the results of cell therapy in DMD have been largely ineffective [47]. Obtaining sufficient numbers of transplant-competent muscle progenitor cells remains a difficult process, transplanted cell viability tends to be poor, and donor cell engraftment in terms of Dystrophin restoration and functional outcomes has largely been clinically insignificant.

Here, human skeletal muscle progenitor cells derived with a previously described dual-SMAD inhibition strategy [86] were evaluated for their capacity to serve as donor cells to not only form human muscle fibers but also act as the primary driver of skeletal muscle repair after injury. Additionally, the injectable hyaluronic acid – skeletal muscle ECM hydrogel characterized in **Chapter 2** was utilized to promote the effectiveness of muscle myoblast transplantation in short-term and long-term studies. Through direct visualization and semi-quantitative assessment of cell survival and donor-derived myofiber formation, both the hydrogel and human pluripotent stem cell derived myoblasts were evaluated for their applicability towards cell therapy for DMD.

## Materials and Methods

*Characterization of hESC derived myoblasts*

Human embryonic stem cell derived myoblasts were derived by the Lee Lab as described in Choi et. al. [86], via treatment of hESCs with CHIR99021 for 4 days, followed by DAPT treatment for 8 days, and further maintenance in culture for at least 18 days to allow for differentiation into the myogenic lineage [86]. 2-6 month old male NOD-Rag1$^{null}$-IL2rg$^{null}$ (NRG) or NOD-SCID-IL2rg$^{null}$ (NSG) mice (Jackson Laboratories) mice were irradiated with 18 Gy in the left or both hindlimbs with either a Shepherd Mark I (JL Shepherd) or a micro-CT guided Small Animal Radiation Research Platform (Xstrahl) [104] in order to ablate the endogenous satellite cell population. After three days, irradiated TAs were injured via injection of 100 µL 10 mM cardiotoxin (*Naja Mossambica,* Sigma) or 50 µL 1.2% $BaCl_2$ (Sigma) [102]. 24 hours after injury, 1-3 x $10^6$ cells were injected into the left TA, with the right leg serving as an uninjected control.

All TA muscles were harvested 4-8 weeks after each injection; serially injured mice received a second TA injury of 50 µL 1.2% $BaCl_2$ at six weeks post-transplantation and were harvested two weeks later. TA muscles were flash frozen in chilled isopentane and 7 µm cryosections were taken. Slides were fixed in cold methanol and blocked with 20% normal goat serum (NGS) in 2% bovine serum albumin (BSA). Fixed slides were incubated with primary antibodies against human lamin A+C (NCL-LAM-AC, mouse IgG2b, 1:100, Leica), pan-species Pax7 (PAX7, mouse IgG1, 1:1, DSHB), human laminin (2E8, mouse IgG2a, 1:100, DSHB), and human Dystrophin (MANDYS106, mouse IgG2a,

1:100, Leica), and secondary antibodies (goat anti-mouse IgG1 Alexa Fluor 488 1:500, goat anti-mouse IgG2a Alexa Fluor 647 1:500, goat anti-mouse IgG2b Alexa Fluor 555 1:500, Thermo Fisher). Pax7-stained slides underwent tyramide signal amplification (Thermo Fisher). Stained sections were mounted using Vectashield with DAPI (Vector Laboratories), and imaged using confocal (Olympus) or fluorescence microscopy (Zeiss). Comparison of N=2-3 serially injured muscles versus uninjured controls was performed via Mann-Whitney test in Prism (Graphpad).

*Short-term transplantation of hydrogel-injected myoblasts*

For semiquantitative analysis, 1 month old male immunodeficient NOD-Rag1$^{null}$-IL2rg$^{null}$ (NRG) mice (Jackson Laboratories) were bilaterally injured via intramuscular injection of 100 µL 10 µM cardiotoxin (Roche) [102] into shaved tibialis anterior (TA) muscles. 24 hours post-injury, 0.5x10$^6$ LHCN-LUC7 immortalized human myoblasts [95] suspended in 50 µL PBS or 6% w/v HA-NHS:M-ECM 1:3 hydrogel were subfascially injected above each TA muscle as described previously. 7 days after injection, muscles were frozen in chilled isopentane, cryosectioned, stained with primary antibodies against human lamin A+C (NCL-LAM-AC, mouse IgG2b, 1:100, Leica) and secondary antibodies (goat anti-mouse IgG2b Alexa Fluor 555 1:500, Thermo Fisher) and imaged using fluorescence microscopy (Zeiss). Human Lamin A+C$^+$ nuclei present in each section were manually counted in ImageJ. N=6 sections were analyzed per muscle from regions at least 150 µm apart and

used to calculate percent cell survival. 4 muscles from n=2 animals were analyzed per group. All parameters were analyzed via two-way ANOVA in Prism (Graphpad).

For cytometric analysis, 1.5 month old male immunodeficient dystrophic NOD-SCID-IL2rγ$^{-}$*mdx*-4$^{Cv}$ (NSG-4Cv) mice (University of Minnesota) [105] were irradiated with 18 Gy X-ray radiation with a micro-CT guided Small Animal Radiation Research Platform (Xstrahl) [104], intramuscularly injured with 50 µL 1.2% $BaCl_2$ after 24 hours [102], and transplanted with 1x10$^6$ human ES-derived GFP$^+$ muscle progenitor cells (unpublished) in 50 µL PBS or hydrogel subfascially above the injured TA muscle (n=5 per group) 24 hours after injury. After 10 days post-transplantation, mice were euthanized, TA muscles were removed, and a single cell suspension was yielded as described previously [106]. Each sample was analyzed using a FACS Calibur + CellQuest Pro (BD), and the relative percentages of transplanted GFP$^+$ cells were determined for each sample. Sample group means were compared via Mann-Whitney test using Prism (Graphpad).

*Long-term transplantation of hydrogel-injected myoblasts*

1-2 month old male immunodeficient dystrophic NOD-SCID-IL2rγ$^{-}$*mdx*-4$^{Cv}$ (NSG-4Cv) mice were irradiated with 18 Gy X-ray radiation with a micro-CT guided Small Animal Radiation Research Platform (Xstrahl) [104], intramuscularly injured with 50 µL 1.2% $BaCl_2$ [102] after 24 hours, and transplanted with 1x10$^6$ hESC derived myoblasts [86] in 50 µL PBS or 6% w/v HA-NHS:M-ECM 1:3 hydrogel alone or with 10.75 µg RK35 as described previously (n=1 each). After 4 months post-transplantation, mice were

euthanized and TA muscles were removed. Cryosections were obtained and stained with primary antibodies against human lamin A+C (Mouse IgG2b, 1:100, Leica), pan-species Pax7 (IgG1, 1:1, DSHB), pan-species Dystrophin (Rabbit, 1:100, Abcam), human laminin (IgG2a, 1:100, DSHB), and human Dystrophin (IgG2a, 1:100, Leica), and secondary antibodies (goat anti-rabbit Alexa Fluor 488 1:500, goat anti-mouse IgG1 Alexa Fluor 488 1:500, goat anti-mouse IgG2a Alexa Fluor 647 1:500, goat anti-mouse IgG2b Alexa Fluor 555 1:500, Thermo Fisher). Pax7-stained slides were also subjected to tyramide signal amplification (Thermo Fisher). Stained sections were mounted using Vectashield mounting medium with DAPI (Vector Laboratories), and imaged using fluorescence microscopy (Zeiss). Observed human Laminin$^{+}$ and human Dystrophin$^{+}$ fibers were counted from six 7 µm cryosections from each muscle taken at least 150 µm apart. All groups were compared via one-way ANOVA in Prism (Graphpad).

## Results

*In vivo characterization of human pluripotent stem cell derived myoblasts.*

Human pluripotent stem cells derived to the myogenic lineage using a dual-SMAD inhibition strategy [86] were transplanted into irradiated, myotoxin injured tibialis anterior (TA) muscles of immunodeficient mice. At 4 weeks post-injection **(Figure 4.1)**, viable human nuclei were observed in transplanted TAs as determined by positive staining for the nuclear marker human Lamin A+C. Human skeletal muscle laminin was also observed, consistent with mature myofibers. Some progenitor cells localized within human laminin$^{+}$ fibers, occupying the satellite cell niche **(Figure 4.1 inset).**

Niche occupancy of progenitors was further verified by immunofluorescence labeling of transplanted muscles with antibodies against Pax7, a marker of satellite cells. Co-localization of Pax7 with human Lamin A+C, which is only present in donor-derived human nuclei, confirmed the occupancy of donor myoblasts in the satellite cell niche **(Figure 4.1)**. Since local satellite cells are the primary mediators of skeletal muscle repair after injury, transplanted muscles were subjected to a secondary myotoxin injury to assess this functionality in donor-derived myoblasts. Analysis of injured transplanted TAs revealed a greater proportion of human Laminin$^{+}$ and human Dystrophin$^{+}$ fibers than transplanted TA muscles that were injured only once **(Figure 4.2).**

*Effects of hydrogel on short-term transplantation of human muscle progenitor cells.*

The hydrogel described in **Chapter 2** was further explored by determining its ability to deliver cells *in vivo*. 24 hours after cardiotoxin injury, immunodeficient mice were transplanted with immortalized human myoblasts suspended in saline or hydrogel. After 1 week, visual assessment of each muscle revealed twice as many human nuclei in hydrogel-transplanted mice compared to saline-transplanted mice **(Figure 4.3).** This was confirmed with a human pluripotent stem cell-derived myoblast line [86] modified to constitutively expresses GFP. 10 days after transplantation of these cells into irradiated, myotoxin-injured immunodeficient dystrophic mice, single-cell populations analyzed by flow cytometry revealed a significantly greater percentage of donor-derived $GFP^+$ cells in hydrogel-transplanted muscles when compared to saline **(Figure 4.4).**

*Effects of hydrogel on long-term transplantation of human muscle progenitor cells.*

Four months after irradiation, myotoxin injury, and transplantation of human embryonic stem cell-derived myoblasts into immunodeficient mice, muscles were cryosectioned and the number of human $Laminin^+$ and $Dystrophin^+$ fibers was counted. Significantly greater numbers of human $Laminin^+$ **(Figure 4.5A)** and $Dystrophin^+$ **(Figure 4.5B)** fibers were observed in hydrogel-transplanted mice compared to saline-transplanted mice. Furthermore, nuclei that co-stained human Lamin $A+C^+$ and $Pax7^+$ within human $Dystrophin^+$ fibers were observed in both conditions, verifying the long-term ability of saline- and hydrogel-transplanted human pluripotent stem cell derived myoblasts to occupy the satellite cell niche.

## Discussion

In this study, increased numbers of donor-derived myoblasts were observed in mice transplanted with hydrogel compared to saline **(Figures 4.3-4.4).** The hydrogel may have conferred a number of positive effects on viability and engraftment through mechanisms established in other studies, including protection from a harsh host environment [49] or reduction of anoikis, programmed cell death that occurs in anchorage-dependent cells that are detached from the extracellular matrix [107]. One key property of the hydrogel that may have also played a role is the dispersion of transplanted cells; without adequate spreading, progenitor cells either localize predominantly around the injection site or adopt a perifascicular pattern of engraftment [108], preventing widespread formation of donor-derived myofibers *in situ*.

The slow but defined gelation pattern established with the hydrogel **(Figure 2.2)** allows the gel to travel, but retain its position once injected. Cross-linking between HA-NHS and locally available primary amines may further increase retention of transplanted cells locally, as the adhesive properties of NHS-conjugated polymers has been previously established [93]. Although subfascial injection was established as an efficient method to ensure sufficient spreading of the hydrogel **(Figure 2.4),** intramuscular injection of the hydrogel may allow for further dispersion and delivery of transplanted cells. Also, since myostatin inhibition has been previously demonstrated to have positive effects on skeletal muscle stem cell transplantation [109], future potential studies could

synergistically utilize both hydrogel and the myostatin inhibitor RK35 to further promote the engraftment efficiency of transplanted cells.

Dystrophin-restored fibers and $Pax7^{+}$ / human Lamin $A+C^{+}$ co-stained nuclei were observed histologically in long-term transplanted muscles **(Figure 4.5)**, but they were relatively rare. Cross sections are only representative of a small portion of an entire muscle; some information may be lost due to sampling bias. Purely visual confirmation of human muscle fiber formation also may not completely differentiate between true *de novo* donor-derived human muscle fibers and hybrid fibers formed with host muscle, originating due to ineffective ablation of satellite cell populations via irradiation or incomplete myotoxin injury. Whole-muscle outcomes of engraftment such as flow cytometry for GFP-labeled progenitor cells or Western blotting to precisely quantify levels of restored Dystrophin [110] may present a more representative evaluation of engraftment efficiency. Additionally, harvesting transplanted muscles at shorter or longer-term timepoints may be required to fully appreciate the effects of the hydrogel on donor-driven repair and regeneration. In the longer term, functional outcomes such as electrophysiology or whole-animal studies could also be utilized [103]. Still, despite the phenotypic severity of the *mdx*-$5^{Cv}$ mouse model [105], additional injury may be necessary to further elucidate the differences between treated groups.

Some limitations do exist with the transplanted human pluripotent stem cell-derived myoblasts utilized in this study. Although they form myofiber-like structures that express human laminin **(Figures 4.1-4.2)**, the expression of sarcolemmal proteins such as human Dystrophin **(Figures 4.2, 4.5)** and human Collagen IV (data not shown) remain extremely limited by comparison. The cells in this study were injected after weeks of culture post-derivation without any intermediate purification steps; these cells are technically a heterogeneous population, the transplantation of which may decrease myogenic efficiency, and has had some unintended consequences in the form of possible transdifferentiation *in situ* leading to the formation of counterproductive non-muscular hypertrophy in some cases (data not shown). Purification of these cell populations prior to injection, potentially utilizing GFP or other markers, could potentially yield increased myogenic efficiency upon transplantation *in vivo*.

## Figures

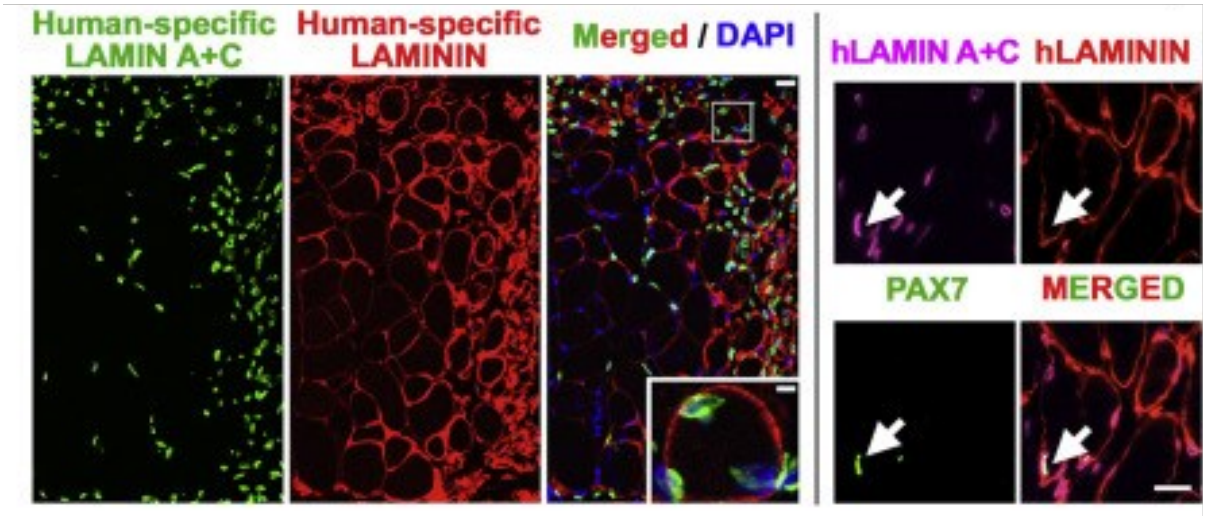


**Figure 4.1. Transplantation of hESC-derived myoblasts in vivo.** Left panels: $1x10^6$ human embryonic stem cell derived myoblasts formed human muscle fibers *in vivo*. Donor-derived nuclei (green) and human skeletal muscle Laminin (red) co-localize (merge) are present at four weeks post-injection with some human nuclei present in the sublaminar space (inset). Figure scale bar = 50 microns, inset scale bar = 5 microns. Right panels: Transplanted hESC-derived myoblasts repopulate the satellite cell niche, as determined by co-localization of human Lamin A+C (magenta) and Pax7 (green) in merged image of cryosectioned TA muscle at 6 weeks post-injection. Scale bar = 50 microns. Images taken from [86] as authorized by Creative Commons Attribution CC-BY-NC-ND 4.0.

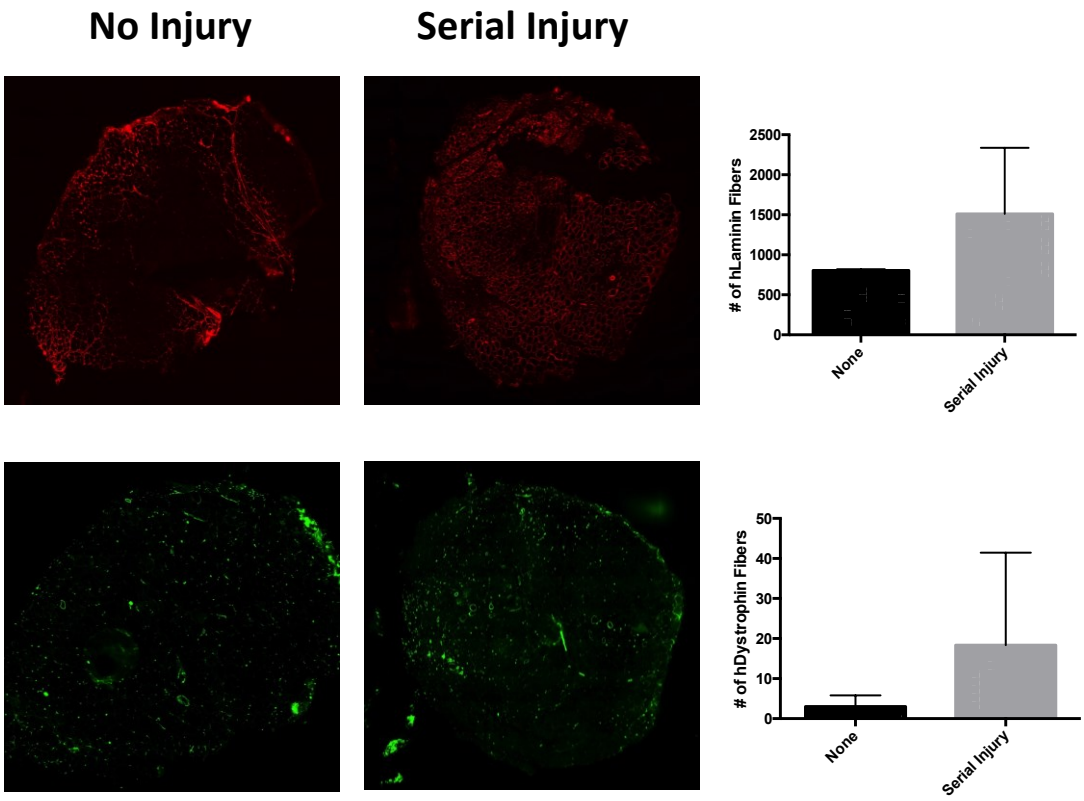


**Figure 4.2. Transplanted hESC-derived myoblasts drive repair after serial injury.** Mice transplanted with human embryonic stem cell derived myoblasts were either harvested at 8 weeks (left column) or injured a second time at 6 weeks prior to harvest at 8 weeks (middle column). Average numbers of human Laminin$^{+}$ (red, top row) and human Dystrophin$^{+}$ (green, bottom row) were counted across whole cryosection mosaics. No injury N=2, serial injury N=3. Data represent means +/- SEM.

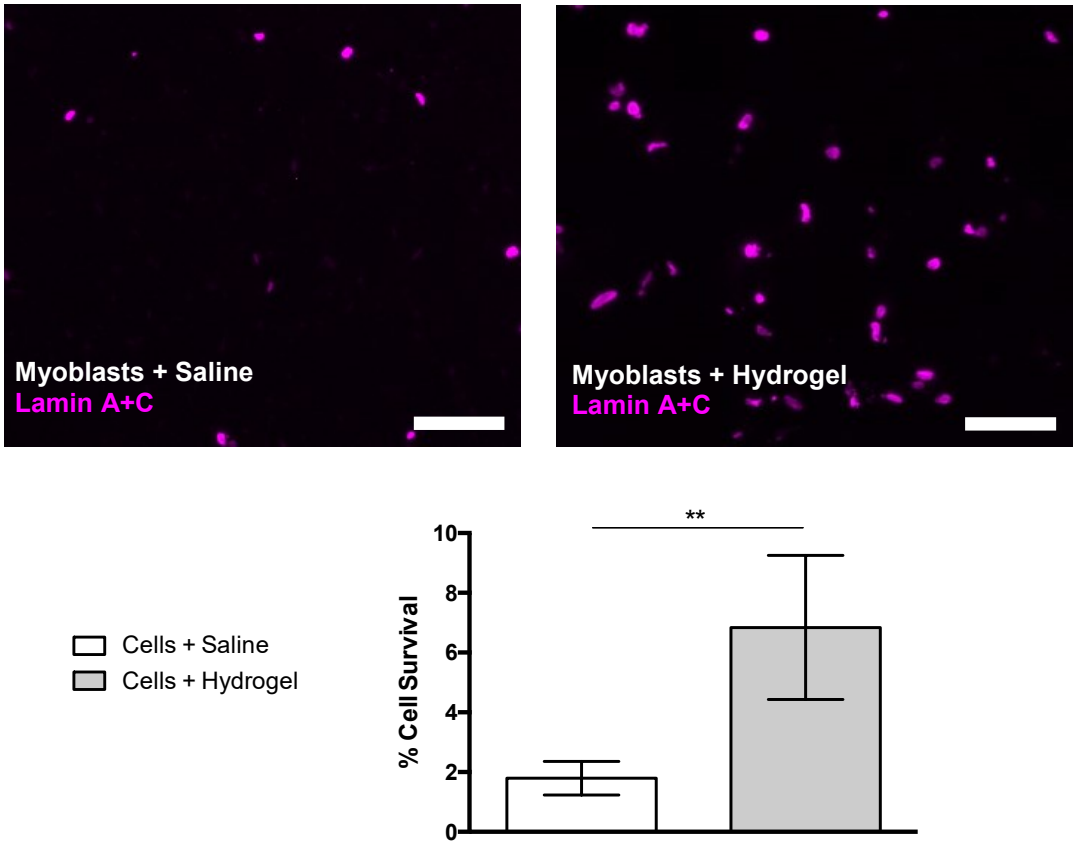


**Figure 4.3. Hydrogel promotes immortalized human myoblast viability after 7 days.** $0.5x10^6$ immortalized human myoblasts were bilaterally injected into the subfascial space of NRG mouse TA muscles 24 hours post-cardiotoxin injury. Immunofluorescence images depict cross-sections of muscles transplanted with cells in PBS (left) or hydrogel (right) 7 days post-transplantation. Scale bars = 200 microns, N=4. All error bars represent means +/- SEM, ** $p<0.01$.

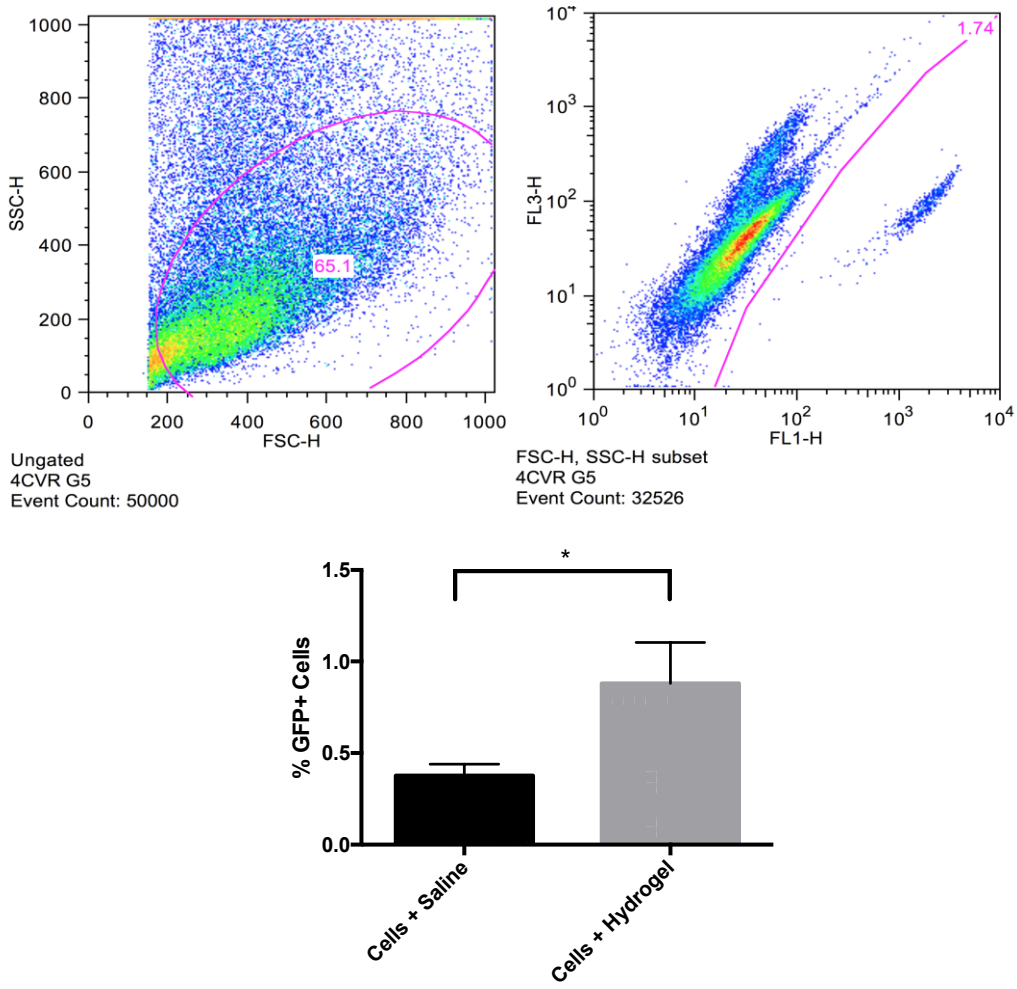


**Figure 4.4. Hydrogel promotes GFP+ hESMyo viability after 10 days.** 1x$10^6$ human embryonic stem cell-derived myoblasts modified to express GFP were unilaterally injected into NOD-SCID-Il2Ɣ$^-$ (NSG) mouse TA muscles 72 hours after irradiation and 24 hours after $BaCl_2$ injury. $GFP^+$ cells were isolated from transplanted TAs and quantified via FACS. Representative FACS plots shown to illustrate isolated population. N=5 mice per condition. Data points on graph represent mean values +/- SEM. ** p<0.05.

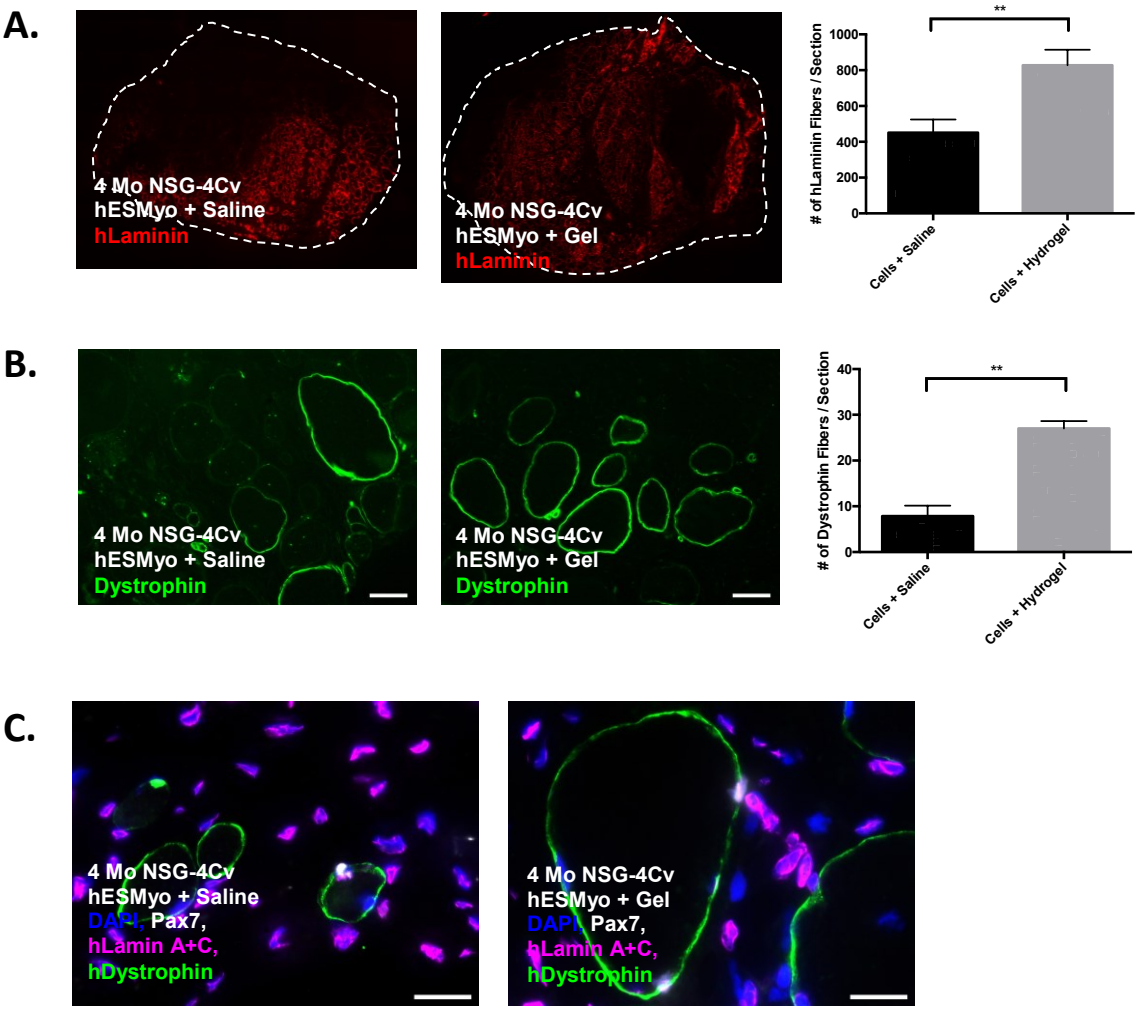


**Figure 4.5. Hydrogel promotes hESMyo engraftment after 4 months.** $1x10^6$ human embryonic stem cell derived myoblasts were injected into NSG-4Cv mice with saline or hydrogel. (A) Number of human Laminin$^+$ fibers. Muscle cross-section boundaries outlined in white. (B) Number of Dystrophin$^+$ fibers. (C) Presence of Pax7$^+$ / human Lamin A+C$^+$ double-positive nuclei co-localized near human Dystrophin$^+$ fibers. 6 sections were counted from N=1 mouse per group. Data points on graphs represent mean values +/- SEM. ** $p<0.01$. Scale Bar = 200 microns.

# Chapter 5: Conclusions and Future Directions

## Conclusions

In this body of work, the principles of biomaterials and tissue engineering were applied to develop a regenerative medicine strategy for the treatment of DMD. We created an injectable biomaterial, known as a hydrogel, with the goal of utilizing it as a carrier to facilitate the delivery of growth factors and muscle progenitor cells in murine models of Duchenne Muscular Dystrophy. The hydrogel is composed of hyaluronic acid succinimidyl succinate (HA-NHS), a modified form of the glycosaminoglycan functionalized with *N*-hydroxysuccinimide groups to promote crosslinking to local primary amines and subsequent hydrogel formation. This was combined with decellularized porcine skeletal muscle extracellular matrix (M-ECM), a material noted for its utility in tissue engineering applications and its ability to modulate type 2 immune responses to promote pro-regenerative outcomes in skeletal muscle.

HA-NHS and M-ECM combined to form a hydrogel at physiologic temperatures *in vitro*, as determined by time sweep rheology. The hydrogel was determined to be cytocompatible *in vitro* when immortalized human myoblasts were cultured on the material over the course of four days. The hydrogel demonstrated excellent injectability and spreading when injected into the subfascial space above mouse tibialis anterior and quadriceps muscles, and was shown to degrade *in situ* over the course of 21 days. Additionally, the hydrogel promoted the controlled release of incorporated myostatin inhibitors *in vitro* and increase their bioactivity *in vivo*, both over the course of five days.

Given the role of the immune system in shaping the course of skeletal muscle repair, the immunomodulatory properties of the hydrogel were evaluated. Immunofluorescence-labeled cryosections from wild type and dystrophic muscles revealed the elevated presence of $Fizz1^+$ macrophages in hydrogel-injected muscles when compared to saline. This was further confirmed by flow cytometry, which verified elevated levels of $CD206^+$ macrophages in hydrogel-injected wild type and dystrophic mice. Furthermore, elevated levels of the pro-regenerative type 2 cytokine interleukin-4 were observed in the inguinal lymph nodes of hydrogel-injected wild type and dystrophic mice. However, increased expression of the inflammation-mediating cytokine interleukin-10 was only observed in the inguinal lymph nodes of wild type hydrogel-injected mice.

The immunomodulatory properties of the hydrogel were further characterized by evaluating its individual components (HA-NHS, M-ECM) in dystrophic mice. Additionally, the potential immunomodulatory effects of myostatin inhibition were evaluated by analyzing the immune microenvironment of dystrophic mice injected with RK35 alone or RK35 in hydrogel. Immunofluorescence analysis revealed the presence of $Fizz1^+$ macrophages in M-ECM, hydrogel, and hydrogel+RK35 injected dystrophic mouse muscles. Cytometric analysis confirmed the elevated presence of $CD206^+$ macrophages in hydrogel and hydrogel+RK35 injected mice, and inguinal lymph node cytokine analysis revealed significantly elevated levels of interleukin-4 in M-ECM, hydrogel, and hydrogel+RK35 injected mice. Analysis of $CD3^+$ T cell population subsets revealed significant increases in the $CD4^+$ T helper cells and $Foxp3^+$ regulatory T cells in mice

injected with hydrogel+RK35. Increases in these key cell populations, which mediate effective skeletal muscle regeneration, were not observed with any of the individual hydrogel components, the hydrogel alone, or the myostatin inhibitor alone, suggesting a novel immunomodulatory functionality present with the combination of biomaterials implantation and myostatin inhibition in dystrophic mice.

The multifunctionality of the hydrogel was further evaluated by utilizing it as an injectable carrier for transplanted skeletal muscle stem cells. Human embryonic stem cells derived to the myogenic lineage via treatment with CHIR99021 and DAPT were transplanted into immunodeficient mice and verified to form human muscle fibers *in situ*, reoccupy the endogenous skeletal muscle progenitor cell niche, and promote long-term repair after injury. Short-term evaluation of the hydrogel as a cell carrier revealed increased numbers of immortalized human myoblasts transplanted with the hydrogel visible in serial cryosections after 7 days, and increased numbers of $GFP^+$ human embryonic stem cell derived myoblasts present in single cell suspensions derived from hydrogel-injected muscles 10 days after transplantation. A longer-term study of hESC-derived myoblasts transplanted into immunodeficient dystrophic mice revealed their capability to reoccupy the satellite cell niche after 4 months, and increased numbers of human $Laminin^+$ and $Dystrophin^+$ fibers in hydrogel-transplanted muscles.

## Future Directions

Given the interdisciplinary nature of this project, which lies at the interface of bioengineering and skeletal muscle biology, numerous potential future experimental directions remain. Proteomic analysis of extracellular matrix components of the hydrogel [111] could be used to isolate the specific factors that promote regeneration *in vivo*. Delivery of RK35 with HA-NHS or M-ECM alone could be used to not only determine mechanisms of increased bioactivity, but potential synergistic immunomodulatory effects as well. Efficacy of myostatin inhibitor delivery could be further assessed by morphometric, physiologic, or functional assays of RK35-injected muscles, and longer-term studies could further clarify the effect of the hydrogel. Co-administration of hydrogel and RK35 in other form factors such as systemic, intramuscular, or extended-release formulations may help verify the role of sustained myostatin inhibition on the immune microenvironment in DMD.

Immunomodulatory evaluation of the materials and myostatin inhibitor was only performed at 1 week; shorter or longer timepoints where different populations such as neutrophils, eosinophils, or regulatory T cells predominate could clarify the effects of both injected components on the entire course of immune-mediated skeletal muscle regeneration. Any one of these populations could also be isolated and subjected to transcriptome analysis. Systemic effects of these materials on distal lymph nodes or distal muscles such as the diaphragm (the most profoundly affected muscle in dystrophic mice) could also be evaluated. These materials were also only tested in

healthy wild type and dystrophic animals; various models of muscle injury [102] could be applied in conjunction with these genotypes in order to reveal defects in regeneration that could be positively mediated with the myostatin inhibitor or hydrogel.

Eventually, future therapeutic developments could include combinatorial delivery of muscle progenitor cells and myostatin inhibitors with the hydrogel, potentially increasing the efficacy of cell therapy for DMD. Transplantation of progenitor cells with reporters to isolate specific cell populations such as Pax7 could not only promote transplantation efficacy, but also facilitate visualization and verification of engraftment. Given the profound effects of the immune system on skeletal muscle and local muscle progenitor cells, a hydrogel such as the one described here could not only create a microenvironment in which transplanted cells could survive and thrive, but also shape the host immune microenvironment to promote donor cell engraftment and myofiber formation *in situ*. The use of mouse myoblasts in transplantation assays could allow for the use of immunocompetent mice, allowing for elucidation of the direct effects of immunomodulation on cell transplantation efficiency. Overall, this study represents the first observation of the combined effect of biomaterials and myostatin inhibition on the musculoskeletal immune microenvironment, providing novel insights into potential immunomodulatory therapies for Duchenne Muscular Dystrophy.

# References


1. Jane Larkindale, e.a., *Cost of Illness for Neuromuscular Diseases in the United States.* Muscle and Nerve, 2014. **49**(3): p. 431-438.

2. Jerry R. Mendell, C.S., Nancy D. Leslie, Kevin M. Flanigan, Roula al-Dahhak, Julie Gastier-Foster, Kelley Kneile, Diane M. Dunn, Brett Duval, Alexander Aoyagi, Cindy Hamil, Maha Mahmoud, Kandice Roush, Lauren Bird, Chelsea Rankin, Heather Lilly, Natalie Street, Ram Chandrasekar, Robert B. Weiss, *Evidence-based path to newborn screening for Duchenne muscular dystrophy.* Annals of Neurology, 2012. **71**(3): p. 304-313.

3. Hoffman, E.P., R.H. Brown, and L.M. Kunkel, *Dystrophin: The protein product of the duchenne muscular dystrophy locus.* Cell, 1987. **51**: p. 919-928.

4. Sahenk, Z. and J.R. Mendell, *The muscular dystrophies: distinct pathogenic mechanisms invite novel therapeutic approaches.* Current Rheumatology Reports, 2011. **13**: p. 199-207.

5. Kevin M. Flanigan, A.v.N., Diane M. Dunn, Jonathan Alder, Jerry R> Mendell, Robert B. Weiss, *Rapid Direct Sequence Analysis of the Dystrophin Gene.* American Journal of Human Genetics, 2003. **72**(4): p. 931-939.

6. Andrew H. Ahn, L.M.K., *The Structural and Functional Diversity of Dystrophin.* Nature Genetics, 1993. **3**(4): p. 283-291.

7. Rebecca J. Fairclough, M.J.W., Kay E. Davies, *Therapy for Duchenne muscular dystrophy: renewed optimism from genetic approaches.* Nature Reviews Genetics, 2013. **14**(6): p. 373-378.

8. Surinder M. Singh, N.K., Javier Cabello-Villegas, and Krishna M. G. Mallela, *Missense mutations in dystrophin that trigger muscular dystrophy decrease protein stability and lead to cross-$\beta$ aggregates.* Proceedings of the National Academy of Sciences, 2010. **107**(34): p. 15069-15074.

9. Luca Cartegni, S.L.C., Adrian R. Krainer, *Listening to silence and understanding nonsense: exonic mutations that affect splicing.* Nature Reviews Genetics, 2002. **3**(4): p. 285-298.

10. Christophe Beroud, S.T.-G., Masafumi Matsuo, Dalil Hamroun,, N.M. Veronique Humbertclaude, Marie-Pierre Moizard, Marie-Antoinette Voelckel,, and P.B. Laurence Michel Calemard, Martine Blayau, Christophe Philippe, Mireille Cossee, Michel Pages, Francois Rivier, Olivier Danos, Luis Garcia, Mireille Claustres, *Multiexon skipping leading to an artificial DMD protein lacking amino acids from*

*exons 45 through 55 could rescue up to 63% of patients with Duchenne muscular dystrophy.* Human Mutation, 2007. **28**(2).

11. J.R. Mendell, R.T.M., R.C. Griggs, M.H. Brooke, G.M. Fenichel, J.P. Miller, W. King, L. Signore, S. Pandya, J. Florence, J. Schierbecker, J. Robison, K. Kaiser, S. Mandel, C. Arfken, and B. Gilder, *Randomized, Double-Blind Six-Month Trial of Prednisone in Duchenne's Muscular Dystrophy.* The New England Journal of Medicine, 1989. **320**(4): p. 1592-1597.

12. Robert D. Griggs, P.M., Cheryl R. Greenberg, Darcy L. Fehlings, Alan Pestronk, Jerry R. Mendell, RIchard T. Moxley, Wendy King, John Kissel, Valerie Cwik, Michel Vanasse, Julaine M. Florence, Shree Pandya, Jordan S. Dubow, James M. Meyer, *Efficacy and safety of deflazacort vs prednisone and placebo for Duchenne muscular dystrophy.* Neurology, 2016. **87**(20): p. 2123-2131.

13. Maaike van Putten, M.H., Vishna Devi Nadarajah, Sandra H. van Heiningen, Ella van Huizen, Maarten van Iterson, Peter Admiraal, Tobias Messemaker, Johan T. den Dunnen, Peter A. C. 't Hoen, Annemieke Aartsma-Rus, *The Effects of Low Levels of Dystrophin on Mouse Muscle Function and Pathology.* PLoS One, 2012. **7**(2): p. e31937.

14. Richard S. Finkel, K.M.F., Brenda Wong, Carsten Bönnemann, Jacinda Sampson, H. Lee Sweeney, Allen Reha, Valerie J. Northcutt, Gary Elfring, Jay Barth, Stuart W. Peltz, *Phase 2a Study of Ataluren-Mediated Dystrophin Production in Patients with Nonsense Mutation Duchenne Muscular Dystrophy.* PLoS One, 2013. **8**(12).

15. Manuel Haas, V.V., Pavel Balabanov, Tomas Salmonson, Serge Bakchine, Greg Markey, Martina Weise, Gabriele Schlosser-Weber, Henning Brohmann, Concepcion Prieto Yerro, Macarena Rodriguez Mendizabal, Violeta Stoyanova-Beninska, Hans L. Hillege, *European Medicines Agency review of ataluren for the treatment of ambulant patients aged 5 years and older with Duchenne muscular dystrophy resulting from a nonsense mutation in the dystrophin gene.* Neuromuscular Disorders, 2015. **25**(1): p. 5-13.

16. Stuart P. McElroy, T.N., Leah S. Torrie, Emma Warbrick, Ulrike Gartner, Gavin Wood, W. H. Irwin McLean, *A lack of premature termination codon read-through efficacy of PTC124 (Ataluren) in a diverse array of reporter assays.* PLoS Biology, 2013. **11**(6).

17. Jerry R Mendell, L.R.R.-K., Zarife Sahenk, Kandice Roush, Loren Bird, Linda P. Lowes, Lindsay Alfano, Ann Maria Gomez, Sarah Lewis, Janaiah Kota, Vinod Malik, Kim Shontz, Christopher Walker, Kevin Flanigan, Marco Corridore, John R. Kean, Hugh D. Allen, CHris Shilling, Kathleen R. Melia, Peter Sazani, Jay B. Saoud, Edward M. Kaye, the Eteplirsen Study Group, *Eteplirsen for the treatment of Duchenne muscular dystrophy.* Annals of Neurology, 2013. **74**(5): p. 637-647.

18. M. Carrie Miceli, S.F.N., *The case for eteplirsen: Paving the way for precision medicine.* Molecular Genetics and Metabolism, 2016. **118**(2): p. 70-71.

19. Courtney S. Young, A.D.P., *Exon Skipping Therapy.* Cell, 2016. **167**(5): p. 1144.

20. Andrea M. Reinig, S.M., Daniel J. Berlau, *Advances in the treatment of Duchenne muscular dystrophy: New and emerging pharmacotherapies.* Pharmacotherapy, 2017.

21. Christopher R. Heier, J.M.D., Qing Yu, Blythe C. Dillingham, Tony Huynh, Jack H. Van der Meulen, Arpana Sali, Brittany K. Miller, Aditi Phadke, Luana Scheffer, James Quinn, Kathleen Tatem, Sarah Jordan, Sherry Dadgar, Olga C. Rodriguez, Chris Albanese, Michael Calhoun, Heather Gordish - Dressman, Jyoti K. Jaiswal, Edward M. Connor, John M. McCall, Eric P. Hoffman, Erica K. M. Reeves, Kanneboyina Nagaraju, *VBP15, a novel anti - inflammatory and membrane - stabilizer, improves muscular dystrophy without side effects.* EMBO Molecular Medicine, 2013. **5**(10): p. 1569-1585.

22. Kleopas A. Kleopa, A.D., Eleni Mavrikiou, Annita Ormisto, Theodoros Kyriakides, *Naturally occurring utrophin correlates with disease severity in Duchenne muscular dystrophy.* Human Molecular Genetics, 2006. **15**(10): p. 1623-1628.

23. Valeria Ricotti, S.S., Helen Roper, Imelda Hughes, Bina Tejura, Neil Robinson, Gary Layton, Kay Davies, Francesco Muntoni, Jonathon Tinsley, *Safety, Tolerability, and Pharmacokinetics of SMT C1100, a 2-Arylbenzoxazole Utrophin Modulator, following Single- and Multiple-Dose Administration to Pediatric Patients with Duchenne Muscular Dystrophy.* PLoS One, 2016. **11**(4).

24. Mary Lynn Mercado, A.R.A., Hiroki Hagiwara, Michael S. Rafii, Beatrice Lechner, Rick T. Owens, David J. McQuillan, Stanley C. Froehner, Justin R. Fallon, *Biglycan targets dystrobrevin, syntrophin and nNOS to the muscle cell membrane.* Federation of American Societies for Experimental Biology, 2006. **20**(10): p. 1724-1726.

25. Alison R. Amenta, A.Y., Sasha Bogdanovich, Beth A. McKechnie, Mehrdad Abed, Tejvir S. Khurana, and Justin R. Fallon, *Biglycan recruits utrophin to the sarcolemma and counters dystrophic pathology in mdx mice.* Proceedings of the National Academy of Sciences, 2010. **108**(2): p. 762-767.

26. Jane T. Seto, J.N.R., Lindsey Muir, Jeffrey S. Chamberlain, Guy L. Odom, *Gene replacement therapies for Duchenne muscular dystrophy using adeno-associated viral vectors.* Current Gene Therapy, 2012. **12**(3): p. 139-151.

27. Scott Q. Harper, M.A.H., Christiana DelloRusso, Dongsheng Duan, Robert W. Crawford, Stephanie F. Phelps, Hollie A. Harper, Ann S. Robinson, John F.

Engelhardt, Susan V. Brooks, Jeffrey S. Chamberlain, *Modular flexibility of dystrophin: Implications for gene therapy of Duchenne muscular dystrophy.* Nature Medicine, 2002. **3**: p. 253-261.

28. Miki Sakamoto, K.Y., Madoka Yoshimura, Toshifumi Yokota, Takaaki Ikemoto, Misao Suzuki, George Dickson, Yuko Miyagoe-Suzuki, Shin'ichi Takeda, *Micro-dystrophin cDNA ameliorates dystrophic phenotypes when introduced into mdx mice as a transgene.* Biochemical and Biophysical Research Communications, 2002. **293**(4): p. 1265-1272.

29. Duan, D., *Dystrophin Gene Replacement and Gene Repair Therapy for Duchenne Muscular Dystrophy in 2016: An Interview.* Human Gene Therapy Clinical Development, 2016. **27**(1): p. 9-18.

30. Jennifer A. Doudna, E.C., *The new frontier of genome engineering with CRISPR-Cas9.* Science, 2014. **346**(6213).

31. Patrick D. Hsu, E.S.L., Feng Zhang, *Development and Applications of CRISPR-Cas9 for Genome Engineering.* Cell, 2014. **157**(6): p. 1262-1278.

32. Christopher E. Nelson Chady H. Hakim, D.G.O., Pratiksha I. Thakore, Eirik A. Moreb, Ruth M. Castellanos Rivera, Sarina Madhavan, Xiufang Pan, F. Ann Ran, Winston X. Yan, Aravind Asokan, Feng Zhang, Dongsheng Duan, Charles A. Gersbach, *In vivo genome editing improves muscle function in a mouse model of Duchenne muscular dystrophy.* Science, 2016. **351**(6271): p. 403-407.

33. Chengzu Long, L.A., Alex A. Mireault, John R. McAnally, Hui Li, Efrain Sanchez-Ortiz, Samadrita Bhattacharyya, John M. Shelton, Rhonda Bassel-Duby, Eric N. Olson, *Postnatal genome editing partially restores dystrophin expression in a mouse model of muscular dystrophy.* Science, 2016. **351**(6271): p. 400-403.

34. Mohammadsharif Tabebordbar, K.Z., Jason K. W. Cheng, Wei Leong Chew, Jeffrey J. Widrick, Winston X. Yan, Claire Maesner, Elizabeth Y. Wu, Ru Xiao, F. Ann Ran, Le Cong, Feng Zhang, Luk H. Vandenberghe, George M. Church, Amy J. Wagers, *In vivo gene editing in dystrophic mouse muscle and muscle stem cells.* Science, 2016. **351**(6271): p. 407-411.

35. Niclas E. Bengtsson, J.K.H., Guy L. Odom, Michael P. Phelps, Colin R. Andrus, R. David Hawkins, Stephen D. Hauschka, Joel R. Chamberlain, Jeffrey S. Chamberlain, *Muscle-specific CRISPR/Cas9 dystrophin gene editing ameliorates pathophysiology in a mouse model for Duchenne muscular dystrophy.* Nature Communications, 2017. **8**.

36. Boldrin, L., F. Muntoni, and J.E. Morgan, *Are human and mouse satellite cells really the same?* The journal of histochemistry and cytochemistry : official journal of the Histochemistry Society, 2010. **58**: p. 941-55.

37. Olguin, H.C. and B.B. Olwin, *Pax-7 up-regulation inhibits myogenesis and cell cycle progression in satellite cells: a potential mechanism for self-renewal.* Dev Biol, 2004. **275**(2): p. 375-88.

38. Brack, A.S., et al., *Increased Wnt signaling during aging alters muscle stem cell fate and increases fibrosis.* Science 2007. **317**: p. 807-10.

39. Scarda, a., et al., *Increased adipogenic conversion of muscle satellite cells in obese Zucker rats.* International journal of obesity (2005), 2010. **34**: p. 1319-27.

40. Terry A. Partridge, J.E.M., Gary R. Coulton, Eric P. Hoffman, Louis M. Kunkel, *Conversion of mdx myofibres from dystrophin-negative to -positive by injection of normal myoblasts.* Nature, 1989. **337**(6203): p. 176-179.

41. Maurilio Sampaolesi, S.B., Giuseppe D'Antona, Nicolas Granger, Rossana Tonlorenzi, Anna Innocenzi, Paolo Mognol, Jean-Lauren Thibaud, Beatriz G. Galvez, Ines Barthélémy, Laura Perani, Sara Mantero, Maria Guttinger, Orietta Pansarasa, Chiara Rinaldi, M. Gabriella Cusella De Angelis, Yvan Torrente, Claudio Bordignon, Roberto Bottinelli, Giulio Cossu, *Mesoangioblast stem cells ameliorate muscle function in dystrophic dogs.* Nature, 2006. **444**(7119): p. 574-579.

42. Emanuela Gussoni, Y.S., Corinne D. Strickland, Elizabeth A. Buzney, Mohamed K. Khan, Alan F. Flint, Louis M. Kunkel, Richard C. Mulligan, *Dystrophin expression in the mdx mouse restored by stem cell transplantation.* Nature, 1999. **401**(6751): p. 390-394.

43. Antonio Filareto, S.P., Radbod Darabi, Luciene Borges, Michelina Iacovino, Tory Schaaf, Timothy Mayerhofer, Jeffrey S Chamberlain, James M. Ervasti, R. Scott McIvor, Michael Kyba, and Rita C.R. Perlingeiro, *An ex vivo Gene Therapy Approach to Treat Muscular Dystrophy Using inducible Pluripotent Stem Cells.* Nature Communications, 2013. **4**.

44. Courtney S. Young, M.R.H., Natalia V. Ermolova, Haruko Nakano, Majib Jan, Shahab Younesi, Saravanan Karumbayaram, Chino Kumagai-Cresse, Derek Wang, Jerome A. Zack, Donald B. Kohn, Atsushi Nakano, Stanley F. Nelson, M. Carrie Miceli, Melissa J. Spencer, April D. Pyle, *A Single CRISPR-Cas9 Deletion Strategy that Targets the Majority of DMD Patients Restores Dystrophin Function in hiPSC-Derived Muscle Cells.* Cell Stem Cell, 2016. **18**(4).

45. Emanuela Gussoni, G.K.P., Andrea M. Lanctot, Khema R. Sharma, Robert G. Miller, Lawrence Steinman, Helen M. Blau, *Normal dystrophin transcripts detected in Duchenne muscular dystrophy patients after myoblast transplantation.* Nature, 1992. **356**(6368): p. 435-438.

46. Giulio Cossu, S.C.P., Sara Napolitano, Maria Pia Cicalese, Francesco Saverio Tedesco, Francesca Nicastro, Maddalena Noviello, Urmas Roostalu, Maria Grazia Natali Sora, Marina Scarlato, Maurizio De Pellegrin, Claudia Godi, Serena Giuliani, Francesca Ciotti, Rossana Tonlorenzi, Isabella Lorenzetti, Cristina Rivellini, Sara Benedetti, Roberto Gatti, Sarah Marktel, Benedetta Mazzi, Andrea Tettamanti, Martina Ragazzi, Maria Adele Imro, Giuseppina Marano, Alessandro Ambrosi, Rossana Fiori, Maria Pia Sormani, Chiara Bonini, Massimo Venturini, Letterio S Politi, Yvan Torrente, Fabio Ciceri, *Intra - arterial transplantation of HLA - matched donor mesoangioblasts in Duchenne muscular dystrophy.* EMBO Molecular Medicine, 2015. **7**(12): p. 1513-1528.

47. Daniel Skuk, J.P.T., *Cell therapy in muscular dystrophies: many promises in mice and dogs, few facts in patients.* Expert Opinion on Biological Therapy, 2015. **15**(9): p. 1307-1319.

48. Wagner, K.R. and A. McPherron, *Loss of myostatin attenuates severity of muscular dystrophy in mdx mice.* Annals of Neurology, 2002. **52**: p. 832-835.

49. Moyer, A.L. and K.R. Wagner, *Regeneration versus fibrosis in skeletal muscle.* Current Opinion in Rheumatology, 2011. **23**: p. 568-73.

50. McPherron, A.C., A.M. Lawler, and S.J. Lee, *Regulation of skeletal muscle mass in mice by a new TGF-beta superfamily member.* Nature, 1997. **387**: p. 83-90.

51. Markus Shuelke, e.a., *Myostatin Mutation Associated with Gross Muscle Hypertrophy in a Child.* New England Journal of Medicine, 2004. **350**(26): p. 2682-2688.

52. Wagner, K.R., et al., *Muscle regeneration in the prolonged absence of myostatin.* Proceedings of the National Academy of Sciences 2005. **102**: p. 2519-24.

53. Li, Z.B., H.D. Kollias, and K.R. Wagner, *Myostatin directly regulates skeletal muscle fibrosis.* The Journal of Biological Chemistry, 2008. **283**: p. 19371-8.

54. Bo Li, Z., J. Zhang, and K.R. Wagner, *Inhibition of myostatin reverses muscle fibrosis through apoptosis.* Journal of cell science, 2012. **125**: p. 3957-65.

55. Craig Campbell, H.J.M., Jean K. Mah, Mark Tarnopolsky, Kathryn Selby, Ty McClure, Dawn M. Wilson, Matthew L. Sherman, Diana Escolar, Kenneth M. Attie, *Myostatin inhibitor ACE-031 treatment of ambulatory boys with Duchenne*

*muscular dystrophy: Results of a randomized, placebo-controlled clinical trial.* Muscle and Nerve, 2016.

56. James R. Apgar, M.M., Rita Agostinelli, Susan Benard, Peter Bialek, Mark Johnson, Yijie Gao, Mark Krebs, Jane Owens, Kevin Parris, Michael St. Andre, Kris Svenson, Carl Morris, Lioudmila Tchistiakova, *Beyond CDR-grafting: Structure-guided humanization of framework and CDR regions of an anti-myostatin antibody.* mAbs, 2016. **8**(7): p. 1302-1318.

57. Erika L.F. Holzbaur, D.S.H., Nicholas Weber, Karen Wallace, Yijin She, Seung Kwak, Liudmilla A. Tchstiakova, Erin Murphy, Joseph Hinson, Riyez Karim, Xiang Yang Tan, Pamela Kelley, Kevin C. McGill, Gareth Williams, Carl Hobbs, Patrick Doherty, Margaret M. Zaleska, Menelas N. Pangalos, Frank S. Walsh, *Myostatin inhibition slows muscle atrophy in rodent models of amyotrophic lateral sclerosis.* Neurobiology of Disease, 2006. **23**(3): p. 697-707.

58. Tidball, J.G., *Regulation of muscle growth and regeneration by the immune system.* Nature Reviews Immunology, 2017. **17**(3): p. 165-178.

59. S. Armando Villalta, B.D., Chiara Rinaldi, Michelle Wehling-Henricks, James G. Tidball, *IFN-γ promotes muscle damage in the mdx mouse model of Duchenne muscular dystrophy by suppressing M2 macrophage activation and inhibiting muscle cell proliferation.* The Journal of Immunology, 2011. **187**(10): p. 5419-5428.

60. Joanne Tonkin, L.T., Robert D Sampson, Enrique Gallego-Colon, Laura Barberi, Daniel Bilbao, Michael D Schneider, Antonio Musarò, and Nadia Rosenthal, *Monocyte/Macrophage-derived IGF-1 Orchestrates Murine Skeletal Muscle Regeneration and Modulates Autocrine Polarization.* Molecular Therapy, 2015. **23**(7): p. 1189-1200.

61. Davie, P.L.a.J.K., *γ-interferon modulates myogenesis through the major histocompatibility complex class II transactivator, CIITA.* Molecular and Cellular Biology, 2011. **31**(14): p. 2854-2866.

62. Davie, P.L.a.J.K., *Interferon-γ Resets Muscle Cell Fate by Stimulating the Sequential Recruitment of JARID2 and PRC2 to Promoters to Repress Myogenesis.* Science Signaling, 2013. **6**(305).

63. Daniela Palacios, C.M., Silvia Consalvi, Giuseppina Caretti, Valentina Saccone, Valentina Proserpio, Victor E. Marquez, Sergio Valente, Antonello Mai, Sonia V. Forcales, Vittorio Sartorelli, Pier Lorenzo Puri, *TNF/p38 α/Polycomb Signaling to Pax7 Locus in Satellite Cells Links Inflammation to the Epigenetic Control of Muscle Regeneration.* Cell Stem Cell, 2010. **7**(4): p. 455-469.

64. Swarnali Acharyya, S.M.S., Alfred S. Cheng, Katherine J. Ladner, Wei He, William Kline, Huating Wang, Michael C. Ostrowski, Tim H. Huang, Denis C. Guttridge, *TNF Inhibits Notch-1 in Skeletal Muscle Cells by Ezh2 and DNA Methylation Mediated Repression: Implications in Duchenne Muscular Dystrophy.* PLoS One, 2010. **5**(8).

65. Dalia Burzyn, W.K., Dmitriy Kolodin, Jennifer L. Shadrach, Massimiliano Cerletti, Young Jang, Esen Sefik, Tze Guan Tan, Amy J. Wagers, Christophe Benoist, Diane Mathis, *A special population of regulatory T cells potentiates muscle repair. .* Cell, 2013. **155**(6): p. 1282-1295.

66. Valerie A. Fadox, D.L.B., Anatole Konowal, Peter W. Freed, Jay Y. Wescott. Peter M. Henson, *Macrophages that have ingested apoptotic cells in vitro inhibit proinflammatory cytokine production through autocrine/paracrine mechanisms involving TGF-beta, PGE2, and PAF.* Journal of Clinical Investigation, 1998. **101**(4): p. 890-898.

67. Valerie A. Fadok, D.L.B., Lindsay Guthrie, Peter M. Henson, *Differential Effects of Apoptotic Versus Lysed Cells on Macrophage Production of Cytokines: Role of Proteases.* The Journal of Immunology, 2001. **166**(11): p. 6847-6854.

68. Jose E. Heredia, L.M., Francis M. Chen, Alisa A. Mueller, Rahul C. Deo, Richard M. Locksley, Thomas A. Rando, Ajay Chawla *Type 2 Innate Signals Stimulate Fibro/Adipogenic Progenitors to Facilitate Muscle Regeneration.* Cell, 2013. **153**(2): p. 376-388.

69. S. Armando Villalta, A.S.R., Jeffrey A. Bluestone, *The immune system in Duchenne muscular dystrophy: Friend or foe.* Rare Diseases, 2015. **3**(1).

70. Cezar, C.A. and D.J. Mooney, *Biomaterial-based delivery for skeletal muscle repair.* Adv Drug Deliv Rev, 2015. **84**: p. 188-97.

71. Nenad Bursac, M.J., Thomas A. Rando, *Synergizing Engineering and Biology to Treat and Model Skeletal Muscle Injury and Disease.* Annual Review of Biomedical Engineering, 2015. **17**: p. 217-242.

72. Hyun-Wook Kang, S.J.L., In Kap Ko, Carlos Kengla, James J Yoo, Anthony Atala, *A 3D bioprinting system to produce human-scale tissue constructs with structural integrity.* Nature Biotechnology, 2016. **34**(3): p. 312-319.

73. Koffler, J. and K. Kaufman-Francis, *Improved vascular organization enhances functional integration of engineered skeletal muscle grafts.* Proceedings of the National Academy of Sciences, 2011. **108**: p. 14789-14794.

74. Fuoco, C., et al., *Injectable polyethylene glycol-fibrinogen hydrogel adjuvant improves survival and differentiation of transplanted mesoangioblasts in acute and chronic skeletal-muscle degeneration.* Skeletal muscle, 2012. **2**: p. 24.

75. Fuoco, C., et al., *In vivo generation of a mature and functional artificial skeletal muscle.* EMBP Molecular Medicine, 2015. **7**(4): p. 411-22.

76. Wolf, M.T., et al., *Naturally derived and synthetic scaffolds for skeletal muscle reconstruction.* Adv Drug Deliv Rev, 2015. **84**: p. 208-21.

77. Roberto Gaetani, C.Y., Neha Srikumar, Rebecca Braden, Pieter A. Doevendans, Joost P.G. Sluijter, Karen L. Christman, *Cardiac-Derived Extracellular Matrix Enhances Cardiogenic Properties of Human Cardiac Progenitor Cells.* Journal of Cell Transplantation, 2016. **25**(9): p. 1653-1663.

78. Sicari, B.M., et al., *An acellular biologic scaffold promotes skeletal muscle formation in mice and humans with volumetric muscle loss.* Science Translational Medicine, 2014. **6**(234): p. 234ra58.

79. Kaitlyn Sadtler, A.S., Matthew T. Wolf, Xiaokun Wang, Drew M. Pardoll, Jennifer H. Elisseeff, *Design, clinical translation and immunological response of biomaterials in regenerative medicine.* Nature Reviews Materials, 2016. **1**.

80. Jenna L. Dziki, B.M.S., Matthew T. Wolf, Madeline C. Cramer, Stephen F. Badylak, *Immunomodulation and Mobilization of Progenitor Cells by Extracellular Matrix Bioscaffolds for Volumetric Muscle Loss Treatment.* Tissue Engineering Part A, 2016. **22**(19-20): p. 1129-1139.

81. Kaitlyn Sadtler, K.E., Brian W. Allen, Matthew T. Wolf, Hongni Fan, Ada J. Tam, Chirag H. Patel, Brandon S. Luber, Hao Wang, Kathryn R. Wagner, Jonathan D. Powell, Franck Housseau, Drew M. Pardoll, Jennifer H. Elisseeff, *Developing a pro-regenerative biomaterial scaffold microenvironment requires T helper 2 cells.* Science, 2016. **352**(6283): p. 366-370.

82. Jordan J. Green, J.H.E., *Mimicking biological functionality with polymers for biomedical applications.* Nature, 2016. **540**(7633): p. 386-394.

83. Kaitlyn Sadtler, B.W.A., Kenneth M. Estrelas, Franck Hosseau, Drew M. Pardoll, Jennifer H. Elisseeff, *The Scaffold Immune Microenvironment: Biomaterial-Mediated Immune Polarization in Traumatic and Nontraumatic Applications.* Tissue Engineering Part A, 2016.

84. Calve, S., et al., *Hyaluronic acid, HAS1, and HAS2 are significantly upregulated during muscle hypertrophy.* American Journal of Physiology Cell Physiology, 2012. **303**: p. C577-88.

85. Chang, C.Y., et al., *Hyaluronic acid-human blood hydrogels for stem cell transplantation.* Biomaterials, 2012. **33**: p. 8026-8033.

86. In Young Choi, H.L., Kenneth Estrellas, Jyothi Mula, Tatiana V. Cohen, Yuanfan Zhang, Christopher J. Donnelly, Jean-Philippe Richard, Yong Jun Kim, Hyesoo Kim, Yasuhiro Kazuki, Mitsuo Oshimura, Hongmei Lisa Li, Akitsu Hotta, Jeffrey Rothstein, Nicholas Maragakis, Kathryn R. Wagner, Gabsang Lee, *Concordant but Varied Phenotypes among Duchenne Muscular Dystrophy Patient-Specific Myoblasts Derived using a Human iPSC-Based Model.* Cell Reports, 2016. **15**(10): p. 2301-2312.

87. Nenad Bursac, M.J., Thomas A. Rando, *Synergizing Engineering and Biology to Treat and Model Skeletal Muscle Injury and Disease.* Annual Review of Biomedical Engineering, 2015. **17**: p. 217-242.

88. Cristina Borselli, H.S., Frank Benesch-Lee, Dmitry Shvartsman, Christine Cezar, Jeff W. Lichtman, Herman H. Vandenburgh, David J. Mooney, *Functional muscle regeneration with combined delivery of angiogenesis and myogenesis factors.* Proceedings of the National Academy of Sciences, 2010. **107**(8): p. 3287-3292.

89. Borselli, C., et al., *The role of multifunctional delivery scaffold in the ability of cultured myoblasts to promote muscle regeneration.* Biomaterials, 2011. **32**: p. 8905-14.

90. Harsha Kabra, Y.H., Hang Liang Lim, Mrityunjoy Kar, Gaurav Arya, Shyni Varghese, *Biomimetic Material-Assisted Delivery of Human Embryonic Stem Cell Derivatives for Enhanced In Vivo Survival and Engraftment.* ACS Biomaterials Science & Engineering, 2015. **1**(1): p. 7-12.

91. Jennifer M. Singelyn, J.A.D., Sonya B. Seif-Naraghi, Robert B. Littlefield, Pamela J. Schup-Magoffin, Karen L. Christman, *Naturally derived myocardial matrix as an injectable scaffold for cardiac tissue engineering.* Biomaterials, 2009. **30**(29): p. 5409-5416.

92. Jessica A. DeQuach, J.E.L., Cynthia Cam, Diane Hu, Michael A. Salvatore, Farah Sheikh, Karen L. Christman, *Injectable skeletal muscle matrix hydrogel promotes neovascularization and muscle cell infiltration in a hindlimb ischemia model.* European Cells and Materials, 2012. **23**: p. 400-412.

93. Iossif Strehin, Z.N., Karun Arora, Thao Nguyen, Jennifer Elisseeff, *A Versatile pH Sensitive Chondroitin Sulfate-PEG Tissue Adhesive and Hydrogel.* BIomaterials, 2010. **31**(10): p. 2788-2797.

94. Jonathan M. Zuidema, C.J.R., Ryan J. Gilbert, Faith A. Morrison, *A protocol for rheological characterization of hydrogels for tissue engineering strategies.*

Journal of Biomedical Materials Research Part B: Applied Biomaterials, 2013. **102**(5): p. 1063-1073.

95. Chun-Hong Zhu, V.M., Raquel N. Cooper, Kamel Mamhaoui, Anne Bigot, Jerry W. Shay, James P. Di Santo, Gillan S. Butler-Browne, Woodring E. Wright, *Cellular senescence in human myoblasts is overcome by human telomerase reverse transcriptase and cyclin- dependent kinase 4: consequences in aging muscle and therapeutic strategies for muscular dystrophies.* Aging Cell, 2007. **6**: p. 515-523.

96. R. Scott Thies, T.C., Monique V. Davies, Kathy N. Tomkinson, Adele A. Pearson, Quazi A. Shakey, Neil M. Wolfman, *GDF-8 Peopeptide Binds to GDF-8 and Antagonizes Biological Activity by Inhibiting GDF-8 Receptor Binding* Growth Factors, 2001. **18**: p. 251-259.

97. Nicholas Beastrom, H.L., Allison Macke, Benjamin D. Canan, Eric K. Johnson, Christopher M. Penton, Brian K. Kaspar, Louise R. Rodino-Klapac, Lan Zhou, Paul M.L. Janssen, *mdx5cv Mice Manifest More Severe Muscle Dysfunction and Diaphragm Force Deficits than Do mdx Mice* The American Journal of Pathology, 2011. **179**(5): p. 2464-2474.

98. Jianyu Li, D.M., *Designing hydrogels for controlled drug delivery.* Nature Reviews Materials, 2016. **1**.

99. S. Armando Villalta, W.R., Leonel Martinez, Amanjot Kaur, TIm Sparwasser, James G. Tidball, Marta Margeta, Melissa J. Spencer, Jeffrey A. Bluestone, *Regulatory T cells suppress muscle inflammation and injury in muscular dystrophy.* Science Translational Medicine, 2014. **6**(258).

100. Suniti Misra, V.C.H., Roger R. Markwald, Shibnath Ghatak, *Interactions between Hyaluronan and Its Receptors (CD44, RHAMM) Regulate the Activities of Inflammation and Cancer.* Frontiers in Immunology, 2015. **6**.

101. Berno Dankbar, M.F., Daniela Brunert, Silvia Hayer, Svetlana Frank, Corinna Wehmeyer, Denise Beckmann, Peter Paruzel, Jessica Bertrand, Kurt Redlich, Christina Koers-Wunrau, Athanasios Stratis, Adelheid Korb-Pap, Thomas Pap, *Myostatin is a direct regulator of osteoclast differentiation and its inhibition reduces inflammatory joint destruction in mice.* Nature Medicine, 2015. **21**(9): p. 1085-1090.

102. David Hardy, A.B., Mathilde Latil, Gregory Jouvion, David Briand, Cedric Thepenier, Quentin Pascal, Aurelie Guguin, Barbara Gayaraud-Morel, Jean-Mark Cavaillon, Shahragim Tajbakhsh, Pierre Rocheteau, Fabrice Chretien, *Comparative Study of Injury Models for Studying Muscle Regeneration in Mice.* PLoS One, 2016. **11**(1).

103. Annemieke Aartsma Rus, M.v.P., *Assessing Functional Performance in the Mdx Mouse Model.* Journal of Visualized Experiments, 2014. **85**.

104. Wong, J., et al., *High-resolution, small animal radiation research platform with x-ray tomographic guidance capabilities.* Int J Radiat Oncol Biol Phys, 2008. **71**(5): p. 1591-9.

105. Robert W. Arpke, R.D., Tara L. Mader, Yu Zhang, Akira Toyama, Cara-lin Lonetree, Nardina Nash, Dawn A. Lowe, Rita C.R. Perlingeiro, Michael Kyba, *A New Immuno-, Dystrophin-Deficient Model, the NSG-mdx-4Cv Mouse, Provides Evidence for Functional Improvement Following Allogeneic Satellite Cell Transplantation.* Stem Cells 2013. **31**(8): p. 1611-1620.

106. Partridge, T.A., *Tissue Culture of Skeletal Muscle*, in *Basic Cell Culture Protocols*, J.M.W. Jeffrey W. Pollard, Editor. 1997, Humana Press. p. 131-144.

107. Lindsay A. Muir, C.E.M., Jeffrey S. Chamberlain, *Prosurvival Factors Improve Functional Engraftment of Myogenically Converted Dermal Cells into Dystrophic Skeletal Muscle.* Stem Cells and Development, 2016. **25**(20): p. 1559-1569.

108. Jinhong Meng, C.F.A., Shi-Wen Xu, Francesco Muntoni, Jennifer E. Morgan, *Contribution of human muscle-derived cells to skeletal muscle regeneration in dystrophic host mice.* PloS one, 2011. **6**(3).

109. Fakhfakh, R., S.-J. Lee, and J.P. Tremblay, *Administration of a soluble activin type IIB receptor promotes the transplantation of human myoblasts in dystrophic mice.* Cell transplantation, 2012. **21**: p. 1419-30.

110. Karen Anthony, V.A.-G., Laura E. Taylor, Adeline Vulin, Yuuki Kaminoh, Silvia Torelli, Lucy Feng, Narinder Janghra, Gisèle Bonne, Maud Beuvin, Rita Barresi, Matt Henderson, Steven Laval, Afrodite Lourbakos, Giles Campion, Volker Straub, Thomas Voit, Caroline A. Sewry, Jennifer E. Morgan, Kevin M. Flanigan, and Francesco Muntoni, *Dystrophin quantification: Biological and translational research implications.* Neurology, 2014. **83**(22): p. 2062-2069.

111. Vince Z. Beachley, M.T.W., Kaitlyn Sadtler, Srikanth S. Manda, Heather Jacobs, Michael R. Blatchley, Joel S. Bader, Akhilesh Pandey, Drew Pardoll, Jennifer H. Elisseeff, *Tissue matrix arrays for high-throughput screening and systems analysis of cell function.* Nature Methods, 2015. **12**(12): p. 1197-1204.

# Curriculum Vitae

KENNETH M. ESTRELLAS
Kenneth.estrellas@gmail.com

Education

2011-17: JOHNS HOPKINS UNIVERSITY. BALTIMORE, MD. PhD Candidate, Graduate Training Program in Cellular and Molecular Medicine.
Dissertation: Development of a Regenerative Medicine Strategy for the Treatment of Duchenne Muscular Dystrophy.

2011: BROWN UNIVERSITY. PROVIDENCE, RI. Master of Science in Biology.
Dissertation: Synthesis and Evaluation of Time-Dependent Mucoadhesion of Novel Bioadhesive Polymers.

2010: BROWN UNIVERSITY. PROVIDENCE, RI. Bachelor of Science in Biology with Honors.
Thesis: Fabrication of Double-Walled Nanospheres by Sequential Phase Inversion Nanoencapsulation.

2010: BROWN UNIVERSITY. PROVIDENCE, RI. Bachelor of Arts in Economics.

Research Experience

2012-2017: PhD Candidate. Johns Hopkins University. Baltimore, MD.
Co-Mentors: Dr. Kathryn Wagner, MD PhD (Director, Center for Genetic Muscle Disorders, Kennedy Krieger Institute) and Dr. Jennifer Elisseeff, PhD (Director, Translational Tissue Engineering Center, Johns Hopkins School of Medicine).
Development of biomaterial hydrogel for use in myogenic progenitor cell transplantation and growth factor delivery for the treatment of muscular dystrophies.
Analysis of regenerative capacity of transplanted human muscle stem cells.
Determination of immunomodulatory properties of implanted biomaterials.

2011: Rotation Student. Johns Hopkins University. Baltimore, MD.
Mentor: Dr. Charles Rudin, MD PhD (Co-Director, Druckenmiller Center for Lung Cancer Research, Memorial Sloan Kettering Cancer Center).
Investigation of the role of autophagy and apoptosis in small cell lung cancer.

2009–2011: Research Assistant. Brown University. Providence, RI.

Mentor: Dr. Edith Mathiowitz PhD (Director, Biotechnology Graduate Program, Brown University). Fabrication and characterization of double-walled polymer nanospheres for use in drug delivery. In vivo rodent studies of uptake, biodistribution, and bioadhesion.
2008–2009: Research Assistant. Brown University. Providence, RI.
Mentor: Dr. Sorin Istrail PhD (Professor, Computer Science, Brown University).
Study of cis -regulation of transcription factor expression and conversion of genetic annotation data from primary literature into browser-based database (Project CYRENE).

## Publications

K.N. Sadtler, B.W. Allen, K.M. Estrellas, J.D. Powell, F. Hosseau, D.M. Pardoll, J.H. Elisseeff. The Scaffold Immune Microenvironment: Biomaterial-Mediated Immune Polarization in Traumatic and Non-Traumatic Applications. Tissue Engineering Part A. October 2016.

I.Y. Choi, H.T. Lim, K.M. Estrellas, J. Mula, T.V. Cohen, Y Zhang, C.J. Donnelly, J.P Richard, Y.J. Kim, H. Kim, Y. Kazuki, M. Oshimura, H. Li, A. Hotta, J. Rothstein, N. Margakis, K.R. Wagner, G. Lee. Concordant but varied phenotypes among patient-specific myoblasts of Duchenne muscular dystrophy revealed by human iPSC-based model. Cell Reports. May 2016.

K.N. Sadtler, K.M. Estrellas, B.W. Allen, M.T. Wolf, H. Fan, A.J. Tam, C. Patel, B.S. Luber, H. Wang, K.R. Wagner, J.D. Powell, F. Hosseau, D.M. Pardoll, J.H. Elisseeff. Developing a Pro-Regenerative Biomaterial Scaffold Micronevironment Requires T Helper 2 Cells. Science. April 2016.

B. Laulicht, A. Mancini, N. Geman, D.Y. Cho, K.M. Estrellas, S. Furtado, R. Hopson, A. Tripathi, E. Mathiowitz. Bioinspired Bioadhesive Polymers: Dopa-Modified Poly(acrylic acid) Derivatives. Macromolecular Bioscience. September 2012.

R.S. Patel, D.Y. Cho, C. Tian, A. Chang, K.M. Estrellas, D. Lavin, S. Furtado, E. Mathiowitz. Doxycycline delivery from PLGA microspheres prepared by a modified solvent removal method. Journal of Microencapsulation. January 2012.

## Conference Proceedings

K.M. Estrellas, J. Mula, K.N. Sadtler, L. Cheu, S. Madjumadar, L. Chung, M. Wolf, E. Velarde, I.Y. Choi, G. Lee, J.H. Elisseeff, K.R. Wagner. Injectable Biomaterial Increases the Myogenic Capacity of Transplanted Human Skeletal Muscle Stem Cells In Vivo. Tissue Engineering and Regenerative Medicine International Society Americas - Annual Meeting. San Diego, CA. December 2016.

K.M. Estrellas, K. Sadtler, S. Madjumadar, J. Mula, E. Velarde, L. Cheu, I.Y. Choi, H.T. Lim, G. Lee, J.H. Elisseeff, K.R. Wagner. Injectable Biomaterials Facilitates Controlled Release of Myostatin Inhibitors and Promotes Viability of Transplanted Myogenic Progenitor Cells In Vivo. 9th Annual Maryland Stem Cell Research Symposium. Silver Spring, MD. May 2016.

K.M. Estrellas, T. Criswell, J. Temenhoff. Co-Chairs, Musculoskeletal Tissue Regeneration Concurrent Session. Tissue Engineering and Regenerative Medicine International Society Annual Conference and Exposition. Washington, DC. December 2014.

K.M. Estrellas, J.H. Elisseeff, K.R. Wagner. Development of a Biomaterial-Based Hydrogel for the Delivery of Myogenic Progenitor Cells Towards the Treatment of Muscular Dystrophy. 7th Annual Maryland Stem Cell Research Symposium. Silver Spring, MD. December 2014.

D.Y. Cho, C. Tian, K.M. Estrellas, Y.T. Liu, J.J. Reineke, S. Furtado, E. Mathiowitz. Bioadhesive Double-Walled Nanospheres as an Oral Insulin Delivery Platform. 38th Annual Meeting and Exposition of the Controlled Release Society. Baltimore, MD. July 2011.

L. Quattrochi, D.Y. Cho, K.M. Estrellas, N.L. Wicks, E. Oancea, E. Mathiowitz. Development of an Artificial Melanosome Utilizing a Lipid-Polymer Hybrid Microparticle. 38th Annual Meeting and Exposition of the Controlled Release Society. Baltimore, MD. July 2011.

D.Y. Cho, K.M. Estrellas, C. Tian, J. Reineke, E. Mathiowitz. A Novel Method for the Fabrication of Double-Walled Nanospheres by Sequential Phase Inversion Nanoencapsulation. 37th Annual Meeting and Exposition of the Controlled Release Society. Portland, OR. July 2010.

D.Y. Cho, C. Tian, K.M. Estrellas, E. Mathiowitz. Effect of Encapsulation Method on Protein Loaded Nanospheres Fabricated by Phase Inversion Nanoencapsulation. 37th Annual Meeting and Exposition of the Controlled Release Society. Portland, OR. July 2010.

## Technical Skills

Rodents: Small Rodent Surgical Models (Cell Transplantation, Hydrogel/Biomaterials Implantation), Small Rodent Injury Models (Volumetric Muscle Defect, Muscle Myotoxins (Cardiotoxin, Notexin, Barium Chloride), Muscle Irradiation), Small Rodent Anesthesia (Isoflurane, Ketamine/Xylazine), Small Rodent Drug Administration (Intraperitoneal, Subcutaneous, Intramuscular), Small Rodent Functional Testing

(Treadmill Exhaustion, Grip Strength), Small Rodent Breeding/Husbandry and Genotyping.

Cellular: Cell Isolation (Muscle Progenitors, Lymphoid/Myeloid Immune Cells), Multiplex/Multicolor Flow Cytometry Staining, Cell/Tissue Culture, Cell Viability (Live/DEAD), Cell Proliferation (MTS/MTT, AlmarBlue/PrestoBlue).

Genetic: RNA Isolation, RNA Quantification (Nanodrop), cDNA Synthesis, Quantitiative RT-PCR (qPCR), DNA Isolation, PCR.

Protein: Protein Isolation, Protein Quantification (BCA), Western Blotting, ELISA.

Histology: Cryosectioning, Multiplex Immunofluorescence, Hematoxylin & Eosin (H&E), Masson's Trichrome.

Imaging: Mutiplex/Multicolor Epifluorescence Microscopy (Zeiss Axio Imager M2), Mutiplex/Multicolor Confocal Microscopy (Olympus FV1000), Brightfield Microscopy (Zeiss Axio Imager M2).

Muscle: Cross-Sectional Area Muscle Regeneration Analysis, Muscle Histology and Immunofluorescence.

Bioengineering: Cell Encapsulation, Animal Tissue Decellularization, Hydrogel Fabrication, Polymer Synthesis, Hydroxamate Assay, Rheology, Differential Scanning Calorimetry.

Software: Zeiss AxioVision, Olympus FluoView, Microsoft Image Composite Editor (ICE), GraphPad Prism, Microsoft Office, EndNote, Adobe Photoshop, iMovie, Sony Vegas.

## Honors/Awards

2016 Maryland State Champion, 3 Minute Thesis Competition - University of Maryland. Baltimore, MD. Summary of PhD thesis in three minutes. Explanation of complex scientific concepts to general audience.

2016 3rd Place Winner, 3 Minute Thesis Competition - Johns Hopkins University. Baltimore, MD. Summary of PhD thesis in three minutes. Explanation of complex scientific concepts to general audience.

2016 1st Place Winner, Baltimore Underground Science Space x Project Bridge Science Slam. Baltimore, MD. Summary of PhD thesis in three minutes. Explanation of complex scientific concepts to general audience.

2010 Graduate Honors, ScB Biology. Brown University. Providence, RI. Honors conferred upon Brown University ScB Biology graduates upon completion of thesis.

2010 The Alfred H. Joslin Award for Student Leadership and Involvement. Brown University. Providence, RI. Awarded to graduating seniors who have demonstrated extensive student leadership and involvement.

Leadership Experience

2015–17 Graduate Student Mentor, JHU Undergraduate Neuroscience Program. Baltimore, MD. Individualized mentorship / research training of JHU undergraduate student, Lindsay Cheu.

2015–16 Co-Chair, Brown University Alumni Interviewing Program, Area 210. Baltimore, MD. Organized admissions interviews for ~300 Baltimore area high school applicants to Brown University.

2014–17 Director of Operations, Baltimore Dance Crews Project Collective. Baltimore, MD. Scheduled rehearsals & logistical support for urban dance organization.

2011–14 Workshop Coordinator/Instructor, Baltimore Dance Crews Project. Baltimore, MD. Planned beginner-advanced urban dance workshops for public audiences.

2009-11 Primary Organizer, Free Open Hip Hop Dance Workshops. Brown University. Providence, RI. Planned intermediate-advanced urban dance workshops for public audiences.

2009-11 Co-Director, imPulse Dance Company. Brown University. Providence, RI. Creative and logistical direction of a collegiate urban dance organization.

2008–09 Co-Founder / Organizer, “Dancing With The Professors.” Brown University. Providence, RI. Co-developed charity event pairing Brown professors with Brown Ballroom Dance Team members.

2007–08 Co-President, Filipino Alliance. Brown University. Providence, RI. Creative and logistical direction of organization dedicated to spreading awareness of Filipino culture.

Professional Experience

2016 Equity Research Extern. T. Rowe Price / BCI Equity Research Externship. Baltimore, MD. Performed due diligence on mid-cap life sciences companies and formulated biotech stock pitch.

2013 Consulting Case Competition. Johns Hopkins University Graduate Consulting Club. Baltimore, MD. Participated in team-based business consulting life sciences case competition.

2010–11 NSF EPSCoR Entrepreneurial Fellow. Slater Technology Fund. Providence, RI. Biopharmaceutical venture capital development and startup formation.

2008–11 Intern. New Age Marketing, Inc. Conway, NH. Viability assessment of college marketing methods; production of training materials.